View metadata, citation and similar papers at core.ac.uk
brought to you by CORE
provided by Scholarly Materials And Research @ Georgia Tech

POLYSTYRENE COMPOSITES FILLED WITH MULTI-WALL CARBON NANOTUBES AND INDIUM TIN OXIDE NANOPOWDERS: PROPERTIES, FABRICATION, CHARACTERIZATION

A Thesis
Presented to
The Academic Faculty

by

John M. Boyea

In Partial Fulfillment
of the Requirements for the Degree
Masters of Science in the
School of Materials Science and Engineering

Georgia Institute of Technology
August 2010

COPYRIGHT 2010 BY JOHN M. BOYEA

POLYSTYRENE COMPOSITES FILLED WITH MULTI-WALL CARBON NANOTUBES AND INDIUM TIN OXIDE NANOPOWDERS: PROPERTIES, FABRICATION, CHARACTERIZATION

Approved by:

Dr. Rosario Gerhardt, Advisor
School of Materials Science and Engineering
Georgia Institute of Technology

Dr. Meisha Shofner
School of Materials Science and Engineering
Georgia Institute of Technology

Dr. Gleb Yushin
School of Materials Science and Engineering
Georgia Institute of Technology

Date Approved: 05 / 18 / 2010

To my sister Emma, and the students and faculty of the Materials Science and Engineering department at the Georgia Institute of Technology.

ACKNOWLEDGEMENTS

The most challenging and nurturing people have helped to guide me through the research, analysis, and writing process. As well, I have been graciously helped by my group members and other peers at Georgia Tech. A special thanks to my parents for their constant support and love. I thank my family for being there for me to share in my achievements and support me in my failures. Most importantly in my life I thank God for putting me on this earth and for the strength and courage he provides to me, as well as the guidance through my graduate program. A special thanks to Dr. Rosario Gerhardt for her unwavering support and constant understanding. Without her my M.S. degree would not have been possible. Dr. Gerhardt is an outstanding person all around and I am most grateful to her for many reasons. I would like to thank Dr. Illia Ivanov at Oak Ridge National Laboratory for collaborating with Dr. Gerhardt and I, as well as providing funding and 3D optical micrographs. I am graciously thankful to Dr. Meisha Shofner, and Dr. Gleb Yushin for evaluating this thesis work. My fellow lab mates have helped tremendously with the project, both experimentally and with feed back, whose names are: Salil Joshi, Charlie Capozzi, Kenter Wu, Reggie Krow, Chunqing Peng, Brian Bertram, Cantwell Carson, and Ricky Whelchel. I would also like to acknowledge the funding source from which this project received funding. The National Science Foundation (Award #: 0604211) for funding the research proposal on "Quantitative Structure-Property Relationships in Insulator-Conductor Composites", awarded to Dr. Rosario Gerhardt, that made my degree and research possible. The US Department of Energy (Subcontract Award DOE-EERE under DE-AC05-000R22725) is also acknowledged for funding part of my graduate education.

TABLE OF CONTENTS

LIST OF TABLES

LIST OF FIGURES

LIST OF SYMBOLS AND ABBREVIATIONS

$\|Z^*\|$	Impedance vector
Z'	Real impedance
Z''	Complex impedance
ω	Angular frequency
σ	Conductivity
ρ	Resistivity
γ	Fractal dimensions of the conducting volume
PS	Polystyrene
MWNT	Multi-walled carbon nanotubes
ITO	Indium tin oxide
ABS	Poly(acrylonitrile-co-butadiene-co-styrene)
CB	Carbon black
HDPE	High density polyethylene
TEM	Transmission electron microscopy
SWNT	Single-walled carbon nanotubes
FWHM	Full width half maximum
PMMA	Poly(methyl methacrylate)
CVD	Chemical vapor deposition
phr	parts per hundred resin
PC	Polycarbonate
NMP	N-methyl-2-pyrrolidone
SDS	Sodium dodecyl sulfate
DMF	Dimethylformamide

SUMMARY

This research was designed to fabricate and characterize novel polyhedral phase segregated microstructures of polystyrene (PS)-matrix composites filled with multi-walled carbon nanotubes (MWNT) and indium tin oxide (ITO) nanopowders. PS-composites were compression molded with MWNT and ITO separately first. The resulting composites were conducting, and remained optically transparent. Mixtures of MWNT and ITO were then used to form mixed ITO/MWNT PS-composites in order to optimize their transparency and conductivity. This was achieved by fabricating composites with varying concentrations of fillers. Impedance spectroscopy was used to characterize the electrical properties of the PS-composites. Optical properties were characterized by measuring the transmission of light through the PS-composite in the visible light spectrum using a spectrophotometer. The electrical properties and microstructural attributes of the fillers used were also characterized. The main objective of the project was to understand the relationships between the structural, electrical, and optical properties of the PS-composites. The resistivity of PS-composites filled with MWNT ranged from 10^5 to 10^{13} Ω cm for samples with 0.007 to 0.9 vol% MWNT. The resistivity of PS-composites filled with ITO ranged from 10^7 to 10^{13} Ω cm for PS-composites with 0.034 to 0.86 vol% ITO. PS/ITO composites had a percolation threshold of 0.15, 0.25, or 0.3 phr ITO, depending on the type of ITO used in the composite. The percolation threshold of PS/MWNT composites was found to be 0.01 phr MWNT. Mixed ITO/MWNT PS-composites were already percolated, the concentrations investigated in

this study were already above the percolation threshold of these composites. A time dependence on impedance was found for PS-composites filled with MWNT. As time increases there is a decrease in impedance, and in some cases also a dependence on voltage. All PS-composites showed a dependence on the microstructure of the PS matrix and the filler material. The resistivity and percolation threshold were lower for PS/MWNT composites than PS/ITO composites due to the difference in filler size and aspect ratio, since MWNT have a smaller size. The orientation of PS grains with respect to neighboring grains was found to affect the resistivity of PS/MWNT. PS/MWNT composites with preferentially oriented PS grains were found to have a lower resistivity. Mixed ITO/MWNT PS-composites with the right filler concentrations were able to maintain transmission while decreasing resistivity. The fracture surface of fractured PS-composites prepared in this work indicated that there was bonding between adjacent PS-grains. From this work, it can be concluded that large grain hybrid ITO/MWNT PS-composites provide insight into the effect of combining nanometer sized filler materials together in a polymer matrix on the resultant structural, electrical, and optical properties of the composite. In the future, it is recommended that this study be used to aid research in flexible transparent conducting electrodes using a polymer matrix and hybrid/mixed nanometer sized conducting fillers.

CHAPTER 1

INTRODUCTION

Nanocomposites are an important and widely studied class of materials. The enhancement of specific material properties, by the addition of functional nanometer sized particles, embedded in a matrix material, is the motivation behind nanocomposite research. Nanocomposite properties that are attractive for enhancement are semiconducting electrical properties[1-5], mechanical properties[4-10], optical properties[1, 5], and thermal properties[4, 12-14]. This work focuses on the electrical and optical properties of mixed Polystyrene/Indium Tin Oxide/Multi-walled Carbon Nanotubes (PS/ITO/MWNT) composites. The processing of polymer composites with nanoparticle fillers is performed via various methods, such as solution casting[15-16], latex casting[12, 14, 18, 19, 21], electrostatic spraying[22], compression molding[1, 23-29], etc. Research presented here uses dry blending and compression molding to fabricate PS-composites, which is expected to allow some control of the electrical and optical properties of the composite. These processing methods affect the properties of the polymer-filler mixtures. Polymer-filler mixtures can be formed into various geometries, such as films, tubing, and wires, depending on the various densities and rheological melt behaviors of the polymer-filler mixtures. Polymer composites can be fabricated into different shapes using known polymer melt processing parameters, such as, films, wires, and bulk materials, which is dependent on the rheological melt behavior of the polymer. [5, 23, 25, 30, 37, 62] Such melt

processed polymer composites have a dispersed filler system, more specifically the microstructure of the polymer composite is randomly dispersed.[62, 118]

Electrical applications for polymer-nanocomposites are electromagnetic interference shielding[30], electrostatic protection[30], chemical sensors,[33] supercapacitors for charge storage,[34] and electrical contacts.[21, 27, 31, 32] Carbon nanotubes (CNT), a cylindrical sheet of hexagonal carbon atoms with nanometer diameter, when used as fillers in nanocomposites are excellent for such applications.[35] To achieve improved electrical conductivity randomly, dispersed CNT polymer-nanocomposites require different loadings, or concentrations, of filler material in order to have the conductivity required for each respective application.[36] Solution-processed composites (dispersed microstructure composites) require a higher amount of filler material than phase-segregated composites.[25] The latter use a lower amount of conducting filler material, in comparison, to produce the sufficient conductivity necessary for each respective application.[25, 27] Figure 1.1 shows schematics of the distributions of filler material in both solution-processed composites and phase-segregated composites.[25] The solution-processed composite has a more random and dispersed filler microstructure than the phase-segregated composite.[25] In this figure the microstructure of the filler in the phase-segregated schematic, Figure 1.1a, is separated by the matrix to a large degree.[25]

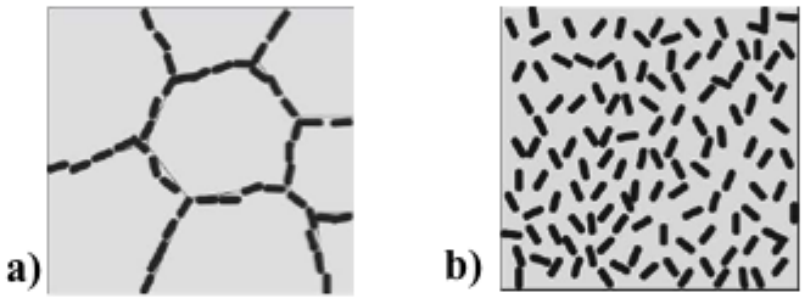

Figure 1.1. Schematic of the distribution of filler material within a polymer-composite, which is the result of a) phase-segregated and b) solution-processing processing. Phase-segregated composites have a filler microstructure that covers the polymer particles surface, while solution-processed composites have a filler microstructure that is randomly distributed in the matrix.[25]

The percolation threshold is an important property to consider when designing a composite system. Percolation is a phenomenon characterized by the filler material forming interconnected wires or pathways through the matrix of the composite.[1, 32, 37, 104] Gupta et. al. fabricated a phase-segregated poly(acrylonitrile-co-butadiene-co-styrene) (ABS) / carbon black (CB) composite, which is an example of a percolated network.[25] In Figure 1.2, an image of an ABS/CB composite shows the CB filler percolating the ABS grain boundaries.[25] The percolation of a conducting filler produces a change in the polymer composite's conductivity.[25] The filler concentration at which the conductivity of the composite drastically changes is defined as the percolation threshold.[1, 25, 37, 38] Figure 1.3 shows the dependence of conductivity on the concentration of CB filler for an ABS/CB phase segregated composite and an ABS/CB solution-processed composite.[25] The drastic change in conductivity, the percolation threshold, occurs at a concentration of 0.01 phr CB and ~10.0 phr CB, respectively.[25]

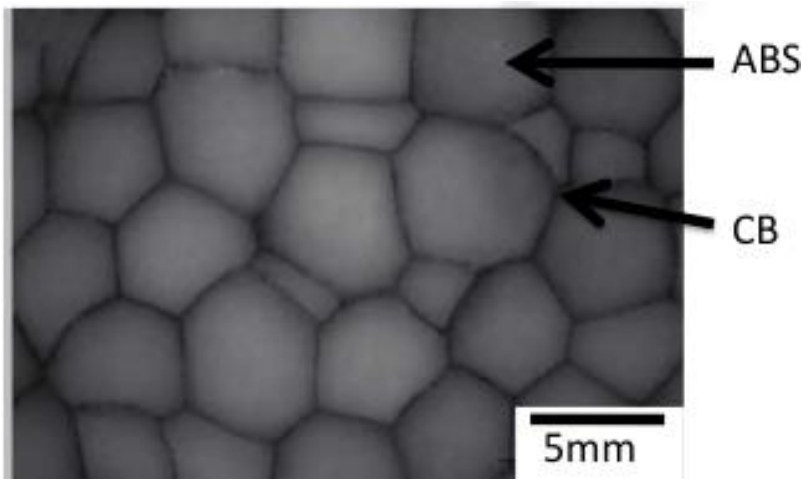

Figure 1.2. Optical micrograph of a phase-segregated ABS/CB composite, the ABS grain boundaries are filled with CB, represented by the dark regions, which forms a honeycomb like structure.[25]

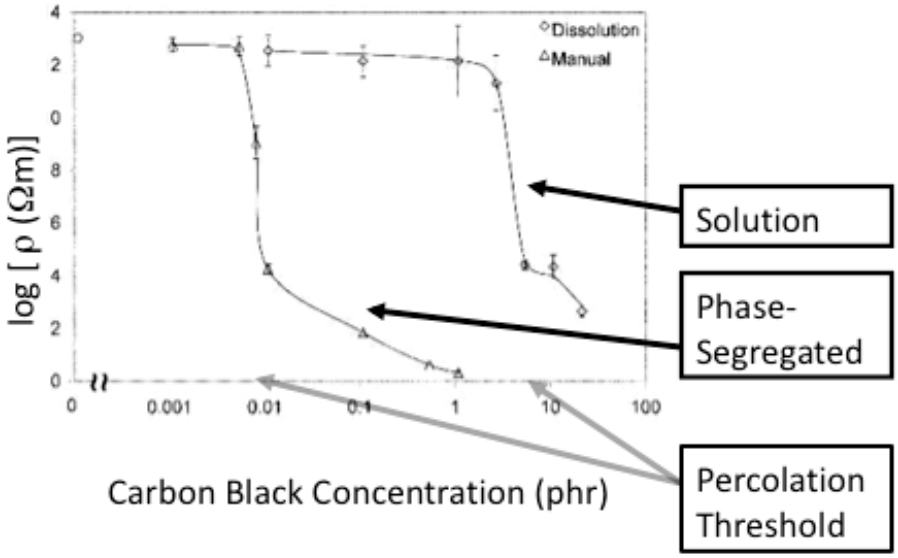

Figure 1.3 Log resistivity versus concentration of carbon black (CB), the drastic decrease in resistivity is the percolation threshold, which occurs at a concentration of 0.01 phr CB for the phase-segregated composites, and at ~10 phr CB for solution-processed composites. ABS/CB phase-segregated composites have a lower percolation threshold than ABS/CB solution processed composites.[25]

The electronic packaging industry uses polymer nanocomposites with conductive properties to protect sensitive electronic components from electrostatic discharge.[30]

Figure 1.4 displays an example of a carbon black (CB), an amorphous carbon, polymer-composite being used to provide electrostatic shielding in the packaging of electronic components, which possesses a dispersed filler microstructure.[41] A high filler loading in such composites is necessary for the composite to reach a sufficient conductivity.[30] High filler loadings are problematic in electronics packaging applications, which is typically due to CB particles that separate from the composite and causes contamination and damage to the enclosed electronics.[30] The mechanical integrity of such composites can decrease at high filler loadings.[30] To meet the required electrical conductivity for such electronics packaging a typical CB polymer-composite contains as much as 15 – 20 wt% CB and has a dispersed filler microstructure.[30] Such composites, require high filler loadings to reach the percolation threshold because the carbon black is randomly dispersed in the manufacturing processes, which are solution or melt processing.[27]

Figure 1.4 Example of a carbon black polymer-composite being used to provide electrostatic shielding in the packaging of electronics components that are sensitive to electrostatic discharge.[41]

A new composite system is proposed in this research to solve the problems associated with high filler loadings and to therefore produce a conducting polymer

nanocomposite with optical transparency properties in the visible spectrum. The proposed composite system uses a transparent grade of polystyrene (PS) with ITO and MWNT fillers to create phase segregated conductive and transparent PS-composites. The electrical and optical properties of MWNT and ITO are of interest to this research in order to enhance the performance of the electrical and optical properties of the PS-composites. Phase segregated composites require low concentrations of filler to achieve percolation which is desired to maintain low scattering of light.[1, 29, 138]

Understanding phase-segregated composites, ITO properties, MWNT properties, and PS properties, presented in Section 1.1, it is necessary to explain the selection of these materials for meeting the goals of this research. Explanation of the research trends of conductive polymer nanocomposites, shown in Section 1.2, provides the background needed to distinguish how this research is unique in comparison. Interpreting the data found during characterization, of the electrical and optical properties of the PS-composites requires an understanding of impedance spectroscopy and optical transmission, as explained later in section 1.3. Further motivation for this research is presented in Section 1.4 after reporting the relevant research and scientific knowledge necessary for understanding the motivation.

1.1. Background on Phase Segregated Polymer Nanocomposites, Indium Tin Oxide (ITO), Multi-Walled Carbon Nanotubes (MWNT), and Polystyrene (PS)

Polymer nanocomposites are formed using several methods and with various materials. Methods of processing polymer nanocomposites, such as melt-processing (a

dispersed filler microstructure method)[45-48], solution-processing (a dispersed filler microstructure method) [15-17], and compression molding[1, 23-29] result in changes to the composite's microstructure, behavior, and properties. Phase-segregated polymer composites, because of their low percolation thresholds, are suitable for application in electronics packaging, electrostatic interference shielding, electrostatic protection, and electrical contacts.[27] Carbon nanotubes are of interest for use as filler material for polymer nanocomposites because nanotubes have unique mechanical, thermal, and electrical properties. Multi-Walled Carbon Nanotubes (MWNT)[49] and Indium Tin Oxide (ITO)[28] can enhance the polymers electrical properties while maintaining a degree of transparency.

1.1.1. Overview of Phase Segregated Polymer Nanocomposites

Phase-segregated polymer nanocomposites exhibit a relatively low percolation threshold compared to composites with a dispersed microstructure.[25, 27] Phase-segregated polymer composites are formed by mixing the filler material and the polymer powders or pellets together, and then compression molding the mixture. Such mixtures undergo particle rearrangement, elastic deformation, and plastic deformation during compression molding.[50] Phase-segregated composites confine the filler particles to the surface of the polymer particles, thus creating an ordered three dimensional structure with a high degree of separation.[1, 23-27, 51-61] During compression molding the polymer matrix is prevented from forming a homogenized structure by the nano-powders coating the polymer.[62] Phase-segregated microstructures are characterized by the separation

between the filler and the matrix phase, in particular these composites have two distinct phases which are discontinuous through the composite.[23, 25, 51]

The distinct separation and ordering of the filler microstructure in phase-segregated polymer nanocomposites causes percolation to occur at low concentrations.[25, 27] In research reported by Gerhardt et. al. a PMMA/CB composite with a phase-segregated microstructure was found to have a percolation threshold at a low volume fraction of 0.26 vol % CB, while a solution processed PMMA/CB composite had a percolation threshold at a higher volume fraction of 2.7 vol % CB.[27]

1.1.2. Indium Tin Oxide (ITO)

Indium tin oxide (ITO) is an important class of materials to the opto-electronic industry.[40, 63, 64] Polycrystalline thin films of ITO possess a conductivity that is near the conductivity of metals, while maintaining a high amount of transparency to visible light.[65] ITO thin films are necessary and well suited for use in a variety of applications, some of which are: liquid crystal displays, solar cells, and photodetectors.[44]

ITO is classified as a wide-band gap semiconductor where the band gap energy is suited for the transmission of visible light.[66] ITO has a unique crystalline structure, the unit cell of ITO is known as cubic bixbyite.[67] A polycrystalline film of ITO has been shown to have a sheet resistivity as low as10^{-4} Ω-cm.[65] The density of the free charge carrier and the mobility of these charge carriers directly affects the resistivity of ITO films, when the number of free charge carriers and the mobility of these carriers increases the resistivity of the ITO films decreases.[44] The microstructure of the deposited ITO affects the before mentioned film properties, which is different between deposition processes and the conditions under which the ITO films are deposited.[44, 68]

There are several deposition techniques used to deposit ITO films, such as dc sputtering, e-beam evaporation, and an arc plasma generator, different sputtering targets and atmospheres are used in each deposition technique, which yield different ITO film microstructures.[63, 65, 68] In-Sn metallic targets, used in a oxygen atmosphere in dc sputtering, can become defective due to poisoning effects.[69] Figure 1.5 shows a schematic of the cross-sectional microstructure and the crystallographic orientation of ITO thin films deposited by dc magnetron sputtering, e-beam evaporation, and an arc plasma generator (HDPE).[68] Such schematics, by showing the resultant microstructure from several ITO thin film deposition techniques, illustrate the microstructural barriers to charge carrier mobility of each film type, such as grain boundaries that act as scattering centers.[68]

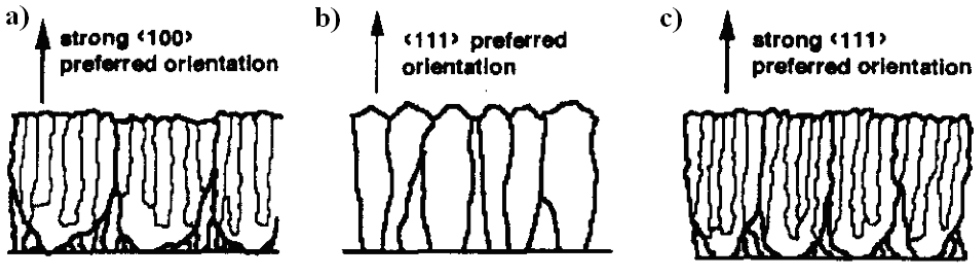

Figure 1.5. Drawings of ITO films, showing a qualitative representation of the microstructure through the thickness of the film, deposited by a) dc magnetron sputtering, b) e-beam evaporation, and c) HDPE. The grain patterns are shown by the shapes growing perpendicular to the substrate. Grain boundaries act as scattering centers which decrease the mobility of the charge carriers.[68]

ITO nanoparticle morphology is different than that of crystalline thin films; instead, nanoparticles consist of individual crystalline ITO particles with nanometer size.[1, 70-72] Solution-processing (dispersed filler microstructure) ITO nanoparticles[70, 73] is attractive because ITO solutions can be coated on a substrate by dipping [5],

spinning[75], and inkjet printing[64, 76]. Figure 1.6 shows the TEM micrograph of ITO nanoparticles produced by thermally oxidizing particle precursors on a substrate via CVD. [77] The figure also shows an analysis of the crystallinity of ITO nanoparticles via TEM diffraction rings.[77]

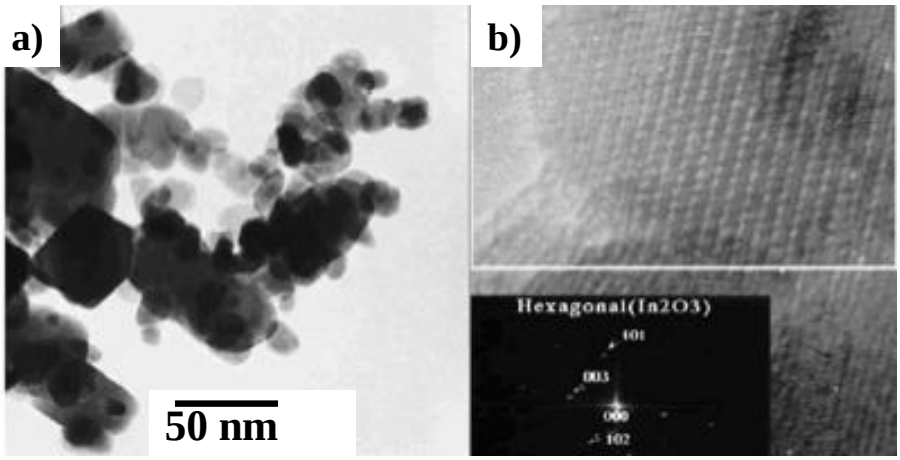

Figure 1.6. a) TEM micrograph of ITO nanoparticles produced via thermal oxidation of precursors on a substrate and b) a high resolution image of a crystalline ITO nanoparticle, confirmed by the electron diffraction pattern.[77]

1.1.3. Carbon Nanotubes (CNT)

Carbon nanotube (CNT) materials, first discovered by Iijima in 1991, posses a unique atomic structure, which has notable optical, mechanical, electrical, and thermal properties.[35, 78, 79] A nanotube can be conceptualized as a graphene sheet, a two-dimensional structure of carbon atoms with a hexagonal arrangement, that is rolled together to form a cylindrical tube.[80] Figure 1.7 shows how the chiral vector, or atomic structure, of a nanotube is defined by picturing the nanotube as an unrolled graphene sheet and defining a vector with respect to the basis vectors of the graphene lattice.[80] An individual carbon nanotube has specific properties that depend on the dimension and chirality of the nanotube.[35] Individually, carbon nanotubes have excellent tensile

strength and elastic modulus.[80] Metallic carbon nanotubes are excellent conductors of electricity as well as thermal energy.[35]

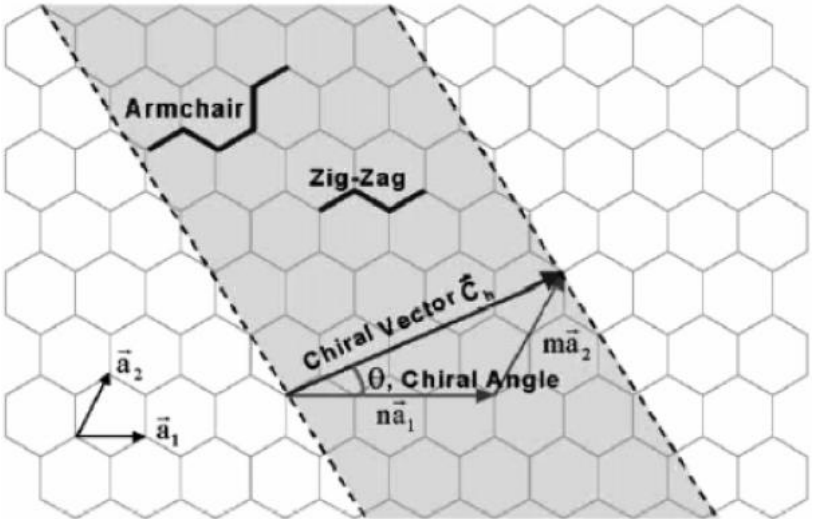

Figure 1.7. Schematic diagram illustrating a hexagonal sheet of graphene and the geometries that the sheet can be rolled into to form a carbon nanotube. CNT geometry is given by the linear combination of the basis vectors of a graphene sheet that defines the repeat unit across the nanotubes diameter, known as the chiral vector. The specific tube geometry shown in the schematic when rolled will form a (3,2) nanotube.[80]

The three main techniques for producing nanotubes are arc discharge, laser ablation, and chemical vapor deposition (CVD).[35, 80] Arc discharge and laser ablation CNT fabrication techniques use a solid carbon source, which is evaporated to create hot carbon atom gas that must condensate to grow CNT.[35] In CVD, hydrocarbon and carbon monoxide gases flow through a furnace, at processing specific conditions, and decompose on the substrates surface (where a catalyst is present) resulting in CNT growth or deposition.[35] CVD is advantageous for the production of CNT due to the high degree of control that this method has of the length and the chirality of the CNT.[35] Each CNT fabrication method and every individual CNT 'batch' made by the various CNT producation techniques creates a combination of CNT types, which vary in chirality,

diameter, length, and impurity atoms.[35] Multi-walled carbon-nanotubes (MWNT) are multiple carbon nanotubes encapsulated within an outer carbon nanotube, where the diameter of the nanotubes increase from the inner to the outer nanotube.[49] Figure 1.8 shows a TEM micrograph of a network of MWNT produced by chemical vapor deposition.[81]

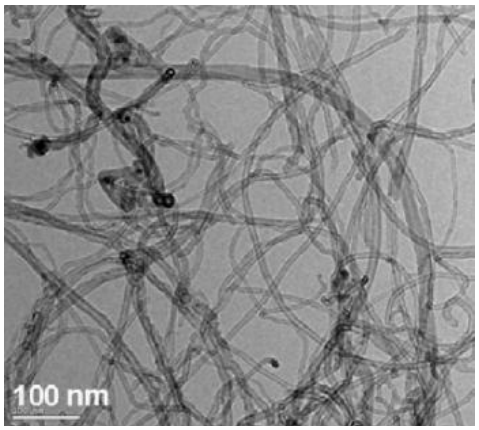

Figure 1.8. TEM image of MWNT with a diameter between 10 and 20 nm and a length between 10 and 50 μm, produced by chemical vapor deposition. The nanotubes are dispersed in a suspension that causes them to exfoliate.[81]

1.1.4 Polystyrene (PS)

Polystyrene (PS) is a widely used commercial polymer that has been investigated extensively for use in carbon filler polymer nanocomposites.[8, 15, 17, 33, 37, 38, 48, 82-85, 87-89] For example, CNT filled PS-composites have been widely studied in hopes of tuning the electrical conductivity properties of nanocomposites.[8, 15, 17, 37, 38] PS is an aromatic polymer polymerized from aromatic monomer styrene.[95] The chemical formula for polystyrene is $(C_8H_8)_n$.[95] PS is a thermoplastic polymer, which is elastic and flexible above the glass transition temperature.[95] The glass transition temperature of PS is

between -92°C and 150°C depending on the molecular weight and network structure of the polymer.[96]

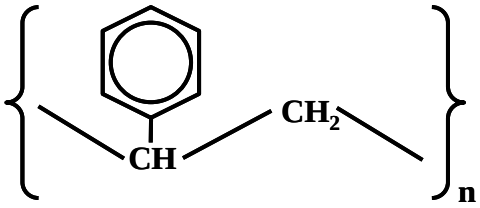

Figure 1.9. A drawing of the polystyrene monomer, a single styrene molecule, with a chemical formula of $(C_8H_8)_n$. The integer n represents the number of styrene molecules that are bonded together to form the polystyrene chain.[95] (Drawing recreated from reference).

1.2. Polymer Nanocomposites with Conductive Fillers

Composites with an insulating polymer matrix containing conducting fillers become electrically conducting when the filler loading exceeds a critical value, known as the percolation threshold.[1, 25, 27, 37, 38, 97] A distinct change in conductivity by many orders of magnitude, attributed to the creation of a three-dimensional conductive network of fillers embedded in the matrix, occurs when the percolation threshold concentration is met or exceeded, as shown in Figure 1.3.[25] When percolation of the conductive filler penetrates the composite, the ac conductivity of the composite scales as a power law function with dependence on the concentration away from the percolation threshold.[99] Quantitative models of percolation in materials science were first explained in experiments by S. Bhattacharyya.[56] In Bhattacharyya's study, percolation was shown to have a specific relationship to the concentration of filler material within the matrix, as well as the ratio between the filler particle size and the polymer matrix particle size.[56] The materials properties and fabrication processes that are used to make polymer composites affects the

percolation threshold of the composite, where the important contributing factors are: the filler size with respect to matrix particle size[32, 51, 53-56, 100, 101] and the composite fabrication method. [25, 27]

1.2.1. Composites Filled with Carbon Nanotubes

Polymer nanocomposites filled with carbon nanotubes (CNT) have been formed as thin film and bulk composites by dip-coating/layer by layer deposition[103], suspension solution polymerization (dispersed filler microstructure)[15], polymer extrusion (a melt processed dispersed filler microstructure)[88], latex technology [19, 104], surface grafting polymerization[105], shear mixing or melt processing (dispersed filler microstructure)[2], and compression molding.[83, 89, 101] Small filler loadings of nanotubes (0.1 wt% or less) have been demonstrated to increase the conductivity of polymer composites by several orders of magnitude.[106] Enhancements in conductivity have been made while maintaining polymer performance properties such as optical clarity[43] and mechanical properties[6, 8, 9, 107, 108]. CNT polymer-composite properties depend in part on several factors independent of the polymer itself: the method of nanotubes production, the state of impurities after purification or the state of impurities without purification, the nanotube morphology and geometry, and the amount of CNT orientation within the composite.[49]

The excellent mechanical properties, fiber like structure, and high aspect ratio of nanotubes have been shown to be viable reinforcements in composite materials.[110] Vigolo et. al. demonstrated a method of producing a CNT polymer composite (PVA/SWNT) with a oriented CNT microstructure called the “coagulation spinning” method, which resulted in a tensile strength of 1.8 GPa.[111] PS-composites filled with

CNT, made using a solution dispersion polymerization method (a dispersed filler microstructure), were investigated using calorimetry in an effort to link the information about percolation, obtained from electrical data, with the calorimetric behavior.[87] Rivin et. al. presented a relationship between the percolation threshold and the integral heat of absorption, this relationship is analogous to the electrical and mechanical property percolation curves.[87]

Nanotubes are often put into suspension using surfactants to separate nanotube agglomerations, which are then mixed with the polymer, and cast into composites, these composites have a dispersed filler microstructure.[15] Exfoliation of CNT has been used to separate nanotube aggregates in order to decrease the percolation threshold. Nanotubes are separated to decrease the percolation threshold of the composite, this separation is known as exfoliation and can lead to more inter-particle contacts between nanotubes in comparison with composites containing agglomerated nanotubes bundles.[112] Agglomeration is an effect of the attraction of CNT with other nanotubes by the van der Waals forces between the two particle surfaces. Pulling apart or physically separating one nanotubes from another is done with a mixture of physical or chemical treatments, such as the addition of surfactants, functionalization of the surface of the nanotubes, and sonication for an extended amount of time.[31, 48, 112-114] Figure 1.10 shows an electrically conductive carbon nanotubes/PS nanocomposite produced by direct mixing a suspension of exfoliated MWNT and PS latex, followed by freeze drying the solution and compression molding the resultant powder.[38] The resulting PS/MWNT nanocomposite is a homogeneous polymer-composite with a well dispersed filler, the maximum

conductivity and percolation of the PS/MWNT composites ranged from $10^{-1.6}$ to $10^{0.8}$ S/m and 0.7 to 1.1 wt % MWNT respectively, depending on pressing conditions.[38]

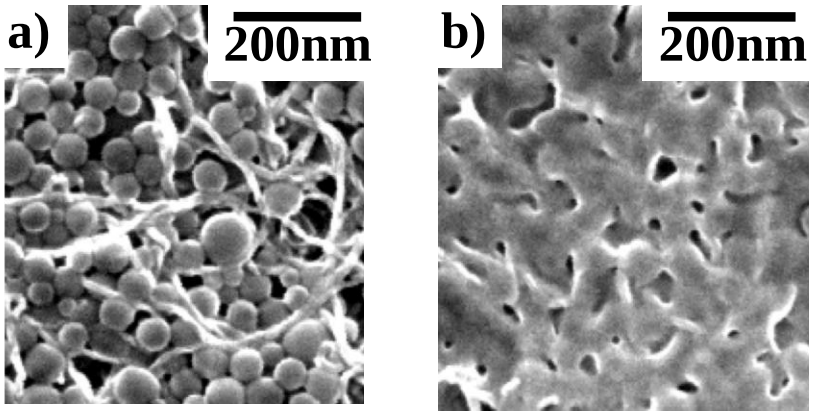

Figure 1.10. SEM image of freeze dried PS/MWNT powder, from an exfoliated MWNT/latex PS solution. Part a) shows the microstructure for the PS/MWNT powder after heating to 60°C, there is no apparent morphology change to the polymer. Part b) displays powder heated to 100°C, the glass transition temperature of PS, the polymer changes morphology.[38]

Above the percolation threshold, typically 0.05 – 10 wt% CNT, CNT polymer-composites have exceptional electrical conductivity.[115] The percolation threshold in nanotube polymer nanocomposites is altered by several nanotube characteristics: aspect ratio[108], dispersion[116], and alignment.[84, 109, 117, 118] Figure 1.11 shows the electrical conductivity of a SWNT/polycarbonate (PC) solution-processed composite as a function of nanotube loading.[36] These solution-blended composites, with loading above 0.3 wt % and 3 wt % SWNT, are acceptable for applications in electrostatic painting and EMI shielding, respectively.[36] A MWNT/epoxy composite was found to have a decrease in the percolation threshold concentration by a factor of eight by Bai and Allaoui,[108] when the MWNT length was varied from 1 to 50 μm. Research described by Z. Wang et. al. describes a solution polymerizing technique for nanotube defloculation, where nanotubes had an absorbed polymer layer providing better dispersion of nanotubes.[15] PS/SWNT

composites prepared by Z. Wang et. al. used a solution polymerization process to form composites which had a minimum dc resistance of 2MΩ.[15] Figure 1.12 shows an SEM micrograph of PS particles coated with SWNT by dissolving the PS in toluene and adding the SWNT to the solution.[15]

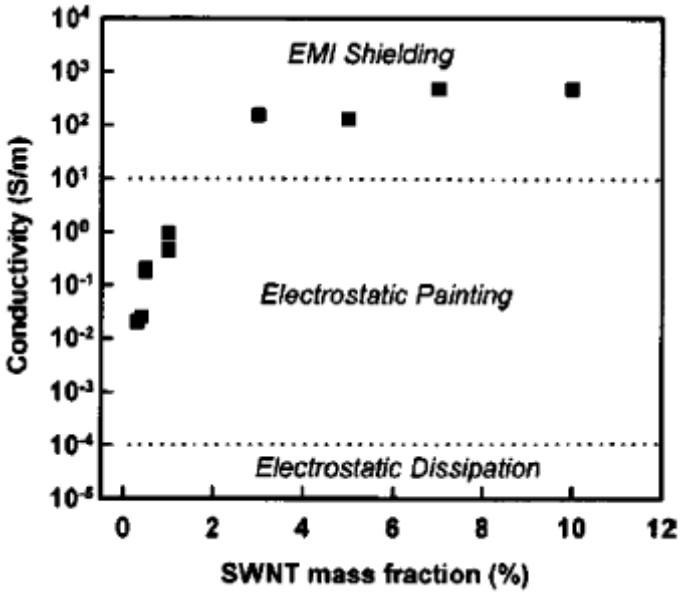

Figure 1.11. Electrical conductivity of a solution-processed SWNT/polycarbonate nanocomposite versus nanotube loading (wt% SWNT), which shows the percolation threshol of these composites. The dashed lines separate the values of conductivity that the composite must meet for use in EMI shielding, electrostatic painting, and electrostatic discharge.[36]

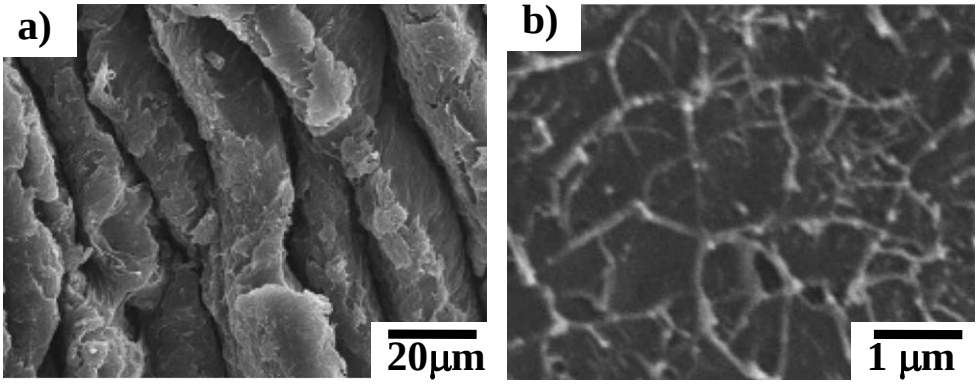

Figure 1.12. SEM micrograph displaying a PS/SWNT solution part a), where PS was dissolved in toluene with SWNT added to the solution, and SEM micrograph at a higher magnification, showing a network of SWNT on the PS surface.[15]

Exfoliated solution CNT-based nanocomposites have a high viscosity which presents issues to the formation of composites when using polymer melt processing (a dispersed filler microstructure).[112, 119, 120] Achieving CNT/polymer nanocomposites with high electrical conductivities and desirable rheological properties is a current challenge in preparing these composites. A PS/MWNT composite with a randomly distributed MWNT microstructure produced using shear mixing was found to have a minimum surface resistivity at 10^3 Ω/square.[85] Cellular structures of phase-segregated SWNT polymer nanocomposites with 0.5 wt% nanotube concentration, studied by Mu. et. al., had a conductivity of ~3 x 10^{-4} Ω-cm.[89] Figure 1.13 shows a phase-segregated compression molded composite film with an ultrahigh molecular weight polyethylene (UHMWPE) matrix and MWNT filler.[45] The nanotubes were placed in an alcohol suspension and were then used to coat the UHMWPE, after which they were compression molded into films.[45] Table 1.1 summarizes PS/CNT research in terms of nanotube type and treatment, the solution used, the fabrication method, the percolation threshold, and the maximum conductivity (σ).

Table 1.1. The percolation threshold, fabrication method, nanotube treatment, suspension solution, and maximum conductivity of MWNT/PS and SWNT/PS composites presented by several references.

Treatment	Solution	Fabrication Method	Perc. Thresh. (wt%)	σ_{max} (S/m)	Ref.
PS/MWNT					
-	Toluene	Sonicated	0.5	10^{0} @10wt%	[8]
-	SDS	Freeze dried, hot pressed	0.9	10^{-1} @2wt%	[38]
C_3H_6O	C_7H_8	Sonicated, hot pressed	<12	300 @25wt%	[121]
-	-	Extruded	0.45		[2]
HNO_3, HCl	-	Sonicated	0.8	10^{-2} @2wt%	[122]
-	C_6H_8O	Sonicated, stirred	0.16	-	[123]
PS/SWNT					
-	Chloroform	Sonicated, stirred	0.17 - 0.3	10^{-7} @6wt%	[16]
-	NMP	Sonicated, dip-coated	0.4	-	[103]
HCl	-	Coated particle process	0.5	10^{-2} @0.5wt%	[89]
-	SDS	Sonicated, freeze dried, hot pressed	0.5		[3]
-	-	Melted, vacuum oven dried	1.5	-	[48]
Annealed	$C_6H_4Cl_2$	Sonicated, stirred	0.44	-	[124]
PEE-functionalized	$CHCl_3$	Shaken, sonicated	0.05	7 @7wt%	[36]
-	H_2O, SDS	Sonicated, centrifuged, hot pressed	0.28	10^{0} @1.5wt%	[21]

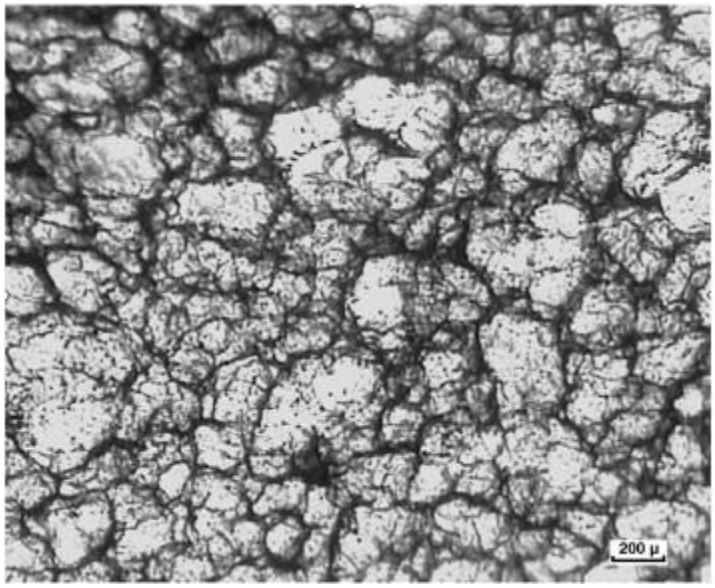

Figure 1.13. Optical micrograph showing the microstructure of a phase-segregated compression molded ultrahigh molecular weight polyethylene (UHMWPE) composite films with a 0.085 vol % concentration MWNT filler (above the percolation threshold). The nanotubes were placed in an alcohol suspension with UHMWPE to coat the polymer particles, after which the alcohol was evaporated and the mixture was compression molded into a film.[45]

Nanotubes can be aligned in a composite during fabrication or after fabrication by mechanical stretching[126], spin-casting[85], wet spinning, melt fiber spinning[84, 118], and electrospinning.[127-129] Using an in-situ polymerization process in combination with the application of an external magnetic field results in the alignment of nanotubes within the polymer-matrix.[109] The mechanical properties of nanotube enriched polymer composites in general show a consistent trend that the tensile modulus and strength of such composites increases with nanotube loading, dispersion, and alignment in the matrix. [8, 9, 12, 108, 124, 126] Du et al. studied the alignment of nanotubes in a SWNT/PMMA composite, controlling nanotubes alignment by varying the melt fiber spinning conditions.[117] The alignment in these studies was quantified by the full width at half-maximum (FWHM) of SWNT form factor scattering, where less SWNT alignment corresponds to higher

FWHM. Fixing the SWNT concentration (2 wt %) and varying the alignment of nanotubes, it was found that the electrical conductivity parallel to the alignment direction increased sharply with decreasing alignment, as shown in Figure 1.14.[117]

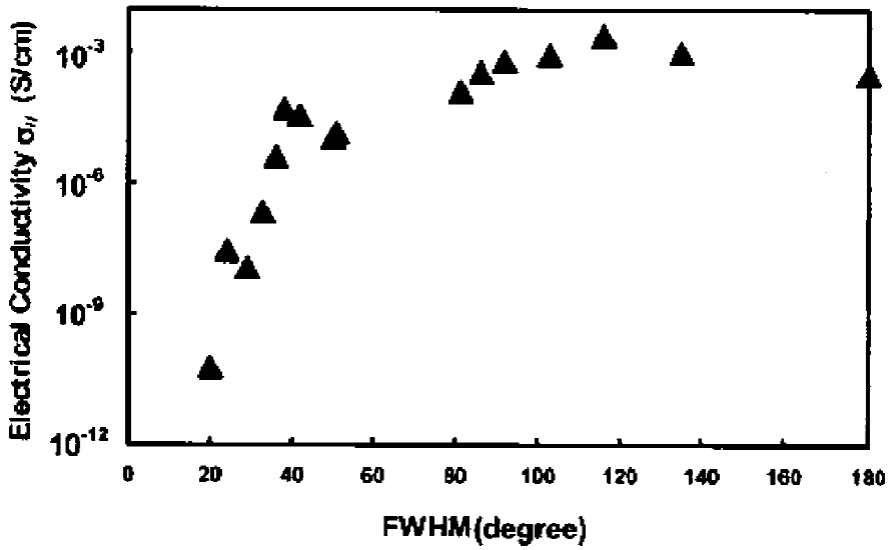

Figure 1.14. Electrical conductivity of a 2 wt % SWNT/PMMA composite along the alignment direction with increasing nanotube isotropy. X-ray scattering is used to determine nanotube alignment where FWHM = 0 is perfectly aligned and FWHM = 180 is isotropic.[117]

1.2.2. Polymer Composites Filled with ITO

ITO nanoparticle/polymer composites have been rarely studied. The possible applications of ITO/polymer composites are similar to CNT/polymer composites, while adding exceptional optical transparency to these composites.[1, 23, 24, 133] Flexible ITO/polymer composites could be used as flexible transparent electrodes for electronics. Phase segregated PMMA/ITO composites reported on by Capozzi et. al. were shown to be transparent and electrically conductive.[1, 23, 24, 28] Figure 1.15 shows a micrograph and image of a PMMA/ITO composite with a PMMA particle size of 5 – 100 μm and a percolation threshold between 0.4 – 1.7 vol% ITO.[28] Polymer ITO composites fabricated

via solution processing making transparent conductive films exhibit poor transparency due to light scattering effects caused by the high ITO filler loadings.[134]

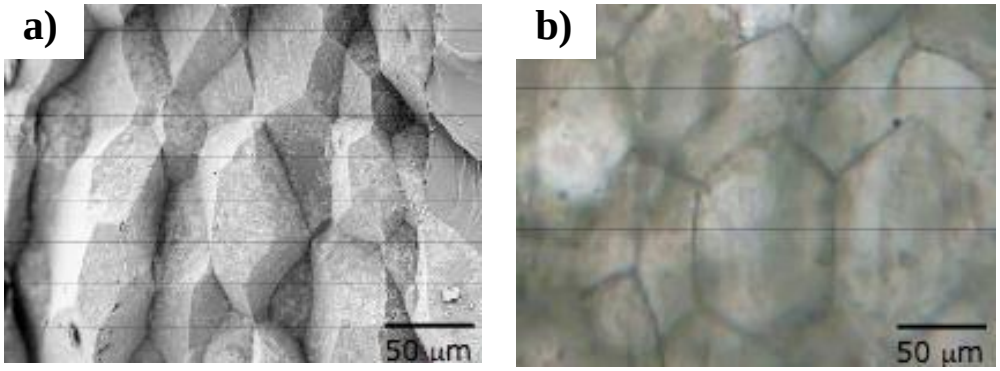

Figure 1.15. PMMA/ITO composites with a phase segregated microstructure. In part a) the cross sectional SEM image of a 0.83 vol% ITO PMMA-composite shows ITO nanoparticles coating polyhedron shaped PMMA particles. In part b) the transmission optical micrograph shows the transparent PMMA grains that are filled with ITO nanoparticles at the grain boundaries.[28]

ITO thin films on polymeric films themselves are a type of composite. In these composites, the interplay between the microstructure and mechanical properties of flexible transparent ITO thin films is a complex system. [135] ITO thin film use in flexible electronics is problematic due to the brittle nature of ITO films when they are under stress.[135] Substrates for flexible organic light emitting devices (OLEDs) are multilayer composite structures, they consist of a polymeric based substrate with various functional coatings.[40] The bending and reliability of the film is dependent on the fracture properties of these extremely brittle films. [136] The mechanical reliability of such films is controlled by the interplay between process induced defects and residual film stresses, cohesive properties and adhesive properties of the individual layers.[136] Figure 1.16 shows an ITO film loaded at a strain of 3.42% where the vertical lines are fracture lines.[135]

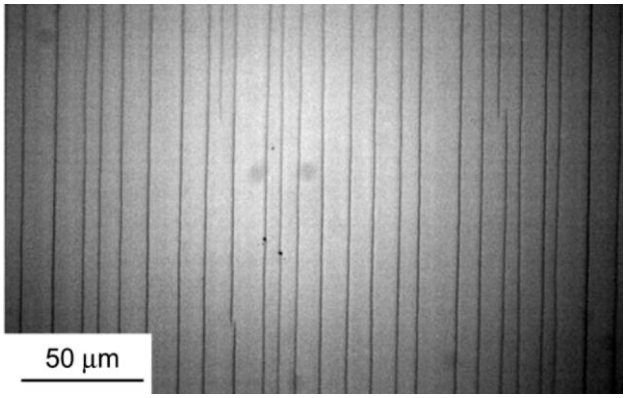

Figure 1.16. ITO film on a flexible substrate, loaded (along the horizontal direction) to a stress of 3.42 %, showing a detrimental failure to the integrity of the electrical conductivity of the film occurs which is seen in the vertical fracture lines of the film.[135]

1.3. Background on Impedance Spectroscopy (IS) and Optical Transmission and Absorbance

Impedance spectroscopy (IS) characterizes the frequency response of the voltage (V) and current (I) as they relate to each other in phase space. Measuring the impedance relates to finding the responses as a function of angular frequency, $\omega = 2\pi f$, which gives the impedance magnitude |Z*|. The impedance vector is given by the following relationship[137]:

$$|Z^*| = \frac{V(\omega)}{I(\omega)} = Z' - jZ'' \qquad \text{Equation 1.1}$$

Where Z' is the real impedance response and Z'' is the imaginary impedance.

The impedance response of composite materials can be modeled with equivalent circuits that can be numerically fitted to the raw data.[137] For example the resistor in parallel with a capacitor circuit has an impedance response that is characterized by Equation 1.2.[137]

$$Z^* = \left[\frac{1}{R1} + j\,\omega\,C1\right]^{-1} \qquad \text{Equation 1.2}$$

Figure 1.17 shows a Nyquist plot of Equation 1.2 with R1 = 10^4 Ωm and C1 = 1 pF. In a Nyquist plot the negative values of Z" are plotted versus Z'. In Figure 1.17 the low frequency intercept of Z'' with the Z' axis is equal to the value of R1.

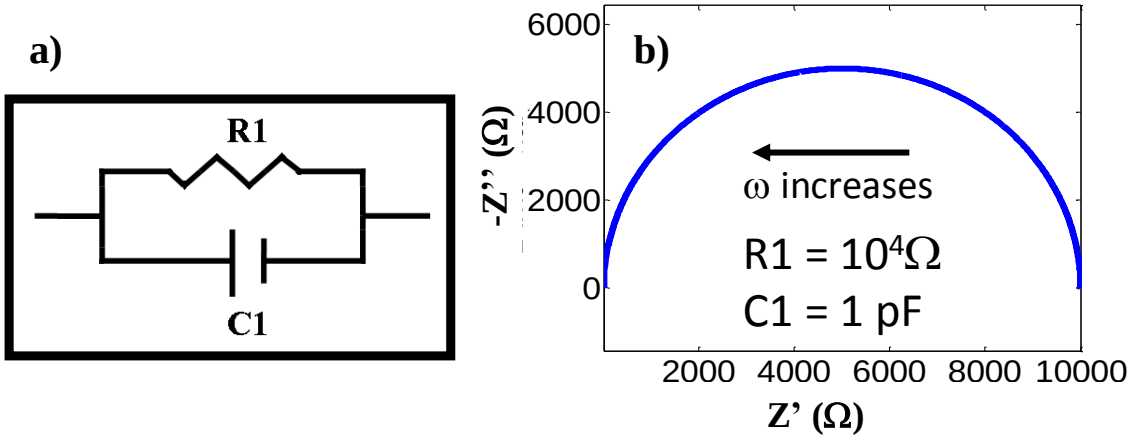

Figure 1.17. Nyquist plot of a resistor in parallel with a capacitor where Equation 1.2 gives the impedance of this circuit. The circuit diagram in part a) is of a resistor in parallel with a capacitor, also known as an RC parallel circuit. In part b) R1 is equal to the intercept of Z'' with Z' in the low frequency region. The value of R1 = 10^4 Ωm is equivalent to this intersection.

The propagation of photon energy in the form of electromagnetic radiation through atomic matter is impeded by absorption, scattering, reflected, and/or refracted.[95] Absorption occurs when energy is lost to molecular interactions that transfer photon energy to phonon energy.[95] Scattering describes the change in direction of electromagnetic wave propagation by interaction with matter where the velocity of the wave is not changed.[95] While refraction is similar to scattering, it is described by Snell's Law as shown in Equation 1.3.[95] Where $\Theta_{\text{incidence}}$ and $\Theta_{refraction}$, $v_{\text{incidence}}$ and $v_{refraction}$, and

$n_{\text{incidence}}$ and $n_{refraction}$ are the angle of incidence and refraction, the velocity of incidence and refraction, and the index of incidence and refraction respectively.

$$\frac{\sin\theta_{incidence}}{\sin\theta_{refraction}} = \frac{v_{incidence}}{v_{refraction}} = \frac{n_{incidence}}{n_{refraction}} \qquad \text{Equation 1.3.}$$

The inline transmission of light can be measured for various wavelengths using a spectrophotometer. The intensity or amplitude of the radiation before and after incidence can be related to the absorbance coefficient using Beer-Lambert's Law in Equation 1.4,[95] where T is the transmittance, I and I_o are the intensity after and before incidence respectively, α' is the absorbance coefficient, and l is the thickness of the material.

$$T = \frac{I}{I_o} = e^{-\alpha' l} \qquad \text{Equation 1.4.}$$

The optical properties of composites are not well described by Beer-Lambert's Law due to the interface between the two constituent phases.[138]

1.4. Research Objectives of Work Presented in this Thesis

This research will separate itself from the existing work on phase-segregated composites by focusing on both the electrical and optical properties of PS-composites. Combining ITO nanoparticles and MWNT as filler materials in any polymer-nanocomposite, as well as PS/ITO, have never been studied. Previous work has looked at phase segregated composites without considering the addition of a second filler material.[27, 59, 139] Although one example did mix CB and CNT in a polymer matrix to enhance electrical properties, it did not focus on both optical properties and conductivity.[81] Phase-segregated composites with a large particulate transparent

polymer matrix are also new to this research area. ITO nanoparticle fillers have been studied in a PMMA matrix, but this research separates itself by combining two fillers to create a mixed PS/ITO/MWNT composite. PS/ITO and PS/MWNT composites are studied first in order to have a reference to compare the optical and electrical properties of these composites and the mixed PS/ITO/MWNT composites. The differences in mixed ITO/MWNT PS-composites are characterized to determine the effect of the particle-particle interactions that occur in the composite. The use of large PS grains is advantageous because it will provide for a more transparent composite, while ITO fillers are predicted to maintain the optical properties of PS as well as add electrical conductivity to the composite. The PS/ITO/MWNT composites are also theorized to be optimal for opto-electronic applications due to the large grains of transparent phase in the composite, as well as the low percolation threshold of filler that a phase-segregated microstructure provides. Lowering the percolation threshold is expected to produce composites with optimized conductivity and reduced scattering and absorbance of light. Taking into consideration the expected properties of a PS/ITO/MWNT composite, experiments were designed to verify the predicted results.

CHAPTER 2

EXPERIMENTAL PROCEDURES

This chapter presents the materials used in the composite fabrication, the methods of fabrication, and the techniques used to characterize the microstructure and properties of the composites synthesized. The various combinations of materials and dimensions of composites sets are outlined to organize this information for the reader. Fabrication procedures for producing composites are explained. Further, microstructure and properties characterization techniques utilized are described.

2.1 Materials

The materials chosen for this experiment were Short-Multi Wall carbon nanotubes (MWNT), Indium Tin Oxide (ITO) nanopowders, and Polystyrene (PS). PS was chosen as the matrix component of the composite materials. ITO and MWNT were chosen as fillers for the composite. The PS was obtained from Polyone Distribution. PS particles are cylindrical with average dimensions of height being 4 mm and the average dimension of diameter being 2.8 mm. Three batches of ITO nanopowder were obtained from Sigma Aldrich. The ITO types will be referred to as ITO #1, ITO #2, and ITO #3. Sigma Aldrich reports that all three ITO types have a size distribution less than 50 nm. Short MWNT were obtained from Cheap Tubes Incorporated. The MWNT were CCVD grown and acid purified, as well as shortened using an extrusion method. The MWNT manufacturer

reports that the MWNT have an outer diameter of 8 – 15 nm, a length of 0.5 – 2.0 μm, a purity greater than 95 wt%, and an ash content less than 1.5 wt%.

2.1.1 Transmission Electron Microscopy of ITO and MWNT

Determination of MWNT and ITO particle size distribution was performed via Transmission Electron Microscopy. Preparation of MWNT powder and ITO powders was performed by ultrasonicating dilute solutions in chloroform. Powders were carefully placed onto a perforated Carbon TEM grid. High magnification images were then obtained with a JEOL 100CX II TEM operating at 100kV at a magnification of 320,000X. TEM micrographs were analyzed to determine the average ITO particle sizes and the average lengths and diameters of the MWNT.

2.1.2 DC Resistivity of ITO and MWNT powders

Two-wire dc resistance measurements were made on bulk powders of ITO and MWNT, to determine the bulk resistivity of the powders separately and also when mixed. A custom pressing die was used to ensure that the powders were compacted enough for a true measure of the bulk resistivity.[28] The bulk powders were loaded into the custom made nylon die cylinder, with a 10 mm inner diameter, then a two-wire connection was made across the opposing stainless steel pistons. Figure 2.1a illustrates the custom pressing die used for the two-wire dc resistance test.[28] The apparatus was placed into a mechanical press and the dc resistance was measured at different compaction pressures. To prevent shorting of the two-wires by touching the pressing plates, an insulating paper sheet was placed between the piston ends and the pressing plates. The die cylinder used was nylon to prevent a two wire short through the die.

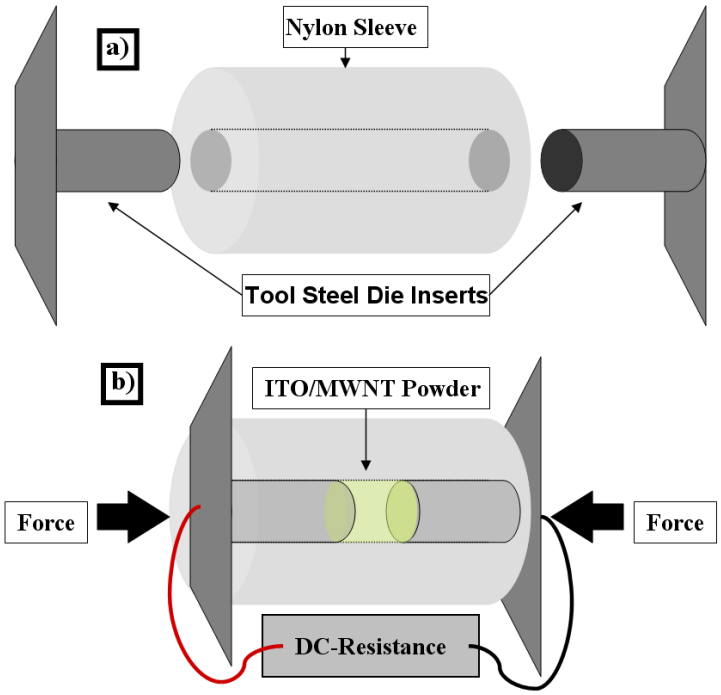

Figure 2.1. Diagram of the experimental setup for measuring bulk resistance of pressed powders, a) a nylon sleeve die and tool steel die inserts for compacting powders, b) after pressing force is set, dc resistance is measured by making electrical connection to the tool steel insert arms.[28]

Figure 2.1b shows the experimental two wire DC resistance setup for measuring the powders bulk resistance. A two-wire DC resistance measurement was taken of ITO #1 powder separately, MWNT powder separately, and a mixture of ITO #1 and MWNT. The bulk powders loaded into the die had a mass of 0.3 g for three different compositions: 100 wt% ITO, a mixture of 59 wt% ITO and 41 wt % MWNT, and 100 wt% MWNT. The resistance of the bulk powders was measured at pressures between 50-370 MPa using a Fluke 8840A multimeter. To find the conductivity of the bulk powders, the resistance of an empty cell was found first. The difference of the empty cell resistance and the measured resistance was taken as the dc resistance through the compacted

powders. The diameter of the die and the thickness of the compacted powders were used to convert the dc resistance to conductivity.

2.2 Composite Preparation

PS-composite fabrication required several steps: mixing different compositions, loading a compaction press, and compression molding at various temperatures and loads. The prescribed combination and concentration of MWNT and ITO were mixed with the PS by mechanical mixing in air. Seven composite sets were made, with variations in processing parameters of thickness, filler type, and concentrations. PS-composite sets are differentiated by filler type or types as well as the composites thickness. To avoid confusion when presenting results PS-composite sets will be referred to by a corresponding Roman numeral. The filler types, concentrations, and thicknesses of all composite sets fabricated are summarized in Table 2.1.

Prepared mixtures were weighed out, mixed and then placed into the compaction press. Composites were hot pressed into their rigid form using a Struers Prontopress-2. All composites formed a rigid disc with a constant diameter, and a variable thickness. Thickness was controlled by using either 1.5 g or 2.5 g of mixed material, the 1.5 g of mixture when pressed had a ~2 mm thickness and 2.5 g of mixture had a ~3 mm thickness. These values are approximate, as the actual thickness varied by ±0.3 mm. The mass of the mixture to be pressed varied somewhat due to the large particle size of the PS, and accounts for the measured tolerance in thickness. All composite sets were prepared by heating the press to 160 ^{o}C at a pressure of 4 MPa for 2 minutes, the pressure

was then increased to 25 MPa for 13 minutes. Following the pressing of the composite, the press cylinder was cooled to room temperature by flowing water through the chamber for 6 minutes. The pressing temperature, pressing pressure, heating time, and cooling time were all manually set using the knobs on the press. To add experimental validity to both electrical and optical characterization, at least three identical composites were made for each concentration within each set. Having multiple samples prepared provides statistical data to the experiments and allows the determination of averages and standard deviations that can account for experimental error.

Table 2.1. Summary of PS-composite sets produced that shows which filler material was used, the concentration range, and the approximate thickness of the fabricated composites.

Set	**Filler Type**	**Concentrations (phr)**	**Thickness (mm)**
I	ITO #1	0.001 - 0.6	2
II	ITO #1	0.001 - 0.6	3
III	ITO #2	0.001 - 1.0	3
IV	ITO #3	0.001 - 1.0	3
V	MWNT	0.001 - 0.13	2
VI	MWNT	0.007 - 0.07	3
VII	MWNT	0.007 - 0.07	3
VIII	ITO #1, MWNT	0.07 ITO, 0.01 - 0.1 MWNT	2
IX	ITO #1, MWNT	0.07 ITO, 0.01 - 0.1 MWNT	3
X	ITO #1, MWNT	0.007 MWNT, 0.01 - 0.4 ITO	2
XI	ITO #1, MWNT	0.007 MWNT, 0.008 - 0.4 ITO	3

PS-composite concentrations were measured in a filler material to composite material ratio called “parts per hundred resin” (phr), which is similar to weight percent.

For example 0.01 phr is equivalent to 1 mg of filler material for every 10 g of matrix material. Table 2.2 shows the conversion between phr, which means "parts per hundred resin," and vol% for all concentrations used for the different composite types. Values of density used for conversion were as follows: $\rho_{PS} = 1.0446$ g / cm^3, $\rho_{MWNT} = 1.3$ g / cm^3, and $\rho_{ITO} = 7.12$ g / cm^3.

Table 2.2. Concentration in "phr" converted to "vol %" of MWNT and ITO fillers in MWNT composites, ITO composites, and combined MWNT and ITO composites.

MWNT Composites		**ITO Composites**		**Mixed Filler Composites MWNT and ITO**			
phr	vol %	phr	vol %	phr MWNT	phr ITO	vol % MWNT	vol % ITO
0.001	0.001	0.001	0.00015	0.01	0.07	0.0080	0.0103
0.005	0.004	0.01	0.00147	0.03	0.07	0.0241	0.0103
0.007	0.006	0.04	0.00587	0.06	0.07	0.0481	0.0103
0.01	0.008	0.045	0.0066	0.1	0.07	0.0802	0.0103
0.015	0.012	0.07	0.01027	0.007	0.008	0.0056	0.0012
0.02	0.016	0.09	0.0132	0.007	0.01	0.0056	0.0015
0.03	0.024	0.11	0.01614	0.007	0.012	0.0056	0.0018
0.035	0.028	0.13	0.01907	0.007	0.05	0.0056	0.0073
0.05	0.040	0.15	0.022	0.007	0.1	0.0056	0.0293
0.07	0.056	0.2	0.02933	0.007	0.3	0.0056	0.0440
0.1	0.080	0.31	0.04546	0.007	0.4	0.0056	0.0586
0.13	0.104	0.6	0.08795	-	-	-	-
-	-	1	0.1465	-	-	-	-

A separate set of PS-composites was made to compare the difference between a composite with an ordered grain structure and a composite with a disordered grain structure. PS particles have a cylindrical shape, which allowed particles to be oriented preferentially before pressing to create an ordered composite, particles were oriented either parallel or perpendicular to the pressing surface. Composites with a parallel

orientation were made by orienting the length direction of PS particles parallel to the surface of the pressing ram. Composites with a perpendicular orientation were made by orienting the axis of the PS particle perpendicular to the plane of the pressing surface.

A perpendicular orientation has the axis of the beads cylinder oriented perpendicular to the plane of the pressing surface. A total of four PS-composites were made for comparing the effect of aligned grains versus disordered grains. PS-composites with ordered and disordered structures had a fixed MWNT concentration of 0.015 phr for better comparison.

2.3 Impedance Spectroscopy Characterization

Impedance spectroscopy was used to measure the electrical properties of the PS-composites. The impedance equipment used was a Solartron SI 1260 interfaced with a Solartron 1296 Dielectric Interface. Initial measurements were made in the frequency range of 10^{-1} to 10^{7} Hz with an ac voltage of 0.1 V. All composite sets were measured 1 – 3 days after fabrication.

Preparation of samples for impedance measurements required applying high purity silver paint (SPI Supplies) to both sides of the PS-composite. Silver electrodes ensure that a true bulk conductivity measurement is made, as well as providing consistent electrical contact. Solvents in the paint were allowed to dry for one day. Flat aluminum electrodes were positioned on each side of the silvered composite and clamped to ensure constant contact. Impedance data resulted in a semicircle in the impedance plane, as similarly shown in Figure 1.17. In some cases the semicircles were incomplete and in

others, there were two consecutive semicircles. DC resistance of a composite with a complete semicircle was taken from the intercept of the imaginary impedance (Z'') on the real impedance (Z') axis.[137] Composites with an incomplete semicircle, which have a strong insulating behavior, were fitted to a least squares model to complete the semicircle. The modeled semicircle is used to find the intercept of Z'' to the Z' axis, to determine the dc resistance. The dc resistance was converted to resistivity using Equation 1.[95]

$$\rho = A \cdot R_{dc} / t \qquad \text{Equation 1.}$$

In Equation 1 the area of the composite electrode surface is A, the thickness of the composite is *t*, and the dc resistance obtained from the impedance plot is R_{dc}.[95]

Impedance measurements on composites were performed initially a few days after fabrication. Additional impedance measurements were carried out again after 6 – 11 months for PS/ITO (sets I, II), PS/MWNT (sets V, VI), and PS/ITO/MWNT (sets I, II, V, VI, and VIII – XI) composites. A newer composite set VII (containing MWNT) had impedance measurements carried out every two to three weeks to detect changes in impedance over shorter periods of time. The effect of the amplitude of the ac voltage was also studied. AC voltage effects were characterized by varying the ac voltage during measurement. The effect of a varying dc bias on the second impedance semicircle was also studied. For ac voltage effect experiments, impedance was measured using ac amplitudes of 0.1V and 1V, dc bias amplitudes of 0.1 V, 0.5 V, and 1V, and a frequency range of 10^{-1} to 10^{8} Hz.

2.4 Optical Characterization

Optical transmittance through the PS-composite was measured using a Beckman DU-640 spectrophotometer with a spot size of 2 mm^2 at a scan speed of 1200 nm/min between 200 nm and 1000 nm. Air was taken as the reference for the spectrophotometer. Prior to the measurement, excess filler material from the surface of the composite was removed. The composite was polished to ensure that the optical properties being characterized were representative of the composites microstructure and not the rough surface of the composite. Grinding the surface of the composite with abrasive 800 grit paper was performed to remove excess filler. Polishing was done with abrasive paper with grit sizes of 1200, 2400, and finally a 1 μm alumina slurry polish on a polishing pad. Transmittance was measured perpendicular to the flat side of the composite or through the thickness of the composite.

2.5 Microscopy Experiments

Optical micrographs of PS-composites were acquired in order to characterize the composites microstructure. Some images were taken with no magnification with a digital camera. Optical microscopy investigation of the composites surface and fracture surface were taken at magnifications of 10 x. Optical micrographs were acquired with a XSB 411 microscope. Composites were fractured through the thickness by hand. Fracture surface micrographs were inspected to determine the fracture behavior of the composite and properties of its microstructure. Additional optical Keyence micrographs with high depth resolution were taken with a Keyence VHX-600 digital microscope.

CHAPTER 3

RESULTS

This chapter presents the results of the experiments described in Chapter 2. The characterization of filler materials is reported first, followed by the results of characterization of the composite materials. Specifically, the ITO and MWNT particle sizes are reported, along with the bulk powder resistivities. PS-composite properties are reported in sections corresponding to filler type. The time-dependent and voltage-dependent impedance behavior of composites is also reported. Optical and Keyence micrographs are presented illustrating the microstructure of the composites. Fracture surface micrographs are presented with a description of the composite's resulting fracture behavior.

3.1 Properties of ITO and MWNT Filler Materials

Filler material particle size and bulk resistivity are reported in this section. Characterization shows differences in properties and structure between the filler types. Figure 3.1 shows high magnification TEM images of ITO nanoparticles; from different batches: ITO #1, #2, and #3. Transmission electron micrographs determine that the size of ITO nanoparticles varies between ITO filler type. Inspection of the TEM micrographs in Figures 3.1a, 3.1b, and 3.1c of different ITO nanoparticles, shows that there is a bimodal distribution of crystalline ITO particles. The particles for ITO #1 (Figure 3.1a) are either spherical with a size of 10 – 20 nm or flat edge crystals with a size of 50 – 100

nm. The particles for ITO #2 (Figure 3.1b) are either spherical with a size of 5 - 25 nm or flat edge crystals with a size of 40 – 100 nm. The particles for ITO #3 (Figure 3.1c) are either spherical with a size of 4 – 20 nm or flat edge crystals with a size of 40 – 100 nm.

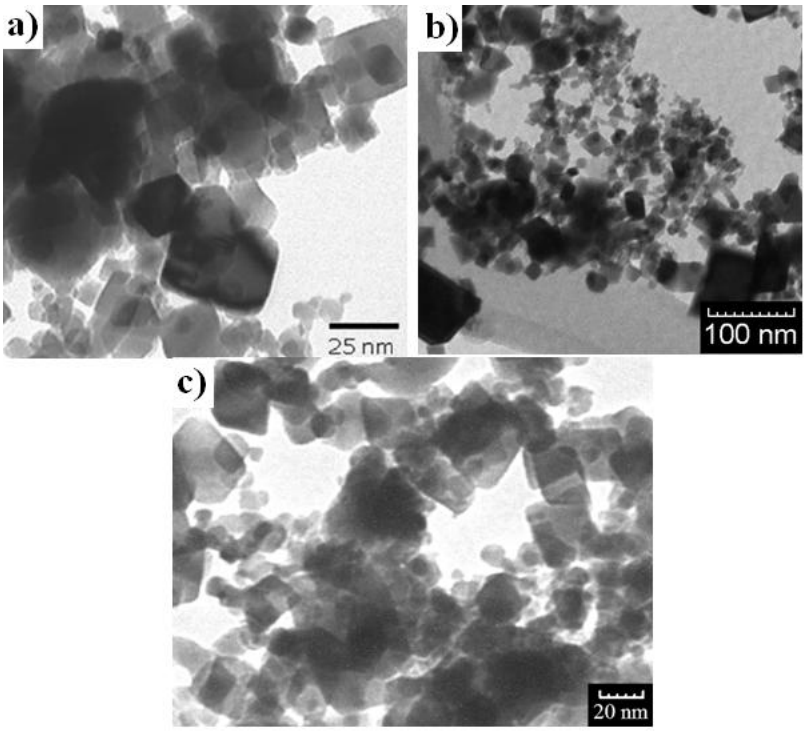

Figure 3.1. TEM micrographs of different ITO nanoparticle fillers, a) ITO #1, b) ITO #2, and c) ITO #3.[28]

Figure 3.2 is a TEM micrograph of dispersed MWNT filler material. The MWNT micrograph shows the outer diameter of the MWNT filler ranges from 8 – 15 nm and a length ranging from 0.5 – 2.0 μm. The MWNT TEM micrograph shows that the MWNT are purified (no inclusions are apparent).

Figure 3.2. TEM micrograph of MWNT filler.[140]

Bulk resistivity values for ITO and MWNT, both pure and mixed, vary with weight percent and compaction pressure. Compacted powders form a brittle disk compact. The resistivity versus MWNT weight percent curve for the mixed ITO/MWNT powders (ITO #1) is reported in Figure 3.3, where the separate curves represent the pressing load. Increasing compaction pressure results in a decrease in the resistivity of the powders. Increases in compaction pressure decrease the 100 wt % ITO/ 0 wt % MWNT mixture's resistivity value by a larger factor (compared to the pressure induced change in resistivity for the mixtures containing MWNT which show essentially no dependence on pressure).

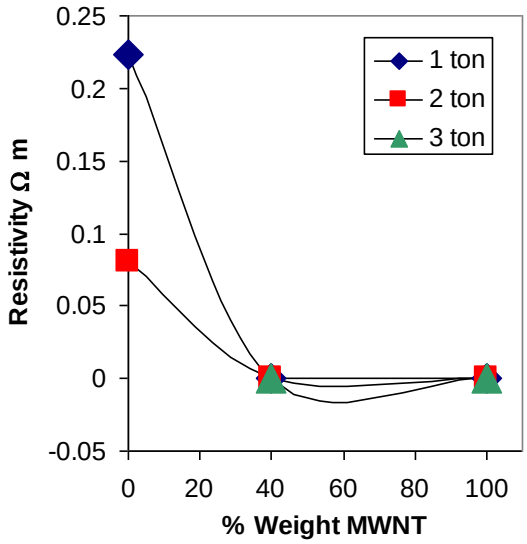

Figure 3.3. Graph of resistivity for ITO/MWNT powder mixtures plotted versus wt. % MWNT, at pressing forces of 1, 2, and 3 tons.

3.2 PS Composites Filled with ITO

ITO and PS composites are optically transparent and electrically conducting. An example of a PS composite filled with ITO is shown in Figure 3.4, where the composite is transparent. In Figure 3.4, an image of a 0.11 phr ITO composite (set I) shows the phase segregation of the filler in the composite, the ITO filler resembles wires or curved lines that surround the PS grains.

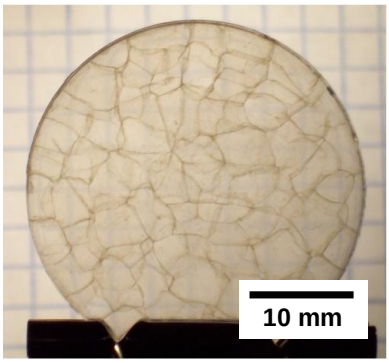

Figure 3.4. Image of a phase segregated PS 0.11 phr ITO composite (set I, ~2 mm).

3.2.1 Impedance Results

PS-composites filled with ITO are conducting after fabrication. Figure 3.5 shows the normalized Nyquist plots ($-\rho''$ vs. ρ') for PS/ITO composites (set II) with ITO #1 filler. The impedance response shows a semicircle in the graph's first quadrant when plotted in a Nyquist plot. The Nyquist plots in Figure 3.5a, b, and c show that the real and imaginary impedance decrease with increases in ITO concentration. Similar results are obtained for ITO composite sets (I - IV) with ITO #1, 2, and 3, and ~ 2 mm and ~ 3 mm thickness, where a decreasing semicircle size occurs for increases in ITO concentration.

Certain PS/ITO composite samples have a tail in the low frequency region of the impedance semicircle, seen in Figure 3.5b and 3.5c. At low frequencies, insulating composite samples have noise or unexpected fluctuations in the impedance data measured, shown in Figure 3.5a.

The average resistivity for 3mm ITO composites with ITO #1, #2, and #3 are compared in Figure 3.6. The percolation threshold is shown to vary with the different ITO filler types. Percolation for ITO #1 occurs at 0.15 phr or 0.022 vol%, for ITO #2 the percolation threshold is 0.25 phr or 0.036 vol%, and ITO #3 has a percolation threshold at 0.3 phr or 0.044 vol%. Minimum resistivity values for ~3 mm ITO composites (sets II, III, and IV) are 1.5×10^4 Ω m for ITO #1, 1.2×10^5 Ω m for ITO #2, and 1.1×10^3 Ω m for ITO #3.

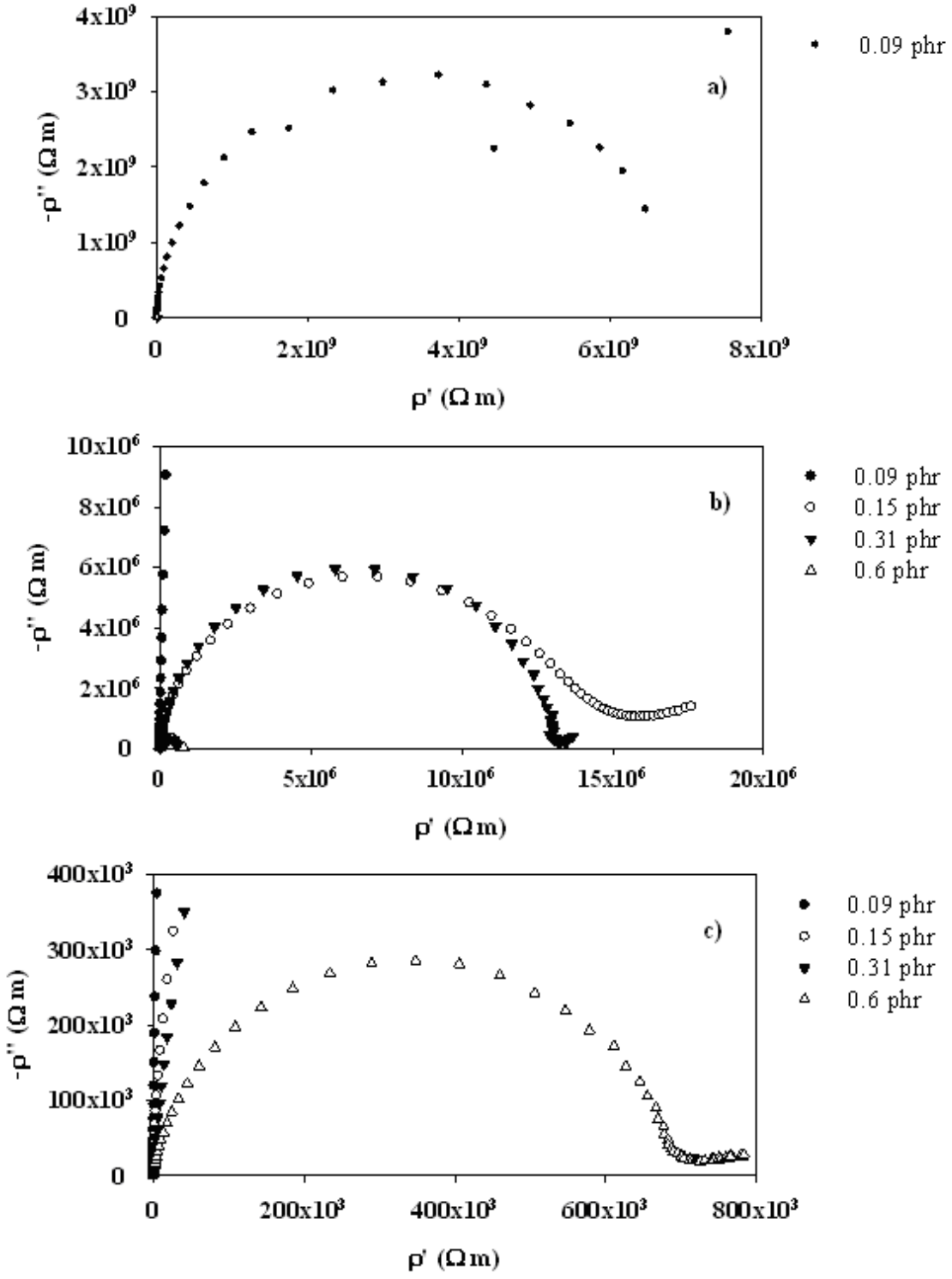

Figure 3.5. Nyquist plots for various concentration of ~3 mm thick ITO/PS composites from set II. Parts (a), (b), and (c) show the $-\rho''$ vs. ρ' of the same composites at different magnifications.

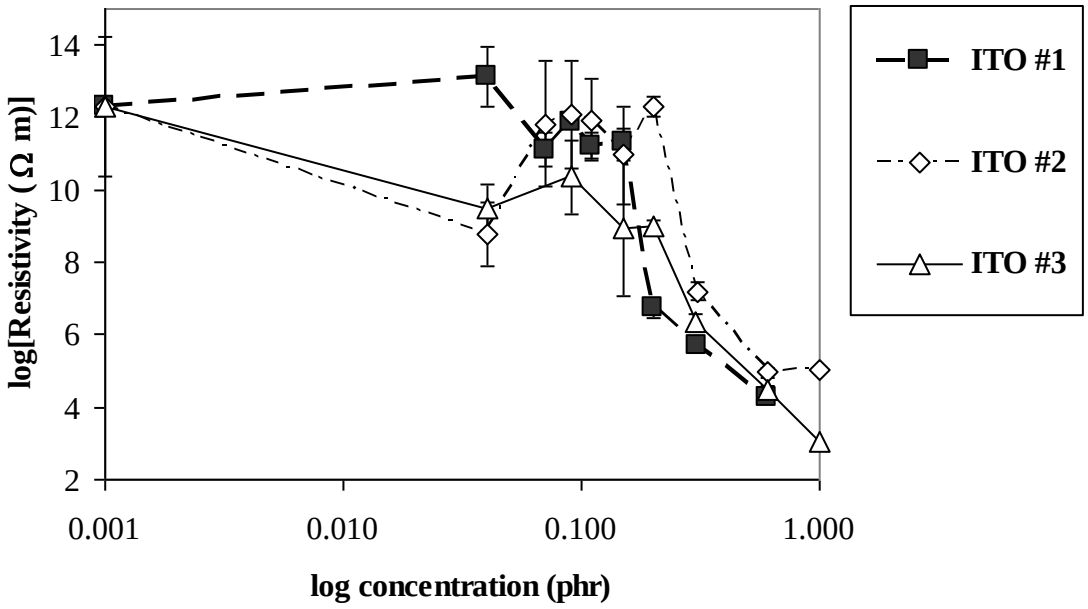

Figure 3.6. Average log resistivity versus concentration for ~3 mm thick ITO composites in (a) set I, ITO filler #1, (b) set II, ITO filler #2, and (c) set III, ITO filler #3.

ITO composite resistivity at high concentrations varies by ITO type. The Nyquist plots of real and imaginary resistivity for three 0.6 phr ITO PS-composites (sets II, III, and IV), with ITO #1, ITO #2, and ITO #3, are shown in Figure 3.7. The dc resistivity of 0.6 phr ITO PS-composites, determined from impedance measurements, of different ITO types varies. The impedance response determined that the 0.6 phr ITO PS-composites with ITO #3 have a lower minimum resistivity (2.1×10^4 Ω m), than the composite made with ITO #1 (3.15×10^4 Ω m). The 0.6 phr ITO composite with ITO #2 has the relatively highest minimum resistivity (2.5×10^5 Ω m).

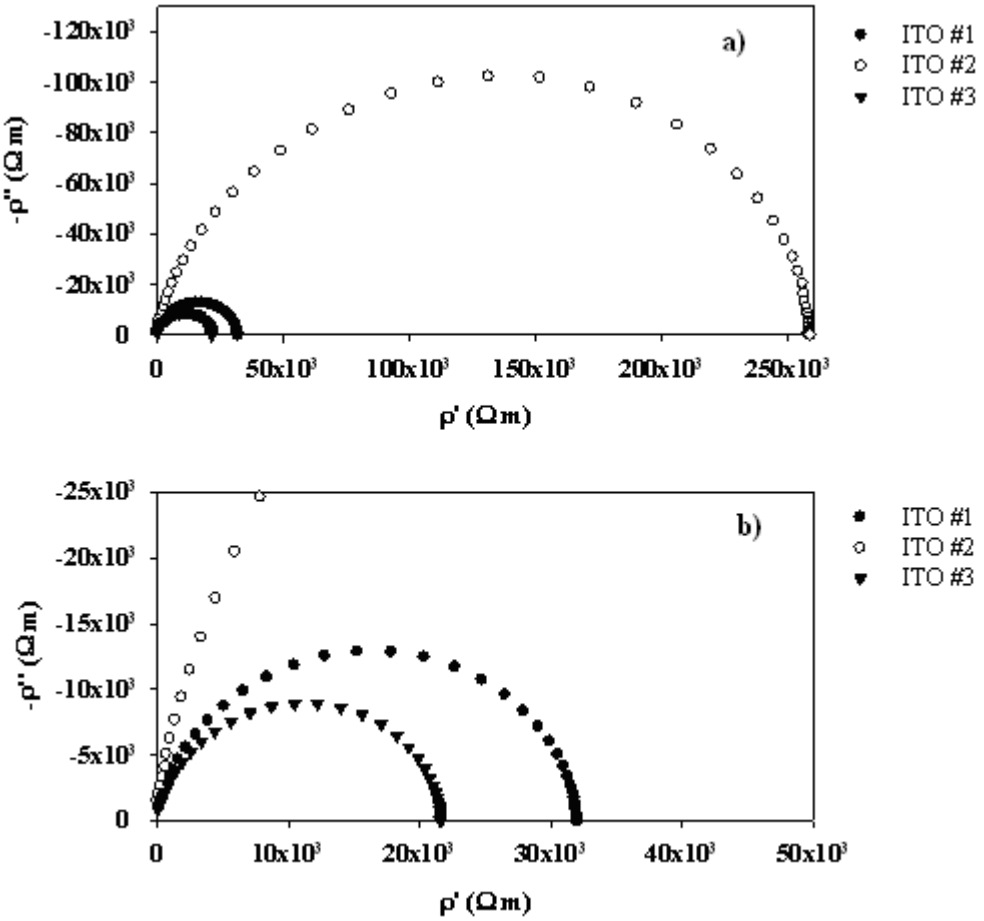

Figure 3.7. Nyquist plots for ~3 mm thick 0.6 phr ITO PS-composites (set II, III, and IV) with ITO #1, ITO #2, and ITO #3 respectively. Bottom figure (part (b)) is a magnified image of figure part (a) on top.

The log of average resistivity versus the log of concentration for ~ 2 mm thick ITO/PS composites (set I) is shown in Figure 3.8. Error bars show the standard deviation from averaging measurements from at least three different composites at each composition. The percolation threshold for ITO composites set I was found to be 0.15 phr or 0.022 vol % ITO. The standard deviation of the average resistivity is larger in magnitude at concentrations below 0.2 phr. The average resistivity of a composite fluctuates between consecutive composite concentrations, for composite concentrations below the percolation threshold. For composites with concentrations above the

percolation threshold, the average resistivity reaches an approximately constant minimum value of 3.7 x 10^7 Ω m, which is about six orders of magnitude smaller than the resistivity of pure PS. The thickness of the sample also affects the resistivity of the composites with the same ITO type (ITO #1).

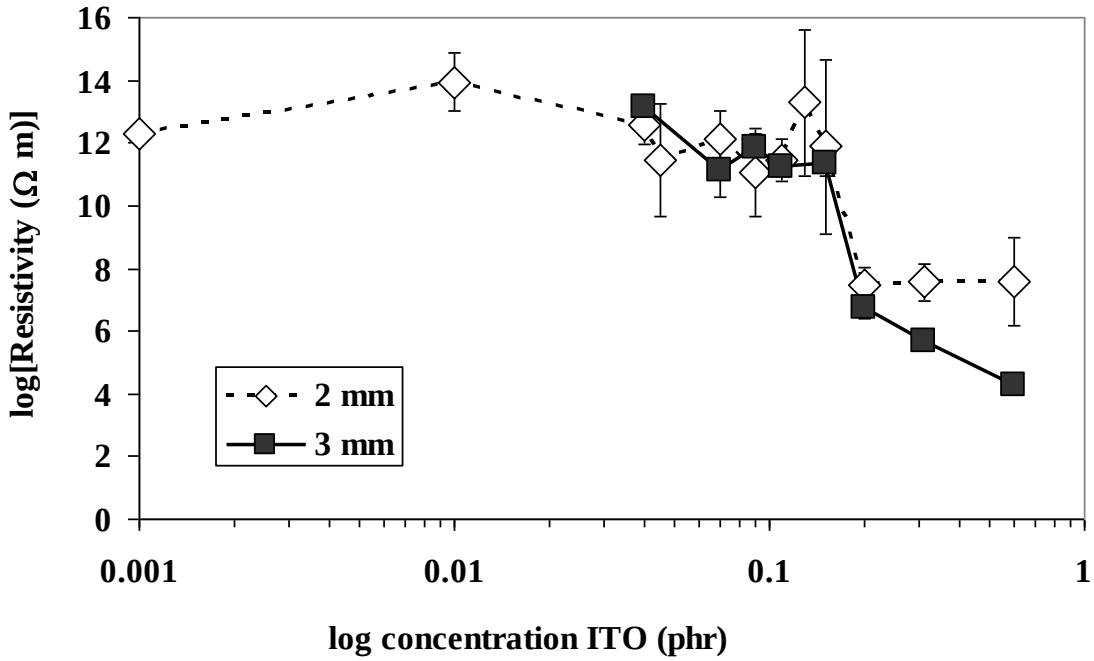

Figure 3.8. Average log resistivity versus concentration for 2mm and 3mm ITO composites filled with ITO #1.

3.2.2 Optical Properties

Composites filled with ITO remain transparent in the visible range after pressing as shown in Figure 3.4. The ITO filler type has an effect on the optical properties of the composites as well. ITO filler type changes the appearance of composites with the same composition, Figure 3.9 is a side by side comparison of composites with equal concentration and different ITO type.

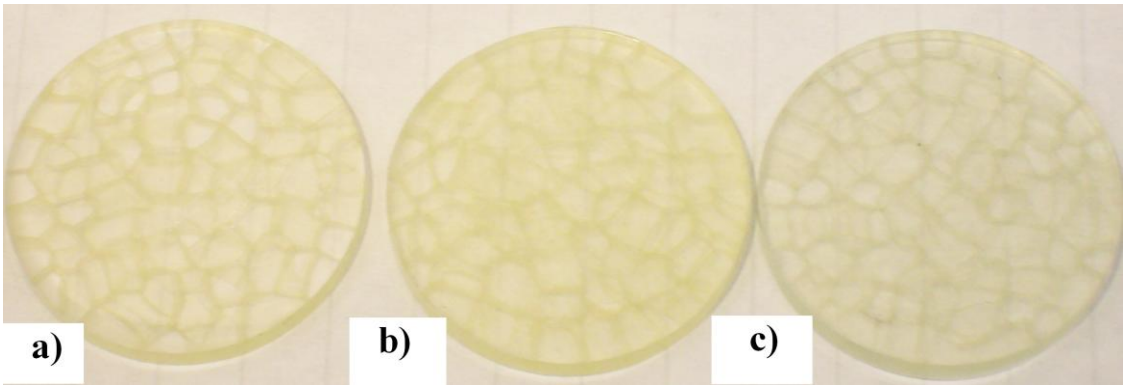

Figure 3.9. Images of 0.3 phr ITO composites sets II, III, and IV.

ITO composites also show a change in the degree of transparency with variation of ITO concentration. Figure 3.10 shows plots of percent transmission of light versus wavelength for ITO composites (set II) containing ITO #1 as a function of ITO concentration. It is clear that as the ITO concentration increases, the percent transmittance decreases. Figure 3.11 shows the percent transmission of light versus concentration at a 600 nm wavelength for ITO composites in set II. Increases in ITO concentration result in a decrease in percent transmission of light through the composite at a given wavelength.

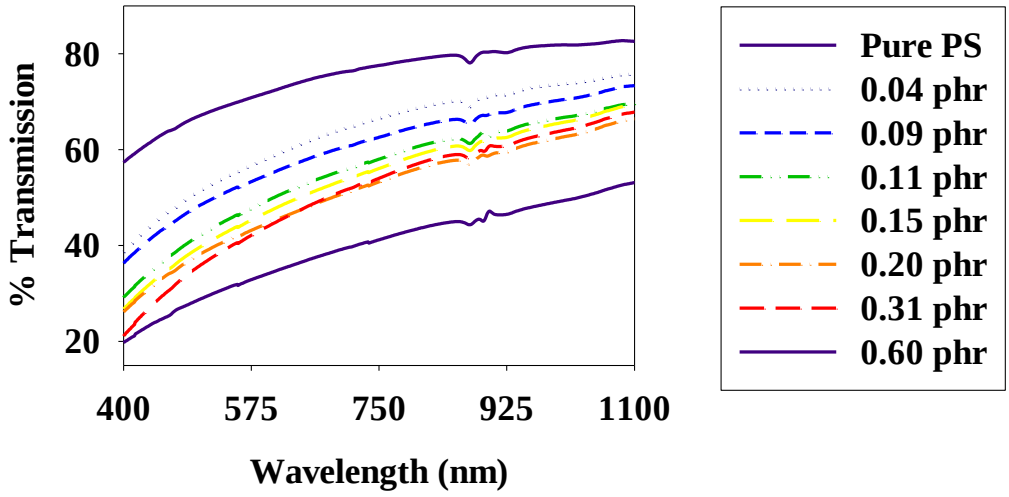

Figure 3.10. Percent transmission versus wavelength for ITO/PS composites (set II, ITO #1) with various ITO concentrations.

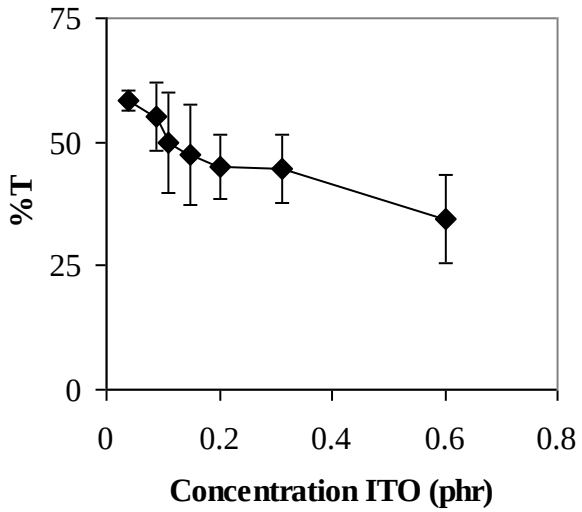

Figure 3.11. Plot of averaged percent transmission versus concentration for ITO/PS composites (set II, ITO #1) at a 600 nm wavelength.

3.3 PS Composites Filled with MWNT

This section presents data from electrical and optical characterization of MWNT filled PS composites. Composites filled with MWNT are electrically conducting and transparent. However, these properties also vary with composition and thickness of the composite. Nyquist plots of varying MWNT concentration are shown. The average resistivity and corresponding percolation threshold is determined for the various composite sets. Optical properties are determined from the data from spectrophotometry characterization.

3.3.1 Impedance Results

Electrical properties of PS composites filled with MWNT (sets V – VII) are presented in this section. Impedance spectroscopy Nyquist plots of MWNT/PS composites indicate that composites have a resistance and capacitance behavior similar to what was observed for ITO/PS composites. Insulating composites have an impedance

response that is approximately equivalent to only a capacitor. Nyquist plots for composite set V with various concentrations are shown in Figure 3.12. The impedance semicircle in the complex impedance plane diminishes in magnitude with increases in concentration of MWNT.

Figure 3.13 shows the average resistivity data for MWNT composite sets V and VI, where set V has a 2 mm thickness and set VI has a 3 mm thickness. The percolation threshold for both composite sets is 0.01 phr or 0.07 vol%. The resistivity of ~2 mm thick MWNT composites (set V) in Figure 3.13 decreases in magnitude from $10^{12 \pm 1.15}$ to $10^{3 \pm 0.2}$ Ω m as MWNT concentration increases. The resistivity of ~3 mm thick MWNT composites (set VI) in Figure 3.13 has a maximum of 10^{8} Ω m and a minimum of 10^{3} Ω m. It is clear that the thickness of the composite affects the composition below the percolation threshold more strongly than those above the percolation threshold.

MWNT/PS composites with an ordered segregated structure showed differences in electrical response from disordered structures. These composites all contain the same concentration of 0.015 phr MWNT. Composites with ordered structures have PS pellets oriented either perpendicular or parallel to the composite's surface. Composites with disordered structures have PS pellets randomly oriented with respect to the pressing direction. PS grains ordered parallel to the pressing direction have a structure as shown in Figure 3.14a. The area of MWNT percolation networks contacting the composite's surface is higher for ordered composites compared to disordered composites. A composite with grains oriented perpendicular to the surface is shown in Figure 3.14c. Composites with an equivalent number of PS grains to the ordered composites are shown in Figures 3.14b and 3.14d.

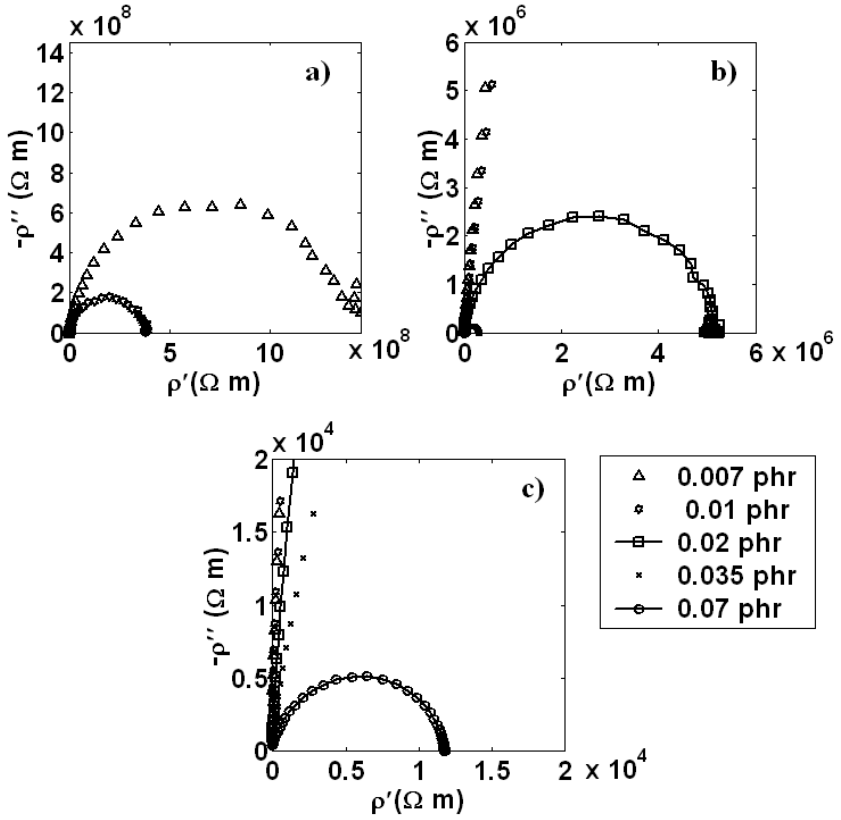

Figure 3.12. Nyquist plots for MWNT/PS composite set V with ~2 mm thickness, with plots for various concentrations at three different magnifications.

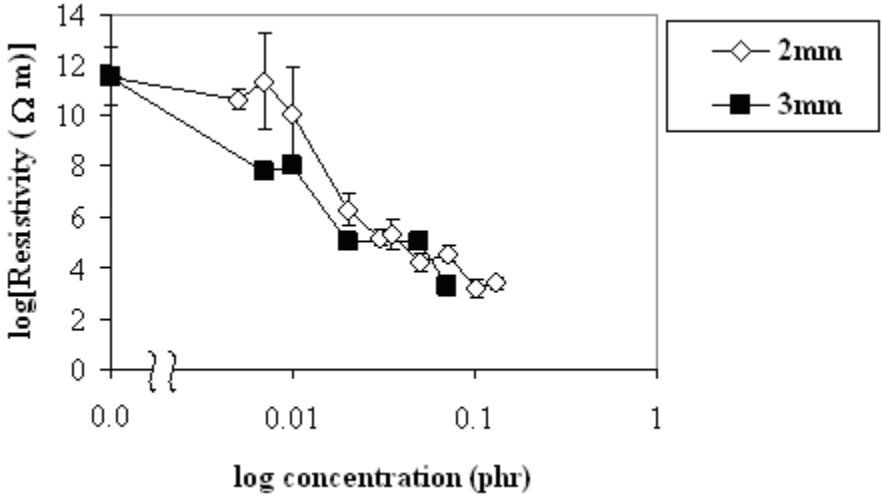

Figure 3.13. MWNT/PS composite average resistivity versus MWNT concentration for composite sets V with a thickness of 2 mm and VI with a thickness of 3 mm.

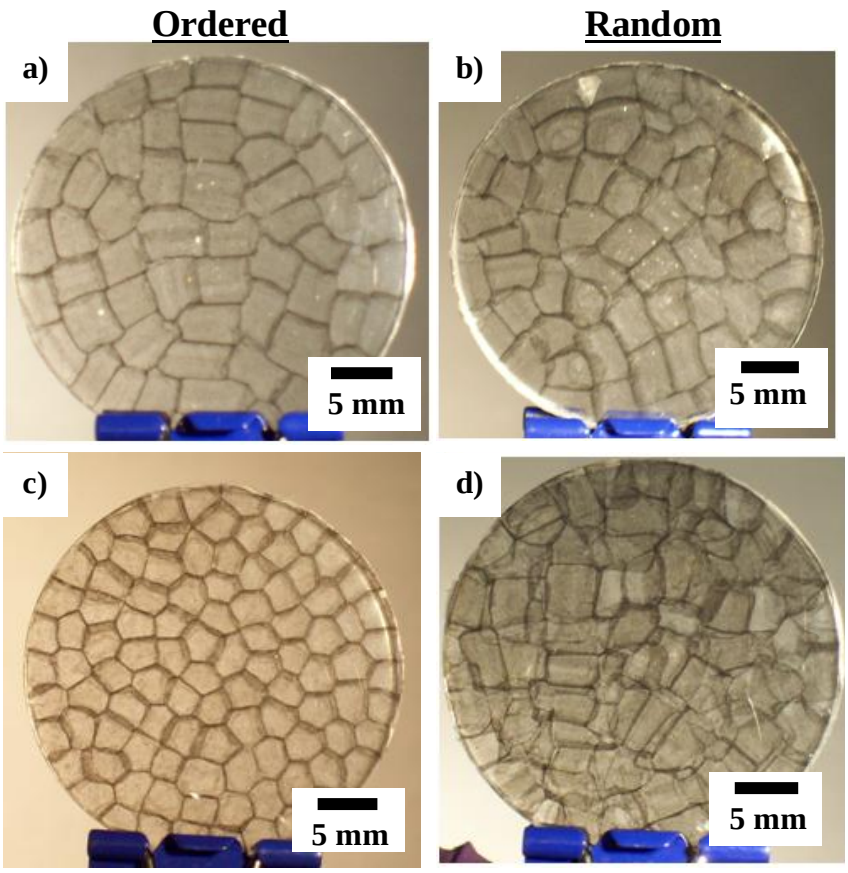

Figure 3.14. Images of ordered (a, c) and random (b, d) MWNT network structures in samples containing the same amount of MWNT, 0.015 phr (a) 57 grains with beads parallel to pressing surface (1.5 mm thickness), (b) 57 grains with random orientation (1.55 mm thickness), (c) 99 grains with perpendicular orientation to pressing surface (2.93 mm thickness), (d) 99 grains with random orientation (2.89 mm thickness).

Composites with ordered grains have a lower resistivity than composites with disordered grains. Figure 3.15 shows the impedance response of a composite ordered parallel with respect to the thickness and the impedance response of an equivalent disordered composite. Figure 3.16 shows the difference in impedance of a composite ordered perpendicular with respect to the thickness and an equivalent disordered composite. In both Figure 3.15 and Figure 3.16 ordered composites have a lower dc resistance than disordered composites.

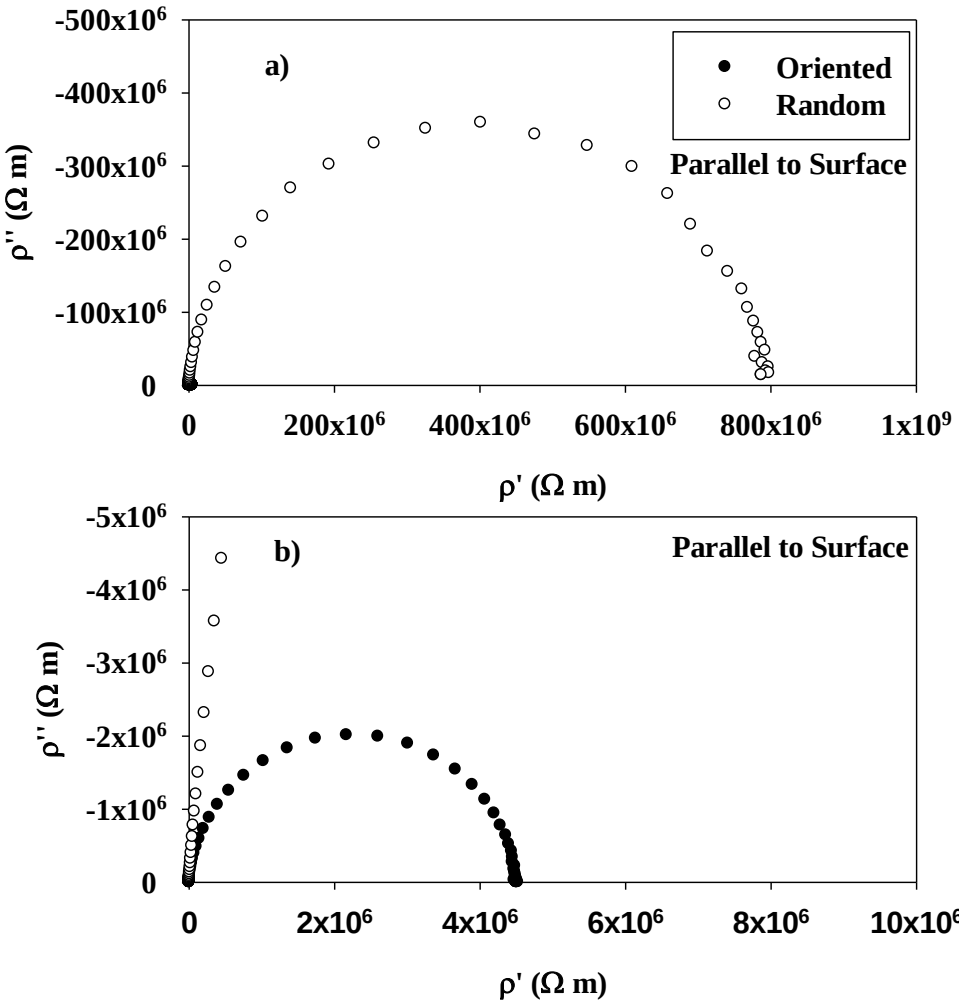

Figure 3.15. Nyquist plots for parallel ordered and equivalent disordered MWNT/PS composites with 57 PS grains whose microstructures were shown in Figure 3.14 a and b: (a) larger scale showing impedance for the disordered composite, (b) smaller scale showing impedance for the ordered composite.

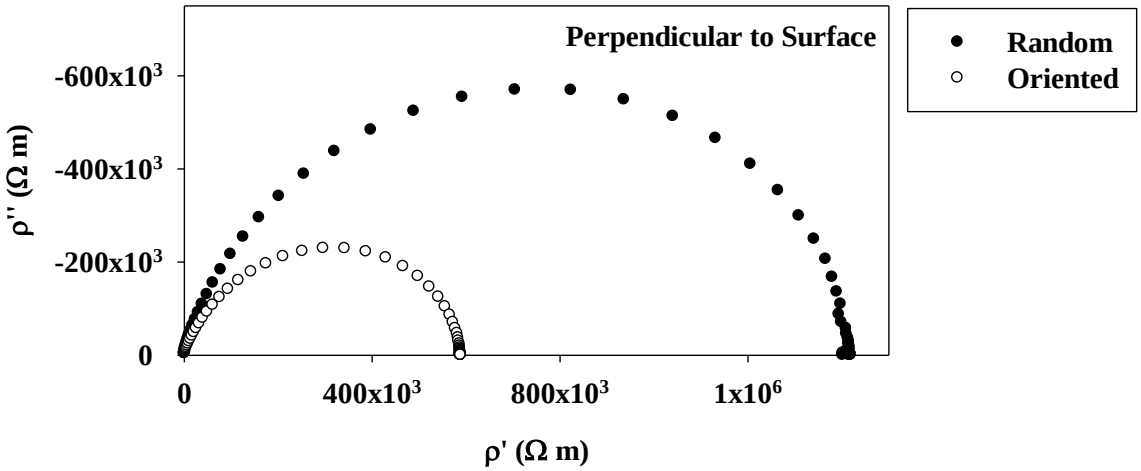

Figure 3.16. Nyquist plots for perpendicular ordered and for an equivalent disordered MWNT composites with 99 PS grains. Microstructures were shown in Figure 3.14 c and d respectively.

3.3.2 Optical Properties

Composites filled with MWNT are transparent and percent transmission of light decreases as filler material concentration increases. Figure 3.17 depicts micrographs illustrating grain boundaries with equal composition showing the various junctions composites make and how the nanotubes agglomerates form at the boundaries.

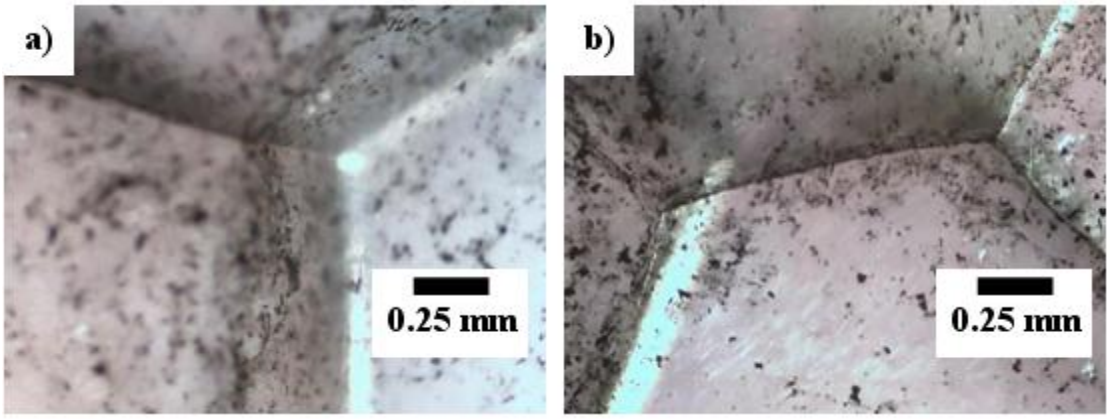

Figure 3.17. Transmission optical micrographs of MWNT/PS composites containing a 0.015 phr concentration of MWNT that were ordered perpendicular to the composites' surface.

Figure 3.18 displays the optical spectrophotometry data showing percent transmission of light over changes in wavelength. Increasing the MWNT concentration in the composite causes the percent transmission to decrease as expected.

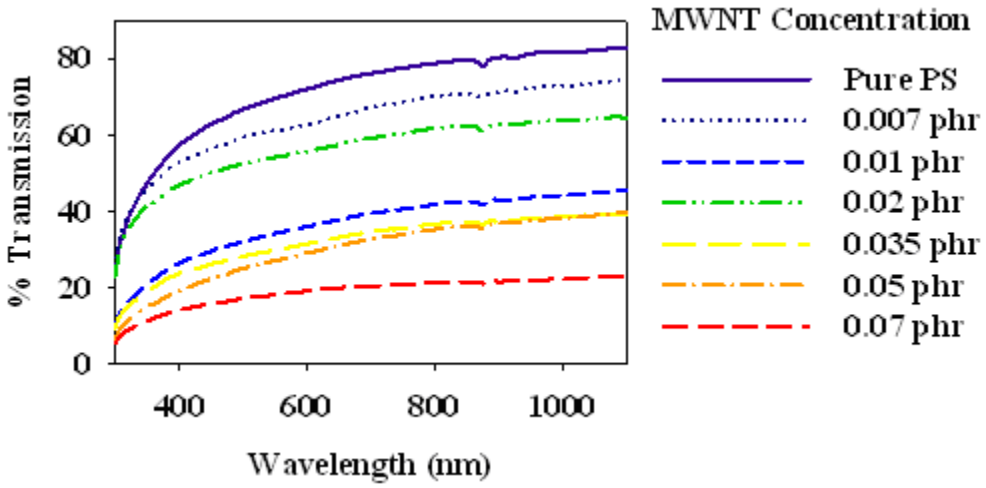

Figure 3.18. Percent transmission versus wavelength for 3mm MWNT/PS composite set VI, plots are shown as a function of MWNT concentration.

Figure 3.19 shows the percent transmission data at a wavelength of 600 nm. The trend of diminishing percent transmission with increasing MWNT concentration is shown in Figure 3.19. It is interesting that the 0.02 phr MWNT composite has a higher percent transmission than the 0.01 phr MWNT composite.

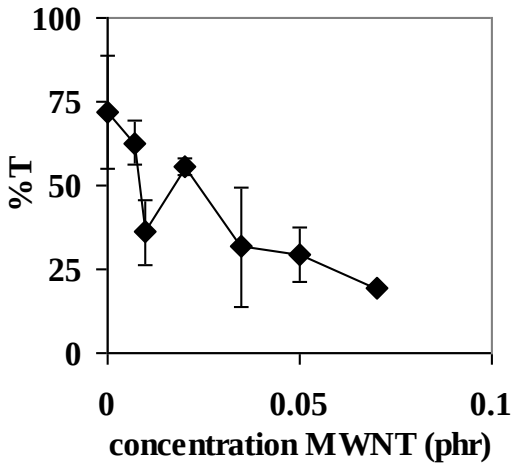

Figure 3.19. Average percent transmission versus concentration at a wavelength of 600 nm for a 3mm thick MWNT/PS composite.

3.4 PS Composites Filled with ITO and MWNT

The electrical and optical properties of PS composites with combined ITO and MWNT fillers are reported in this section. The combination of filler materials results in electrical and optical properties similar to those obtained for the ITO/PS composites and MWNT/PS composites separately. PS composites containing mixed ITO/MWNT are electrically conducting and transparent; these properties vary with composition and composite thickness. Spectrophotometry data for mixed ITO/MWNT/PS composites suggests that there are trends in percent transmission due to composition changes.

3.4.1 Impedance Results

Electrical properties of mixed ITO/MWNT PS-composites (sets VIII – XI) as determined by impedance spectroscopy are presented in this section. Figure 3.20 depicts the Nyquist plot for mixed ITO/MWNT PS-composite (~3 mm) set XI with a constant 0.007 phr concentration of MWNT. The impedance response is equivalent to a RC parallel circuit. Samples containing low concentrations of ITO have semicircles that are

incomplete. Composites with an incomplete semicircle are more insulating. Figure 3.20 indicates that the size of the impedance semicircle decreases with increasing ITO concentration. An impedance decrease associated with increasing ITO concentration is also seen in ~2 mm mixed ITO/MWNT PS-composites (set X, constant 0.007 phr MWNT), this data is not shown. Both ~2 mm and ~3 mm mixed ITO/MWNT PS-composites (set VIII and IX respectively) with a constant concentration of 0.07 phr ITO, where the MWNT concentration is varied, also have a similar impedance response compared to mixed ITO/MWNT PS-composites with a constant concentration of 0.007 phr MWNT, as shown in Figure 3.20.

The log of average resistivity as it relates to the log of concentration of mixed fillers for ~2 mm and ~3 mm mixed ITO/MWNT PS-composite (sets VIII and IX respectively) with a constant concentration of 0.07 phr ITO, are shown in Figure 3.21. The average resistivity for 3 mm composites (set IX) is smaller in value compared to 2 mm thick composites (set VIII), which was determined from Figure 3.21. There is no definable percolation threshold for the measured composition range. Increasing the concentration of MWNT reduces the average resistivity of mixed ITO/MWNT composite sets VIII and IX (~ 2 mm and ~ 3 mm respectively) with a constant concentration of 0.07 phr ITO.

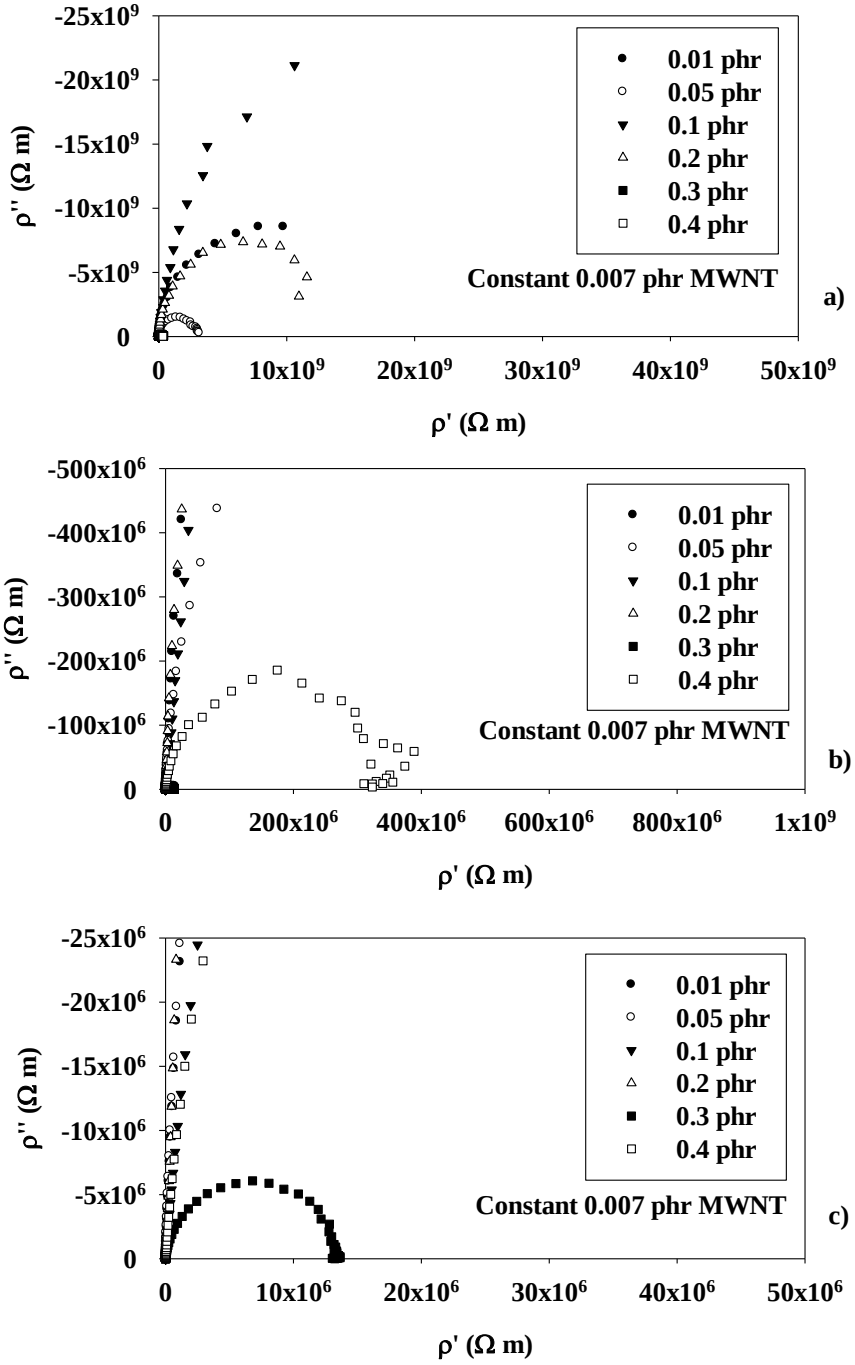

Figure 3.20. Nyquist plots for ~3 mm mixed ITO/MWNT PS-composite set XI where MWNT concentration is held constant at 0.007 phr, and ITO content is varied as shown in the legend. Notice the scale change from plots (a) through (c).

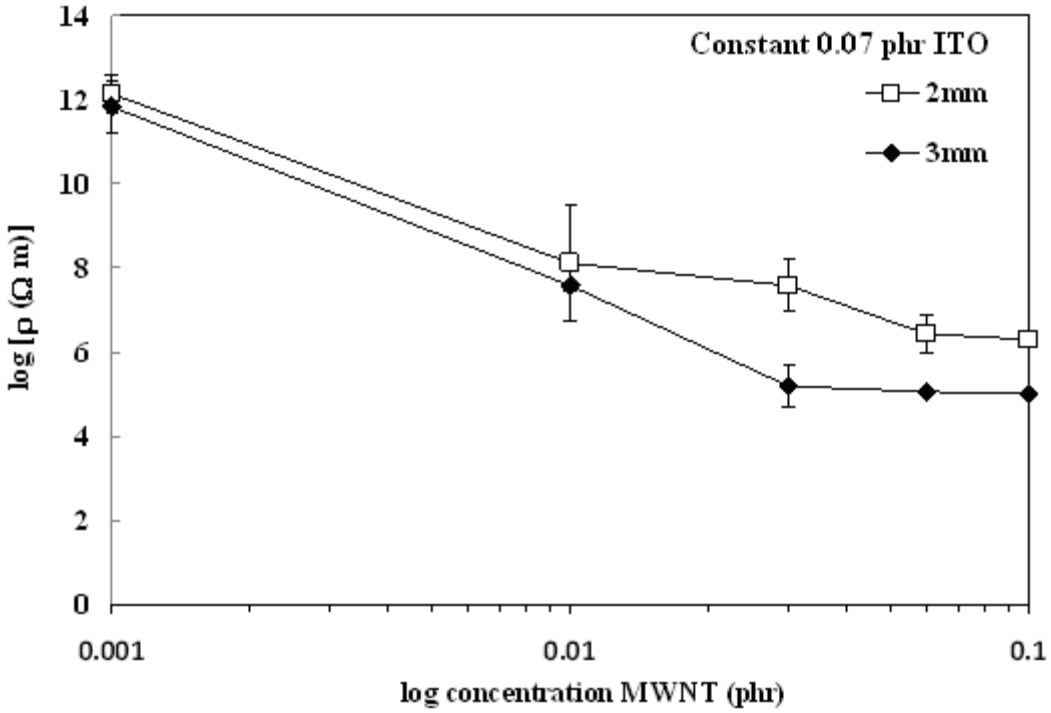

Figure 3.21. Plots of log resistivity versus log MWNT concentration, for ~2 mm and ~3 mm mixed ITO/MWNT PS-composites with a constant concentration of 0.07 phr ITO (sets VIII and IX respectively).

Figure 3.22 plots the log of average resistivity versus the log of concentration of ~2 mm and ~3 mm mixed ITO/MWNT PS-composites with a constant concentration of 0.07 phr ITO (sets VIII and XI respectively). Varying the concentration of ITO while keeping the concentration of MWNT constant at 0.007 phr, in mixed ITO/MWNT PS-composites (sets X and XI, ~ 2 mm and ~ 3 mm respectively), changes the average resistivity, but not in a definable trend. Composite thickness changes the average resistivity of mixed ITO/MWNT PS-composites with a constant concentration of 0.007 phr MWNT (sets X and XI, ~ 2 mm and ~ 3 mm respectively). Specifically, the resistivity of ~2 mm PS-composites is higher than that of PS-composites with a ~3 mm thickness. It is noteworthy that the composites in set XI (~3 mm, constant 0.007 phr MWNT) with a 0.01 phr ITO concentration have a lower average resistivity value

compared to composites containing 0.008 phr ITO and 0.012 phr ITO. Error bars are as shown.

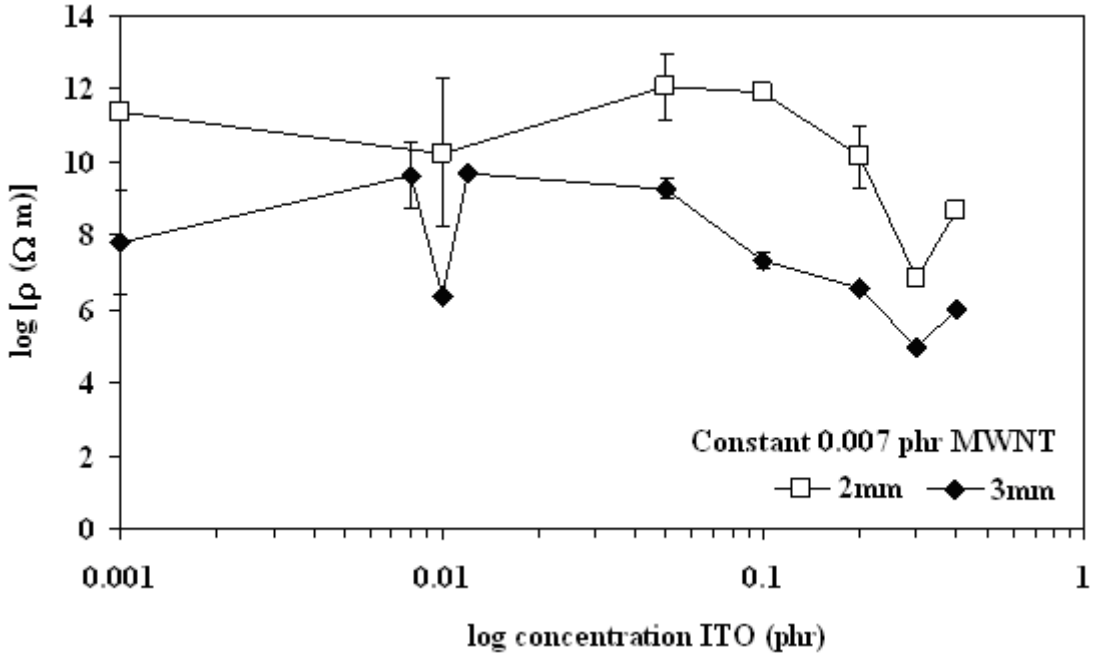

Figure 3.22. Plots of log resistivity versus log ITO concentration, for ~2 mm and ~3 mm mixed ITO/MWNT PS-composites with a constant concentration of 0.007 phr MWNT (sets X and XI respectively).

3.4.2 Optical Properties

Figure 3.23 displays the optical spectrophotometer data plotted as percent transmission of light over a wavelength range for ~2 mm mixed ITO/MWNT PS/composite with a constant concentration of 0.07 phr ITO (set VIII). Increasing the concentration of MWNT, the composite shows no obvious trend in the percent transmission of the composites. Figure 3.24 plots the percent transmission of light over a wavelength range for composite set X (~2 mm) with a constant concentration of 0.007 phr MWNT.

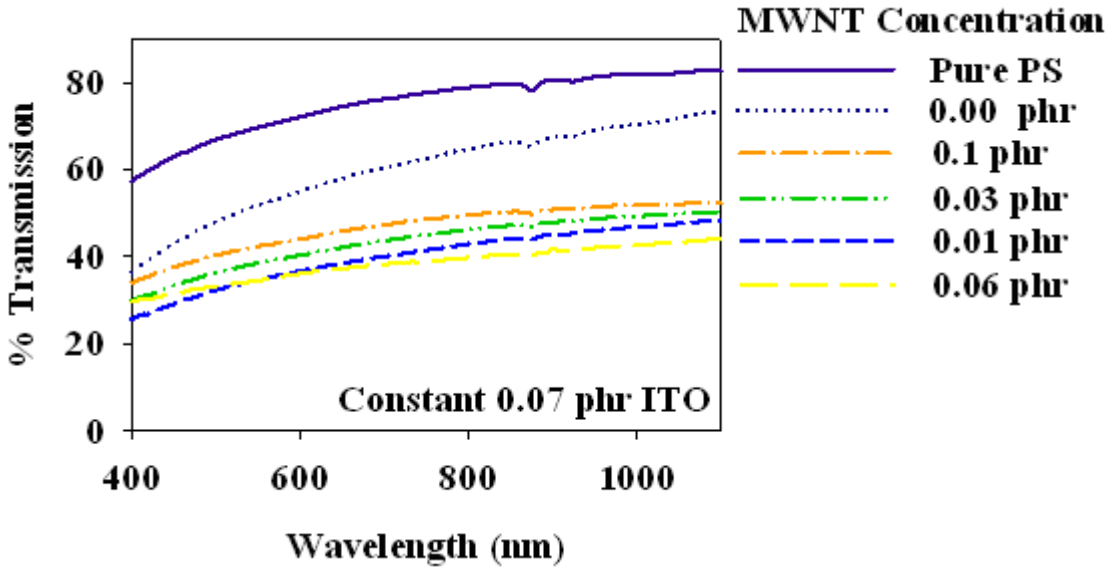

Figure 3.23. Graph of percent transmission versus wavelength for mixed ITO/MWNT PS-composite set VIII (~2 mm, constant 0.07 phr ITO) as a function of MWNT concentration.

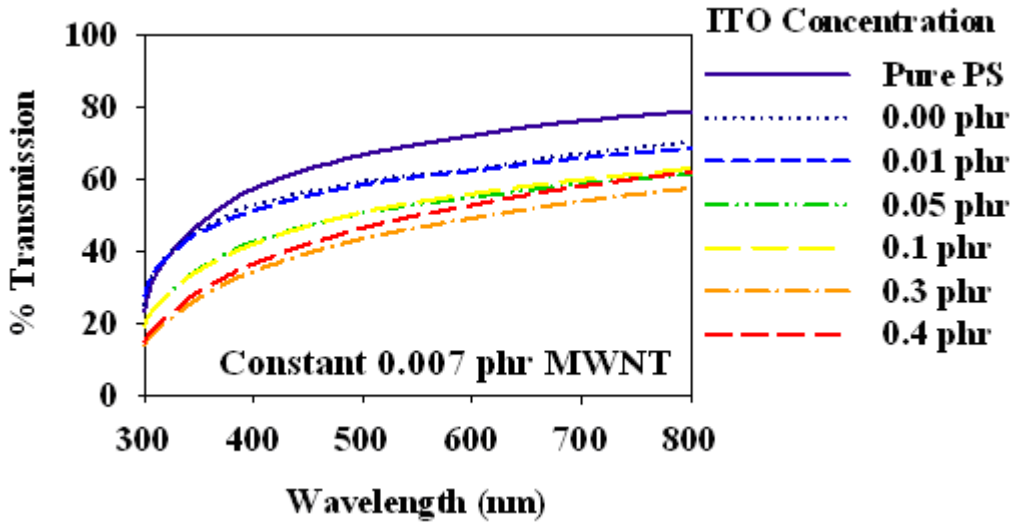

Figure 3.24. Graph of percent transmission versus wavelength for mixed ITO/MWNT PS-composite set X (~2 mm, constant 0.007 phr MWNT) as a function of ITO concentration.

Figure 3.25 shows the percent transmission value at a single wavelength of 600 nm for mixed ITO/MWNT PS-composite set VIII (~2 mm, constant 0.07 phr ITO) as a

function of MWNT concentration and for mixed ITO/MWNT PS-composite set X (~2 mm, constant 0.007 phr MWNT) as a function of ITO concentration.

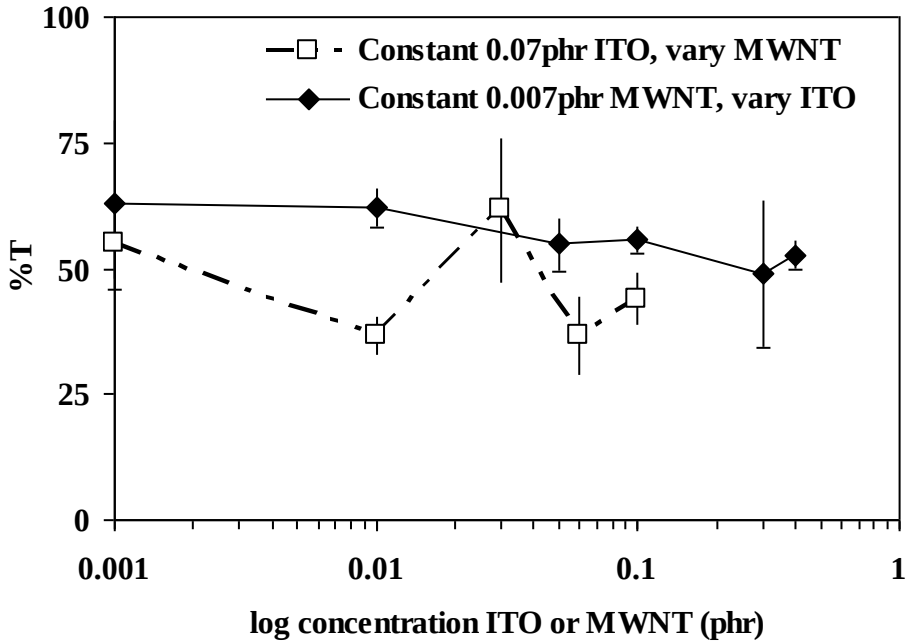

Figure 3.25. Percent transmission versus concentration at 600 nm wavelength for ~2mm mixed ITO/MWNT PS-composites: set VIII (constant 0.07 phr ITO) with varying MWNT filler concentration and set X (constant 0.007 MWNT) with varying ITO filler concentration).

3.5 Time and Voltage Dependence of Impedance

This section reports the changes in impedance response due to measuring the impedance again after a period of several weeks or months, and due to varying the ac and dc voltage while measuring the impedance. Impedance measurements of composites containing MWNT, measured weeks or months after the initial measurements, show a time dependent impedance response which is not observed for the PS-composites containing ITO only. The average resistivity of the composites decreases when measured after a time has elapsed between the initial measurements and the consecutive ones.

The time dependent impedance response is determined by comparison of Nyquist plots of initial and subsequent impedance measurements. Figure 3.26 depicts the Nyquist plots of the initial impedance response (post-fabrication) and the response measured after eight months of a 0.007 phr MWNT PS-composite (~3 mm, set VI). The latter measurement shows that the dc resistivity decreased by four orders of magnitude. The subsequent measurement in Figure 3.26 has a second semicircle, the initial measurement did not.

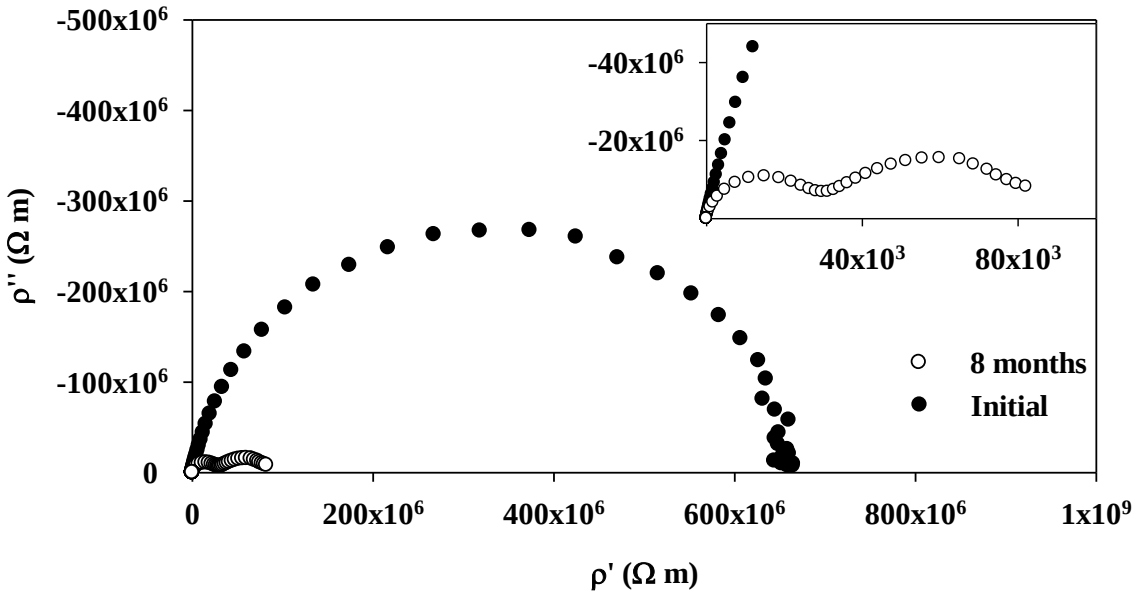

Figure 3.26. Nyquist plots of initial and subsequent (after eight months) impedance measurements of a 0.007 phr MWNT PS-composite (set VI), shown at different magnifications.

Figure 3.27 shows the effect of varying ac and dc voltage on the impedance response of a 0.007 phr MWNT PS-composite (~3 mm, set VI), eight months post fabrication. Increases in the ac or dc voltage parameter for impedance measurements made in Figure 3.27 causes the size of the second semicircle to decrease. AC or dc voltage variations in impedance measurements on a 0.007 phr MWNT PS-composite (~3

mm, set VI) do not affect the high frequency semicircle response. At an ac voltage of 1 V and a dc bias of 5 V the second semicircle substantially decreases.

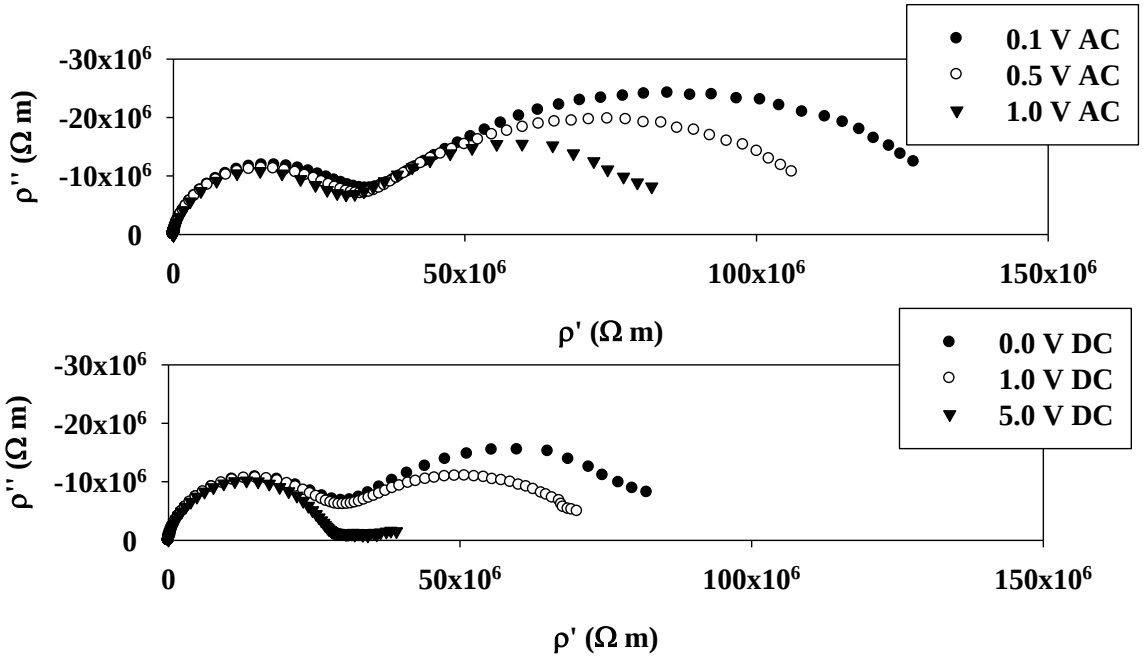

Figure 3.27. Nyquist plots of a 0.007 phr MWNT PS-composite (~3 mm, set VI) measured eight months post fabrication. Impedance measurements are shown as a function of a) ac applied voltage and b) dc applied voltage.

Figure 3.28 displays the plots of the log average resistivity versus concentration for MWNT PS-composite set VI (~3 mm thickness with varying MWNT concentration) comparing the initial impedance measurements and the latter measurement made after eight months. The average resistivity decreases by one to two orders of magnitude for subsequent measurements. At the highest filler content, i.e. 0.07 phr MWNT, the average resistivity remains approximately constant for the subsequent measurement.

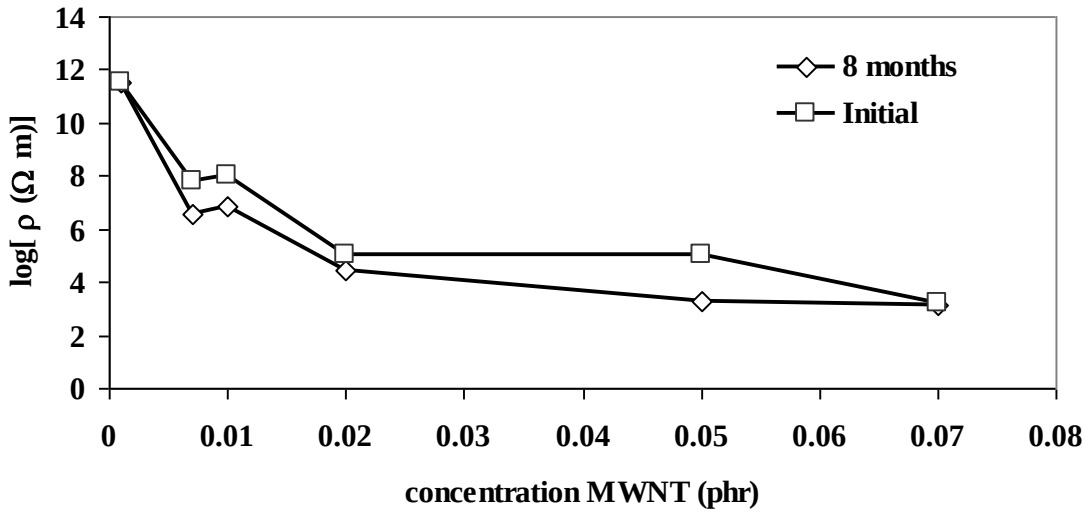

Figure 3.28. Log average resistivity versus concentration plots for MWNT PS-composite set VI (~3 mm, with varying MWNT concentration) determined by initial and eight month subsequent impedance measurements.

Figure 3.29 depicts the plots of the log average resistivity versus concentration for MWNT PS-composite set V (~2 mm, with varying MWNT concentration) determined by the initial impedance measurements and by the nine month subsequent impedance measurements. The average resistivity decreases 1.5 – 80 times for subsequent measurements. The 0.007 phr MWNT composite's (set V) average resistivity remains approximately constant.

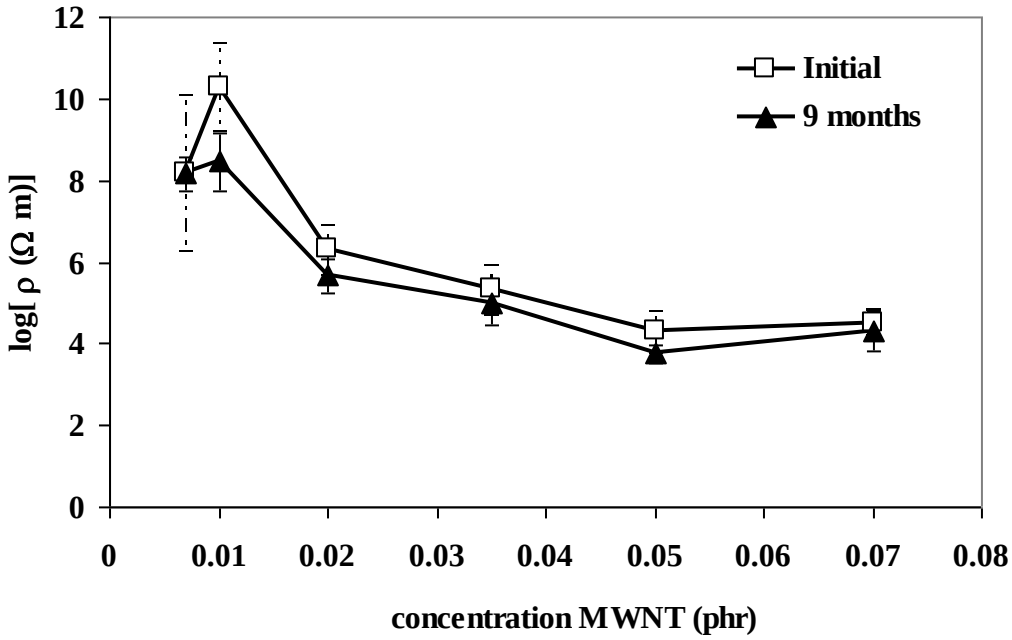

Figure 3.29. Log average resistivity versus concentration plots for MWNT PS-composite set V (~2 mm, with varying MWNT concentration) determined by initial and nine month subsequent impedance measurements.

A new set of MWNT PS-composites was fabricated after the discovery described above. The changes in electrical response were measured as a function of time over a much shorter time lapse. Figure 3.30 displays the plots of the log average resistivity versus concentration for composite set VII determined by the impedance measurements taken at 0, 2, 4, and 6 weeks. From weeks 0 to 2, 2 to 4, and 4 to 6 the average resistivity decreases 8, 2.5, and 16 times respectively for the 0.01 phr MWNT PS-composite's (set V). The 0.02, 0.035, 0.05, and 0.07 phr MWNT PS-composite's (set V) average resistivity remains approximately constant. After 14 weeks the MWNT PS-composites had an electrical response similar to the response of week 6.

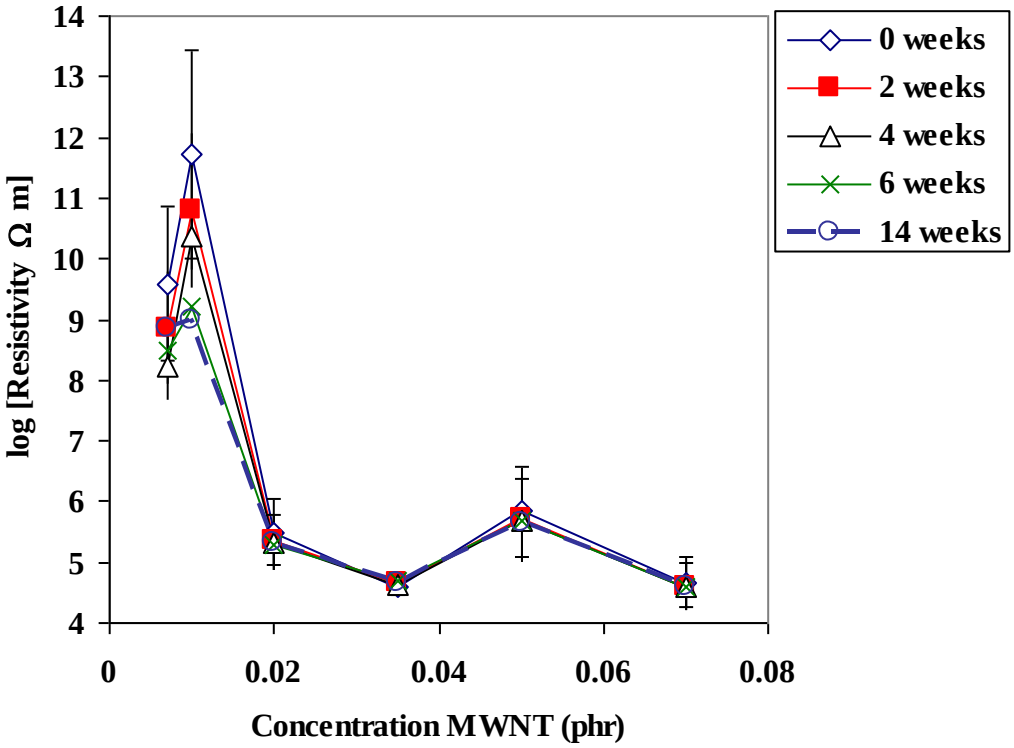

Figure 3.30. Log average resistivity versus concentration for MWNT/PS composites (set VII) measured at 2 week time intervals and also 14 weeks after fabrication.

3.6 Keyence Micrographs and Fracture Surfaces

This section shows Keyence micrographs of conducting planes of filler material and optical micrographs of fractured PS-composites. Figure 3.31 shows Keyence micrographs at different magnifications of a 0.07 phr ITO PS-composite (set I), where the respective magnification of the micrograph is notated: part a) 25x, b) and c) 100x, and d) and e) 200x . In Figure 3.31b ITO agglomeration appears highly concentrated at grain edges. Figure 3.32 shows Keyence micrographs at different magnifications of a 0.07 phr MWNT composite (set V): part a) 25x, b) 100x, and c) 100x. In Figure 3.32b the curvature of the grain boundary layer can be seen, as well as the agglomeration of MWNT that are dispersed on the boundaries surface. Figure 3.33 shows Keyence

micrographs at different magnifications of a mixed 0.01 MWNT / 0.07 phr ITO PS-composite (~2 mm, set VIII). In Figure 3.33 part a), b), and c) the magnification of the micrograph is 25x, 100x, and 200x respectively in the image.

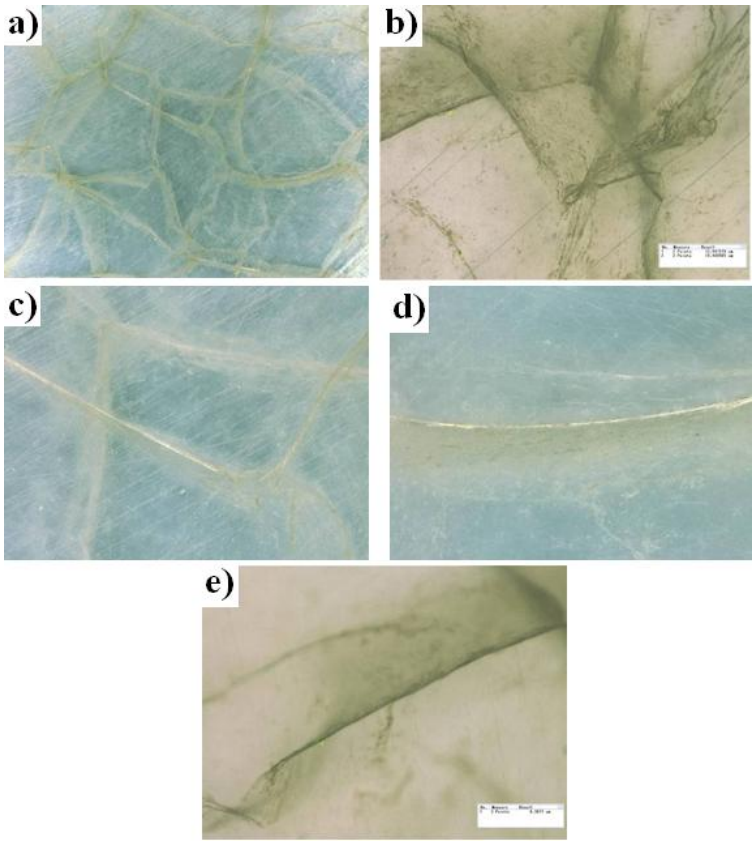

Figure 3.31. Keyence micrographs at different magnifications of a 0.07 phr ITO PS-composite (~2 mm, set I), showing the agglomeration of filler at grain edges, a) 25x, b) 100x, c) 100x, d) 200x, and e) 200x

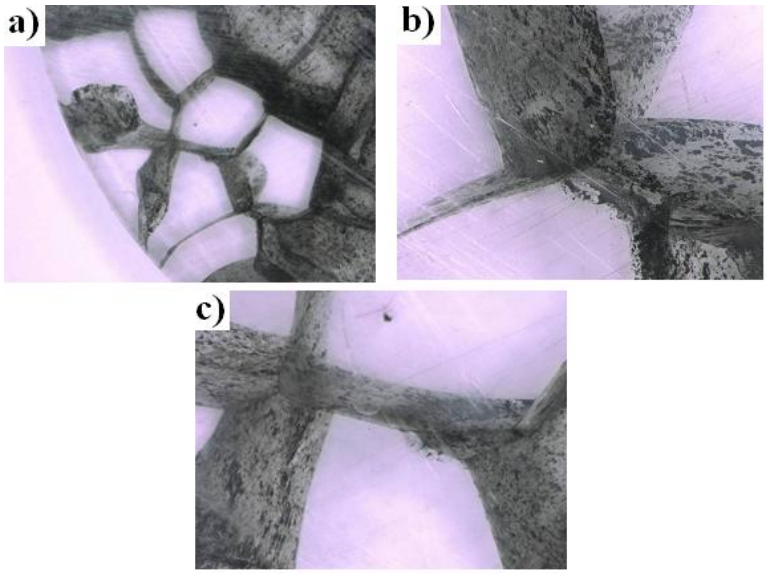

Figure 3.32. Keyence micrographs at different magnifications of a 0.07 phr MWNT PS-composite (~2 mm, set V), showing the meeting of conducting planes and nanotube agglomeration at the PS grain edges, a) 25x, b) 100x, and c) 100x

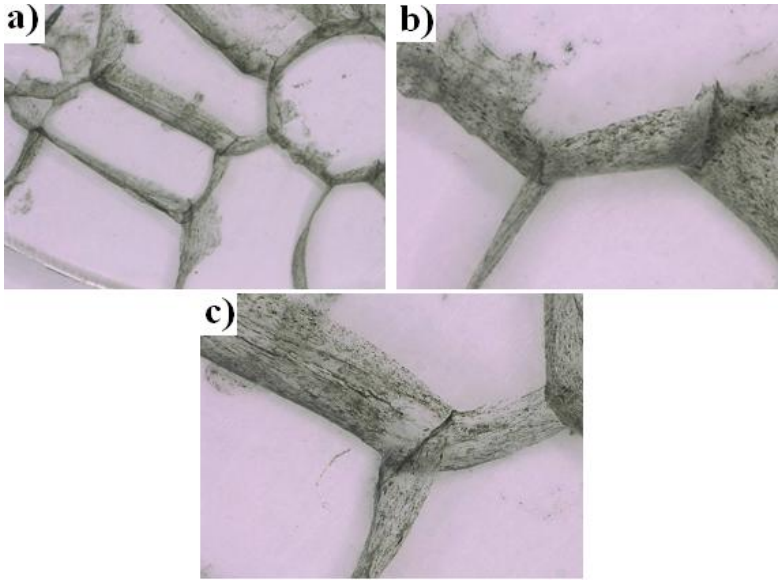

Figure 3.33. Keyence micrograph at different magnifications of a mixed 0.01 MWNT / 0.07 phr ITO PS-composite (~2 mm, set VIII), showing the agglomeration of ITO and MWNT on grain boundary planes and edges, a) 25x, b) 100x, and c) and 100x

Fractured ITO composites broke at areas of applied pressure and not at boundaries between PS-grains. Figure 3.34 shows various fracture surfaces for MWNT composites with a 2 mm thickness at increasing concentrations. Figure 3.35 shows various fracture

surfaces for ITO composites with ITO #1 and a 2 mm thickness at increasing concentrations. The fracture surfaces have striations resembling a series of waves.

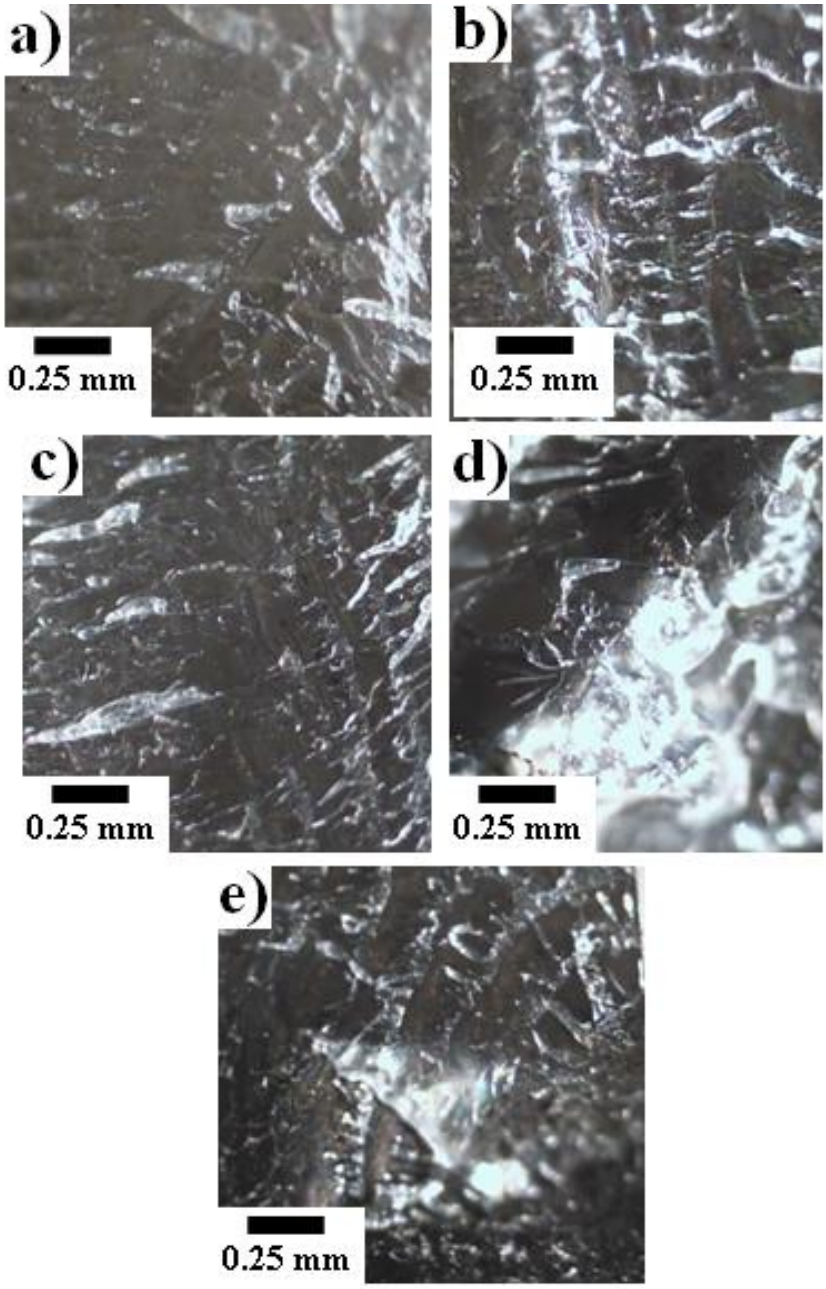

Figure 3.34. Optical micrographs of the fracture surfaces of PS-composites with MWNT filler at concentrations of a) 0.005 phr, b) 0.007 phr, c) 0.01 phr, d) 0.05 phr, and e) 0.07 phr

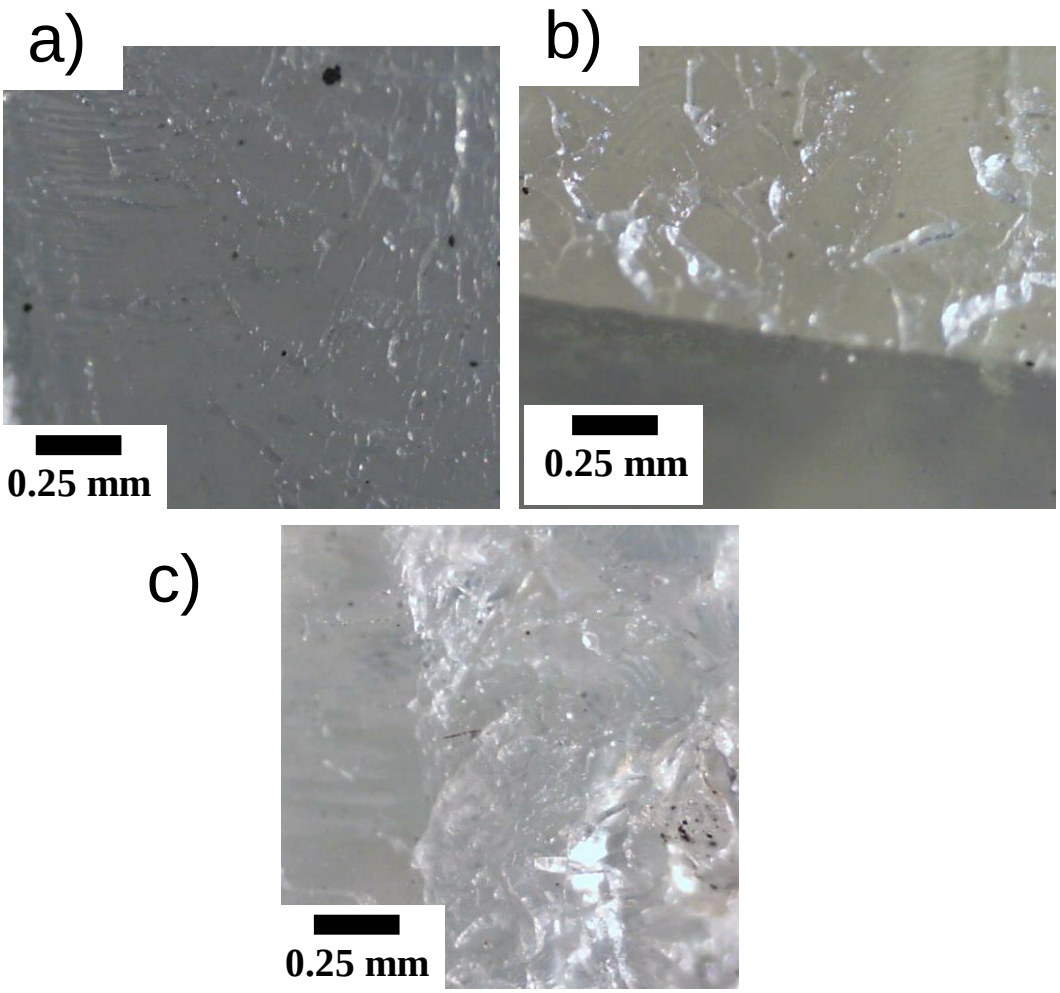

Figure 3.35. Optical micrographs of the fracture surfaces of PS-composites with ITO filler #1 at concentrations of a) 0.01 phr, b) 0.13 phr, and c) 0.31 phr

CHAPTER 4

ANALYSIS AND DISCUSSION

This chapter focuses on the analysis and discussion of experimental results, as they are associated with understanding the changes in the behavior of the PS-composites with changes in the filler concentration and type; the composites microstructure as it relates to its properties, the effect of voltage and incremental changes in properties, and the time dependence of the electrical properties of the composite. The behavior of PS-composites as it relates to changes in the type of filler and its concentration is discussed first. Such discussions compare the effect of filler concentration and type as they are associated with: the properties of individual materials, the composites electrical, optical, and mechanical properties. Correlations are drawn between the materials and composite properties that support the findings from the experiments. Lastly, the effect of time on MWNT composite's electrical properties is discussed.

4.1 Behavior of ITO, MWNT, and Mixed ITO/MWNT PS-Composites as a Function of Filler Concentration and Type

This section describes the behavior of composites with changes to the filler concentration and type, by analyzing and discussing material properties, PS-composite electrical properties, and PS-composite optical properties. The effect of filler concentration is apparent with incremental changes to the filler concentration as well as the concentration associated with the transformation between a non-percolated composite and a percolated composite. Changes in filler concentration also cause a decrease in the transmission of light through the PS-composites. The filler type (MWNT, ITO, or mixed ITO/MWNT) used in the PS-composite affects the maximum and minimum resistivity,

and the transparency of the composite. MWNT composites have a smaller minimum resistivity compared to ITO and mixed ITO/MWNT PS-composites. The electrical and optical properties of ITO and MWNT fillers, as well as the size of the respective fillers, helps to explain the different electrical properties, optical properties, and percolation thresholds between the various PS-composite sets. Analysis of the ac conductivity as it varies with frequency across the PS-composite can be used to determine at what point and to what degree the composite is percolated and the number of percolation mechanisms that exist.

4.1.1 Filler and Matrix Materials Properties Analysis and Discussion

The individual properties of ITO, MWNT, and PS provide an understanding of the electrical and optical properties of the PS-composites, as they are associated with the filler type and concentration. ITO composites have a higher minimum resistivity than MWNT composites. This is true because ITO is more resistive than MWNT, as shown in Figure 3.3. The filler particle size ratio to matrix particle size dictates the percolation threshold in phase-segregated composites.[11, 52] The particle size and geometry of filler materials is related to the percolation threshold difference between PS/ITO and PS/MWNT composites. Capozzi et. al. showed that the size ratio between the matrix particles and the filler particles affects the percolation threshold concentration for phase-segregated composites.[28] MWNT have a much smaller diameter than the average size of ITO nanoparticles as well as a higher surface area. It is therefore expected that PS/MWNT composites will have a lower percolation threshold than PS/ITO composites.

The electrical resistivity of a given filler material is expected to change the behavior of composites as the filler concentration is changed. The DC resistivity of ITO powders is one to two orders of magnitude higher than the DC resistivity of MWNT powders. The mixed ITO/MWNT powders cause a notable decrease in the resistivity between the ITO powders alone and the mixture of 59 wt% ITO and 41 wt % MWNT. The bulk powder resistivity of ITO nanoparticles is higher in comparison to mixed ITO/MWNT particles, as shown in Figure 3.3. The resistivity of ITO PS-composites in comparison with both MWNT PS-composites and mixed ITO/MWNT composites confirms a similar trend. The change in resistivity between ITO powders and MWNT powders is equivalent to the respective difference in minimum resistivity found between ITO composites and MWNT composites. The difference between respective filler powder resistivity and their corresponding composite's minimum resistivity is explained by the composite's microstructure, to be discussed later in Section 4.2.

The decrease in bulk powder resistivity of ITO, MWNT, and mixed ITO/MWNT particles, with increases in compaction pressure, as seen Figure 3.3, is associated with increases in particle-particle contact area. PS-composite compaction pressure effects on resistivity could be correlated with the increased contact area between filler particles in the composites matrix. This will be discussed later in Section 4.2 in the context of the jamming transition phenomenon and its effect on the microstructure of the composite. Work by Capozzi et. al. found that the compaction pressure affects the resistivity of PMMA/ITO composites.[24, 141] The resistivity of PMMA-composites decreases as the compaction pressure is increased during fabrication.[24, 141]

4.1.2 Electrical Properties of Composites Analysis and Discussion

Impedance spectroscopy shows that the electrical properties of the composite are related to the concentration of filler and the filler type. Each composite has a unique Z' value at the low frequency intercept where Z'' = 0, which is related to the concentration of the filler and its type. Variations in Z' and Z'' at specific filler concentrations (seen in the standard deviation values of average resistivity) demonstrate that resistivity is also related to the composites microstructure. A percolated composite has less variation in $|Z^*|$ than a non-percolated composite for example, see Figures 3.6, 3.8, 3.13, 3.21, and 3.22.

Filler concentration changes the dc conductivity of PS-composites (ITO, MWNT, or mixed ITO/MWNT), which was determined by impedance spectroscopy. Figures 3.7, 3.8, 3.13, 3.21, and 3.22 show the effect of concentration on dc resistance in PS-composites. An increase in filler concentration generally decreases the resistivity of the PS-composite. In PS/ITO and PS/MWNT composites, the total resistivity change from the maximum resistivity (at low concentrations) to the minimum resistivity (at high concentrations) is from 10^{13} to $10^{3.1}$ Ωm (PS/ITO) and from $10^{11.4}$ to $10^{3.2}$ Ωm (PS/MWNT) respectively. This change in resistivity from a high value at low concentrations (below percolation) to a low value at high concentrations (above percolation) is seen in log-log plots of resistivity versus concentration, with the exception of mixed PS/ITO/MWNT composites (Figure 3.21, 3.22) where some anomalous results were observed.

Figure 4.1 shows the ac conductivity for a ~3 mm MWNT/PS composite set. By analyzing the ac conductivity of the PS-composites as a function of frequency and concentration, it can be concluded that there are multiple percolation mechanisms in the

composites and that the fractal dimensions of each mechanism are different in complexity.

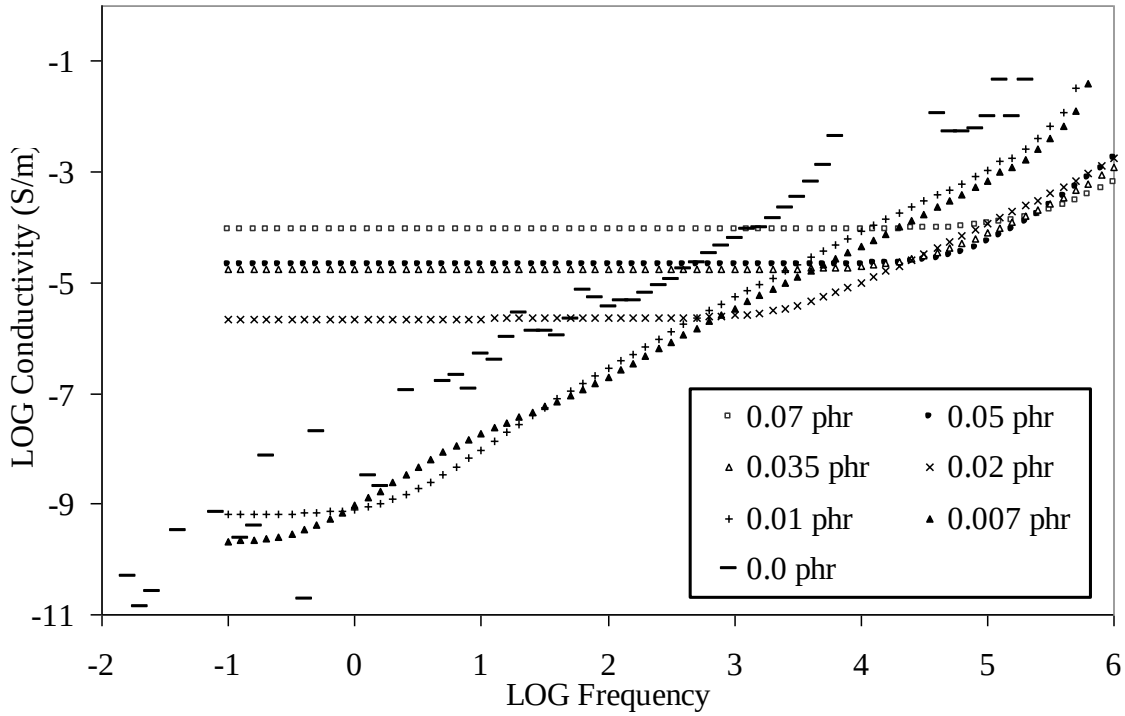

Figure 4.1. Graph of log conductivity versus log frequency explaining how the critical frequency f_c is determined. The impedance spectroscopy data from ~3 mm MWNT/PS composite set was analyzed to determine the AC conductivity. The conductivity in the frequency independent region represents the dc conductivity of the composite, and is an indicator of the occurrence of percolation. 0.007 phr and 0.01 phr MWNT composites are percolated by a different mechanism than that associated with higher concentration composites.

The percolation threshold of PS/MWNT composites is 0.015 phr MWNT and the PS/ITO composites have a percolation threshold between 0.15 phr and 0.3 phr (depending on the ITO filler type used). The difference in the percolation threshold of PS/ITO and PS/MWNT composites is attributed to the filler type and the respective size of that filler.[23, 108]

The electrical properties of mixed ITO/MWNT PS-composites vary in unpredictable and unexpected ways with changes in the concentration of the filler. Mixed PS/ITO/MWNT composites with a ~3 mm thickness (0.01 ITO / 0.007 MWNT phr) exhibit a significant decrease in the measured resistivity, in comparison to composites at concentrations (0.008 ITO / 0.007 MWNT phr and 0.012 ITO / 0.007 MWNT phr), as seen in Figure 3.22. In Figure 3.7 it can be seen that a composite containing only 0.01 phr ITO has a $\rho \sim 10^{12}$ Ωm. The addition of 0.007 phr MWNT to a 0.01 ITO composite decreases the resistivity of that composite significantly. In Figure 3.22 it can be seen that the two surrounding ITO composites (with the same MWNT of 0.007 phr) have much higher resistivity than the samples containing 0.01 phr ITO. The difference between the two composites is that the mixed ITO/MWNT PS-composite has a higher total vol % of filler and the mixed ITO/MWNT composites concentration is above the percolation threshold (0.045 vol % ITO) of ~3mm thick ITO composites (ITO #2). The mixed ITO/MWNT composite has a higher vol % of filler than the 0.3 phr ITO composite by a difference of 0.012 vol %. Mixed ITO/MWNT composites have a distinct correlation to the percolation threshold of both ITO and MWNT composites.

The ITO, MWNT, and mixed ITO/PS composites presented in this research have a large grain size and contain a low number of PS-grains ranging from 50 – 100. The first percolation mechanism for MWNT PS-composites occurs at a concentration of 0.007 phr MWNT. The second percolation mechanism is at 0.15 phr MWNT for the PS/MWNT composites.

Analysis of the ac conductivity, made from impedance data, shows that filler material percolates the composites thickness by multiple percolation mechanisms, which

are concentration dependent. A plot of the ac conductivity as a function of frequency can be used to determine when a PS-composite is percolated by determining the frequency and concentrations where the ac conductivity of the composite transitions to a dc conductivity, where a frequency independent region emerges. Figure 4.1 shows a plot of the composites conductivity versus frequency for a ~3 mm thick MWNT composite set (VII). At 0.007 phr, the ac conductivity reaches a critical frequency showing that at this concentration the composite is percolated, as previously mentioned. Frequency independent conductivity is characterized by the domination of a resistive conducting pathway.[98, 99]

The critical frequency is the frequency at which the transition between the frequency dependent region and the frequency independent region occurs. To determine the critical frequency f_c the data of the frequency dependent region and frequency independent region are fitted with a linear best fit, the intersection of these lines is the critical frequency.[24, 98, 99] Relating the critical frequency of a PS/composite to the absolute value of the difference between volume fraction of filler (p) and the volume fraction at percolation (p_c), which is $| p\text{-}p_c |$, gives the proportionality of f_c to the percolation threshold that can be determined by Equation 3.2 [98, 99]

$$f_c \alpha | p - p_c |^{\gamma} \qquad \text{Equation 3.2}$$

Equation 3.2 can determine such a relationship where p represents the volume fraction at a given composition, p_c represents the percolation threshold volume fraction of filler, and γ is the fractal dimension of the conducting volume.[98, 99] The plots of the log of real conductivity versus the log of frequency for MWNT/PS composites show that percolation exists for two different mechanisms. The conductivity versus frequency

spectra, shown in Figure 4.1, for $p \leq 0.01$ phr MWNT, have a frequency dependent region that intersects with the frequency independent region of spectrums $p \geq 0.02$ phr MWNT. This intersection shows that there are two mechanisms of percolation in PS/MWNT composites. Figure 4.2 shows the numerically calculated percolation threshold for a polymer composite with 75 μm polyhedral grains for a range of filler radii and four possible geometries.[11] The notation for the different geometries describes the geometry of the idealized matrix polyhedral particle, a truncated octahedron (labeled O) or a truncated tetrahedron (labeled T), and the location of filler along either the grain boundary edges (1D) or the grain boundary edges and faces (2D). [11]

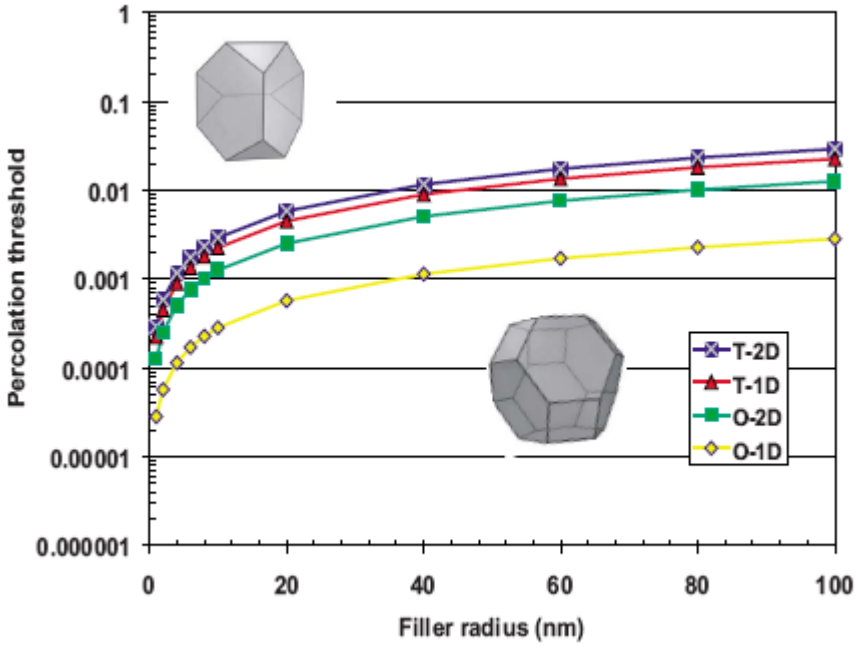

Figure 4.2. The idealized numerical solution to the percolation threshold for four different polyhedra, with a 75 μm size, given the location of filler along the grain boundaries and the radius of the filler particles. Truncated tetrahedron matrix particles, shown in the top left part of the figure (labeled T), and truncated octahedron matrix particles, shown in the bottom right of the figure (labeled O), have filler material located on either the edges of the polyhedral grain boundaries (1D) or on both the edges and the faces (2D). The filler radius and location and the geometry of the grains implies that percolation is affected by the microstructure of the phase segregated polyhedra and the microstructure of the filler. [11]

There are two distributions of filler material that exist to create interconnected pathways in PS/MWNT composites, as shown in Figure 4.2. As the concentration of filler increases, interconnected pathways of filler begin to form at the edges of PS grains (this is along the grain boundaries), this is the first percolation mechanism. Further increases in filler concentration cause the accumulation of filler at the grain edges to saturate, after saturation filler material is forced to agglomerate on PS grain boundaries. At sufficient concentrations of filler, interconnected pathways form on the PS grain faces; this is the second mechanism of percolation. The maximum values of resistivity of 2 mm and 3 mm PS/MWNT composites is10^{11} to 10^{8} Ωm respectively before the concentration of the second percolation threshold is met, after percolation the lowest values of resistivity for each thickness is approximately equal, which is $10^{3.8}$ Ωm.

The value of the fractal dimension of the conducting volume (γ) is specific to the density of interconnected filler in the composite.[98, 99] The conducting volume is the volume of the interconnected conducting filler material; it includes information about the geometry and size of the interconnected pathway within the composite. Analysis of the values of γ, which are found, using Equation 3.2, for PS/MWNT composites determines that the fractal dimensions of the conducting volume are different for the first and second percolation mechanism. Figure 4.3 shows a plot of f_c versus $|p\text{-}p_c|$ for 2 mm PS/MWNT composites, with a varying value of p. The data points are fitted with a linear best fit algorithm and the slope of the line is the values of γ for the respective percolation mechanism. The conducting volume of PS/MWNT composites has two different fractal dimensions, $\gamma = -1.46$ and $\gamma = 1.64$, which represent the conducting volume size and geometry that form via the first and second percolation mechanism respectively. The

larger value of γ for the second percolation mechanism is due to the more dispersed arrangement and larger volume of the interconnected conducting filler that is positioned within the composite Figure 4.2 provides a visualization of the percolated filler structure, which qualitatively shows the arrangement and the conducting volume size of interconnected conducting filler material that result from both percolation mechanisms.

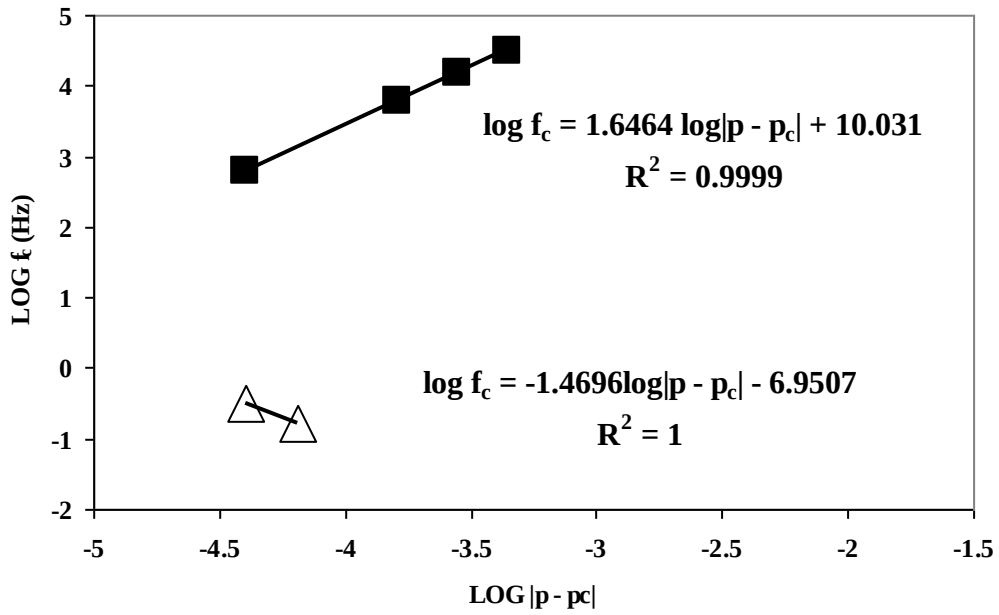

Figure 4.3. The critical frequency f_c as a function of $|p-p_c|$ in a log scale for a 2mm PS/MWNT composites (set V). The data is fitted to two linear best-fit lines. The slopes of the lines represent the fractal dimensions of the conducting volume for the respective concentrations. There are two mechanisms of percolation for the PS/MWNT composites.

The dependence of the average resistivity on the filler concentration, the type of filler (filler to matrix particle ratio, the aspect ratio, the inherent electrical properties), the microstructure of the PS-grains, the thickness of the composite, and its percolation threshold is an expected result. This expectation can be inferred from research reported by Gerhardt et. al., which will now be outlined.[1, 23, 83, 102, 141] PS/CB, PS/SWNT, and PS/MWNT composites which had equivalent PS particles to those used in this work

identical PS particles, presented by Wu et. al.[83] These composites had different percolation thresholds where each depended on the filler type (the filler to matrix particle ratio explains this difference), the best possible conductivity values varied between filler types as well. The concentration of the filler material in the composites presented by Wu affected the resistivity in an analogous manner, as expected.

Furthermore, Wu examined the relationship between the thickness of the composite and its electrical properties; similarly the research presented here agreed with the trend that increases in the thickness cause a decrease in the resistivity of the composite. A project using a phase-segregated ABS/CB and ABS/CNT composites by Talapatra et. al.[102], also found the presence of a relationship between thickness and resistivity. Also, Talapatra found that the resistivity follows a decreasing relationship until the composite reaches ~8 mm and the resistivity drastically increases, which is similar to a point of diminishing return.

The composites prepared by Talapatra were designed to create comparisons between the effect of processing temperature, filler type (CB or CNT), mechanical properties, and electrical properties. The changes in resistivity caused by the extrinsic (mass-dependent) properties of the polymer-composites have a dependence on the samples unique microstructure, which will be explained later. The number of grains in a ~3 mm phase-segregated composite is almost a two fold increase in the number of polymer "grains" relative to the number of grains in a 2 mm thick composites. A higher number of polymer-grains is likely to increase the number of interconnected pathways through the composite, the path-length of the pathway for charge conduction will likely decrease, which promotes charge transfer through the composite. The microstructural

effect on resistivity is seen clearly in the comparison made in this work between PS composites with an ordered and random orientation of PS. In other words, the orientation of the PS-grains with respect to other grains is an important contributing factor to the resistivity, such that a composite with oriented PS-grains is better equipped for promoting conductivity.

A possible inference from the findings presented in this document and the results of prior research is that the thickness effect is caused by an increase in the number of polymer-grains, that have completely different microstructures. Such an inference provides a perspective on the effects of a uniaxial compression on a different number PS-pellets, and that more grains are effective for increasing the interconnectedness of filler through the composite. As well, the surface area of the PS-grain boundaries in the composite for thicker samples is greater, and that this can be used to suggest that a higher surface area of grain boundaries provides a greater number of interconnected filler pathways that may provide a shorter and less resistive charge transfer path.

Given that the PS-composites in this work have ~100 or less PS-grains (depending on the sample thickness) it was expected that there would be a large variation, or spread, in the resistivity data at a given concentration. In other words, the microstructure of PS-composites in this work is a contributing factor to the large standard deviations in the average resistivity and the percent transmission (to be discussed later).

Furthermore, it is a reasonable assumption that an increase in the number of polymer-grains in a phase-segregated composite will cause a decrease in the experimental spread in the average resistivity at a specific filler concentration. Work by Capozzi et. al. and Ou et. al.[23, 27, 141] showed a considerably smaller spread in the average resistivity of

PMMA/ITO composites and PMMA/CB (phase-segregated) at a given composition than work presented here. The PMMA/ITO composite research by Capozzi et. al.[23, 141] and Ou et. al. [27] had micron sized PMMA particles. The density of PMMA-grains in such PMMA/ITO composite research was much greater than the density of PS-grains in the PS-composites presented in this thesis. A higher polymer-grain density lessens the microstructural grain orientation effect on the variance/spread in the average resistivity of the PMMA/ITO composites. The PS-composites have a grain density that is several orders of magnitude lower in comparison. The higher the grain density of the composite is, the lower the variation in the resistivity of the composite is between identically prepared composites.

A correlation between standard deviation magnitude and the concentration of filler with respect to the percolation threshold can be inferred. The spread/variance in the resistivity data at a given concentration may be influenced by whether that concentration is considerably above the percolation threshold or near/below it. The resistivity data implies that when the filler concentration is sufficiently above the percolation threshold, there is less dominance of the microstructure/thickness effect on the resistivity of the PS-composite, which leads to a tighter standard deviation around the average resistivity of the identically prepared PS-composites. Inversely, several PS-composites with a concentration near/below the percolation threshold will have a larger standard deviation around the average resistivity, due to more dominance of the microstructure/thickness effect on the resistivity of the PS-composite. It is important to note that the electrical measurements taken with impedance spectroscopy in this work are precise and represent

the true impedance response of the PS-composites measured and the entire measurement apparatus.

4.1.3 Optical Properties Analysis and Discussion

The concentration of filler material in PS-composites directly affects the amount of in-line transmission of light. The type of filler used in PS-composites also has an effect on the resultant transmission. PS-composites are transparent to light to various degrees depending on the wavelength of the light, in other words the absorption coefficient decreases with increasing wavelength in the range of 200 nm to 1100 nm, as shown in Figures 3.10, 3.18, 3.23, and 3.24. The type of filler used in composites also affects the absorption of visible light.

PS-composites are transparent to light to varying degrees depending on the microstructure and composition of the composite. There is a relationship between the percent transmission of light through the composite and the filler concentration. Increasing the concentration of ITO and/or MWNT in a PS-composite causes a decrease in the value of the percent transmission, in some composites. In PS/ITO/MWNT composite sets, the addition of filler material has a random effect on percent transmission and the spectrophotometer measurement does not completely capture the bulk percent transmission.

By comparing the percent transmission with certain composites with similar resistivity values but different compositions, it is shown that percent transmission can be increased while maintaining conductivity performance. The percent transmission of the PS-composites, at a 600 nm wavelength, versus the concentration of filler was plotted in

Figures 3.11, 3.19, 3.25. These values were shown to vary with filler type and concentration. Figure 4.4 shows the effect of adding ITO to a MWNT PS-composite, which causes an increase in %T, but also increases the composites ρ from 10^5 to $10^{6.1}$. Ω m. Figure 4.5 shows a comparison of two mixed ITO/MWNT PS-composites with a ρ = 10^5 Ωm. Figure 4.5 infers that the addition of a higher wt% of ITO, to the PS-composite, relative to the wt% of MWNT causes an increase in the percent transmission while maintaining the same resistivity.

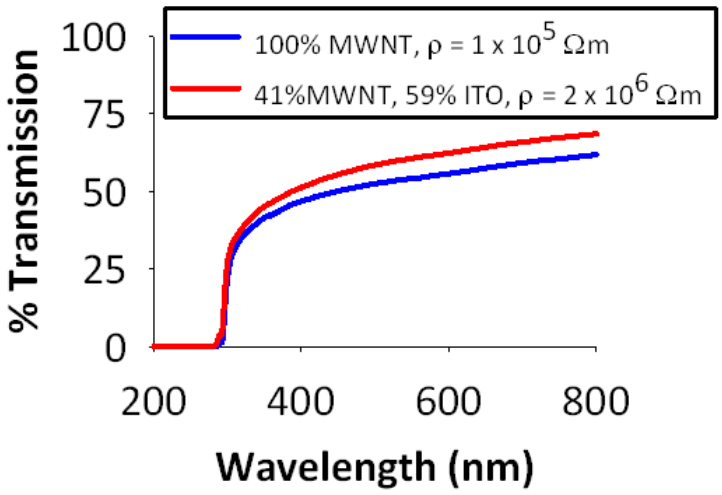

Figure 4.4. %T vs. wavelength of a PS/MWNT composite with and without ITO. The addition of ITO increases the transmission of the composite, however it also increases the resistivity of the PS/MWNT composite

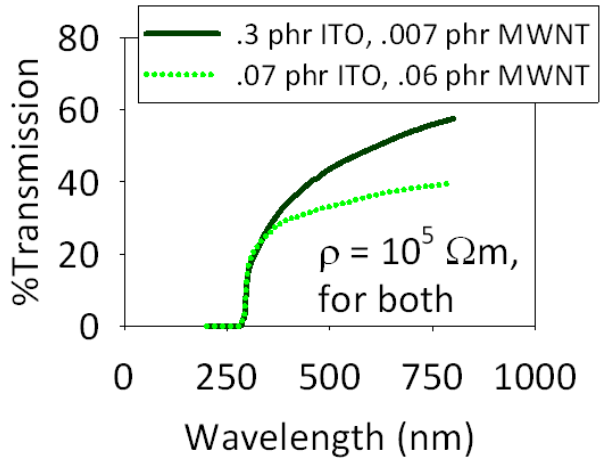

Figure 4.5. %T vs. wavelength of two mixed PS/ITO/MWNT composites with the same resistivity, which is equal to 10^5 Ωm. A higher wt% of ITO relative to the wt% of MWNT can increase the PS-composites transmission, while maintaining the same resistivity.

The amount of scattering that occurs for incident light is increased as the filler concentration is increased. PS/ITO composites are capable of containing a higher weight concentration of filler than PS/MWNT composites, while maintaining a higher value of transmittance. The absorption is affected similarly by changes in filler concentration. An unexpected result occurs for PS/MWNT composites increasing the concentration of MWNT causes an increase in transmittance from 0.01 phr to 0.02 phr MWNT. Such an unexpected result in the transmittance/concentration relationship can be related to the large size of PS grains with respect to the filler size. Figure 4.4 shows a 0.007 phr MWNT PS-composite, which helps to visualize the locations on the surface of the composite that can be probed with the spectrophotometer. The spot size of the spectrophotometer incident on the sample is smaller in area than the PS grain size, and therefore when the transmission measurements are taken, it is possible that the area probed on the sample may have different transmission values. Even though the transmission measurements were averaged it is unavoidable to have large variations.

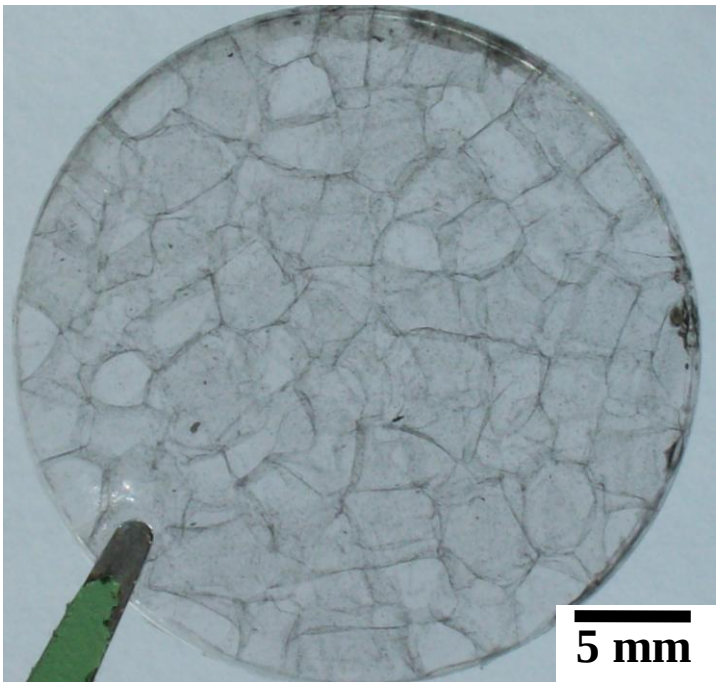

Figure 4.6. An enlarged image of a 0.007 phr MWNT PS-composite, which helps to visualize the lack of uniformity in transmission measurements over different location on the surface of the composite. The small spot size of the spectrophotometer beam (2 mm^2) when placed on the sample is measuring the transmission of the composite at one small spot and can not account for the lack of homogeneity in the composites microstructure.

4.2 The Dependence of Electrical, Optical, and Mechanical Properties on the Microstructure of PS-composites

The microstructure of PS-composites affects the properties of the composite, and correlations can be drawn between the two. The large PS grain boundaries provide a good separation between the interconnected-wires made up of ITO, MWNT, or both. The PS grains are shown in Figures 3.4, 3.9, 3.14, 3.17, and 3.31 – 33. It is important to note that the PS grain boundaries are visible on the bulk scale. A qualitative understanding of the microstructure is used in the following sub-sections to explain the relationship between the properties of the composite and its microstructure.

4.2.1 Microstructure Analysis and Discussion

The composites matrix structure is made up of PS grains or regions of PS phase surrounded by filler material. Grain boundaries are covered by filler material and voids between adjacent filler particles. The compaction of PS at temperatures above the glass transition causes the polymers to enter a viscous state.[95] The applied pressure to the polymers then causes the particles to assume a space filling shape. The resulting space filling shapes are polyhedra.

Mixing PS with composites in a dry atmosphere promotes adhesion between nanoparticles and PS, because of the presence of electrostatic forces.[95] The presence of voids, on PS-grain boundaries, between neighboring filler particles can be inferred from the microstructure of ITO and MWNT materials within the PS-composite, as shown in Figures 3.31 – 3.33. Changing the concentration of filler material directly affects the amount of voids present in a composite, as well as the agglomeration of filler on the PS grain boundaries.

MWNT filler orders itself in between PS grains. The regions of MWNT agglomeration are oriented perpendicular to the pressing direction. Regions of MWNT agglomerates show up as a dark region in optical and Keyence micrographs. Dark regions are mostly situated in lines perpendicular to the pressing direction. This can be explained by the shear forces in the transverse direction during pressing. MWNT are forced together with MWNT on adjacent PS grains during compaction, deformation causes MWNT to agglomerate in higher concentration regions.

In the PS-composite, filler material forms wires and sheets, forming a three dimensional network of filler material, which is separated by PS grains. Concentrations

of filler material above a composites percolation threshold have an interconnected pathway of filler material through the thickness of the composite. This is indicated in optical micrographs as well as a substantial decrease in the resistivity compared to lower concentrations, as shown in Figures 3.7, 3.8, 3.13, 3.21, 3.22, and3.31 – 3.33. The change in resistivity indicates a saturation of filler material on the grains surface. Though there is saturation, the filler material sheet is not completely uniform as there must be connection of adjacent PS beads otherwise the composite would become brittle. Previous work has shown that some polymer filler composites containing large amounts of filler are brittle and grains do not form good adhesion between them.[25, 102, 141]

Contacts between ITO nanoparticles and MWNT in composites are weaker than contacts made during dc resistivity experiments of filler powders alone. The smaller resistivity of ITO and MWNT particles where they are by themselves implies that ITO and/or MWNT particle contact in composites does not have the same microstructure as the pressed powders. A comparison between the bulk resistivity of powders and the minimum resistivity of composites infers that the contacts between the filler particles are weak, or separated by PS. Ideally, composites that are percolated should have a resistivity equal or similar to bulk powders. Therefore, contacts between fillers in the composites studied here are therefore not continuous throughout the composites thickness.

The microstructure of the composites is formed via the deformation of PS and is dependent on other factors. Deformation is sensitive to pressing parameters and processing conditions.[24, 102] Filler size, polymer size, composite thickness, applied pressure, temperature, and heating and cooling rate are all factors that affect the microstructure of a composite.

4.2.2 The Jamming Transition

The jamming transition is a physical concept that describes the point at which a system becomes rigid under increased pressure.[142] In the case of polymer composite systems, the addition of filler material can cause the material to transition from viscous behavior to solid like behavior.[143] In this work the PS/(ITO and/or MWNT) materials are placed under an applied pressure that effectively, after a sufficient amount of heating and pressing time, prevents further motion of the viscous polymer.

PS pellets are uniaxially compressed and undergo deformation, which at some point no longer occurs. The moment at which the kinetic motion of the PS grains and the filler material ceases is the jamming transition.[143] The presence of filler material on and around an effectively porous filler/PS-grain causes the grains to become distinct, when a sufficient temperature and compaction pressure are used to form the PS-composite. The PS-grains maintain the final deformed shape during cooling, while the filler material is positioned on the grain boundary edges. The filler material is positioned at the surface of the PS-grains, which maintains a barrier between adjacent PS-grains. When combining filler material with granular media, such as the nanoparticle fillers used in this thesis, a critical density point can be reached under certain conditions, where pressure and temperature cause a densification or pinning of the media, the deformation and movement will then cease.

The settling of the PS-grains occurs and deformation ceases and the density then increases. Once the jamming transition is met, the cooling of the press under constant pressure preserves the cellular microstructure of the PS-composite at the jamming transition. The cessation of media motion is partly responsible for the definable

agglomerations of filler material. The transverse and axial shear forces and the effects these forces have during impingement also affect the final outcome.

The densification, or settling, of PS pellets under heating and compaction, results in the formation of polyhedron shaped PS-grains, as shown in Figure 3.14. The orientation/position of the PS pellets with respect to the composites surface and the axial direction of the composites describe the orientation of the PS-grains. While the grain orientation is random, such as in typical composites, the direction of pressing dictates the settling or jamming of this viscous granular material as it flows together into polyhedra, and as force used is uniaxial compression. The application of a compression force and temperature at sufficient values to the PS-composites, causes the material to reach a critical density point, where the viscoelastic flow of PS transitions to a zero net flow. Reaching this transformation depends on the mechanics of the deformation, the viscosity of the PS-grains and how it responds to the shear force, and its relationship to the temperature, and pressure. The density of the media reaches a critical value and the transition is complete, the microstructure of the PS grains is set, and the grain boundaries are well defined by a coating of filler material. A notable/interesting effect on the dispersion of filler particles by deformation is that regions of filler particle agglomerates are concentrated on the surface of the PS-grains in the transverse direction, as seen in Figures 3.31 – 3.33.

4.2.3 Electrical Properties Analysis and Discussion

The composite filler concentration reaches a saturation point where resistivity changes drastically, known as the percolation threshold. When the concentration reaches

the percolation threshold, the structure of the filler within the composite exists as a continuous wire through the thickness of the composite. The RC equivalent circuit model can be expected to apply for an insulator conductor composite. Additional agglomeration of filler material between grains fills the grains surface to a point of maximum conductivity for the material. This is best described by log- log plots of average resistivity versus concentration. Work by Gerhardt et. al. showed that CB/ABS phase-segregated composites had percolation at very low filler concentrations, approximately 0.01 phr CB.[25] Table 4.1 summarizes the percolation threshold and minimum resistivity of PS-composite sets by sample thickness and filler type (ITO, MWNT, or mixed ITO/MWNT). It is seen that the percolation threshold for MWNT in PS-composites is the same as that of CB in ABS, because the initial polymer grain size was similar. See Figures 1.2 and 3.4 for a comparison between the two.

Table 4.1. Summarizes the percolation threshold and minimum resistivity of the PS-composites, which is given for all the various types of filler and the approximate sample thicknesses (~2 or ~3mm).

Filler	Percolation Threshold (phr)	Minimum ρ (Ω m)	Thickness of PS-composite (mm)
ITO #1	0.15	$3.7 \times 10^{}$	2.0
ITO #1	0.15	$1.5 \times 10^{}$	3.0
ITO #2	0.25	$1.2 \times 10^{}$	3.0
ITO #3	0.30	$2.1 \times 10^{}$	3.0
MWNT	0.01	$1 \times 10^{}$	2.0
MWNT	0.01	$1 \times 10^{}$	3.0
Constant 0.007 phr MWNT and varying ITO	-	$7.2 \times 10^{}$	2.0
0.007phr MWNT/ varying ITO	-	$8.7 \times 10^{}$	3.0
Constant 0.07 phr ITO and varying MWNT	-	$3.1 \times 10^{}$	2.0
0.07phr ITO/varying MWNT	-	$1 \times 10^{}$	3.0

Modeling a composite with an insulating and conducting phase with an equivalent circuit requires an understanding of impedance and analog electronics.[137] Circuit

elements themselves each have an individual impedance response and adding these elements together, a new impedance equation is acquired. The equivalent circuit that describes the experimental data can be used to draw comparisons between the physical materials phenomenon that affect the composites electrical and dielectric behavior and circuit elements, which have a quantitative solution describing the impedance behavior of the circuit.

Composites with PS grains ordered parallel or tangentially to the pressing surface in comparison with equivalent randomly oriented composites have a lower resistivity, as shown in Figure 3.16. The preferential orientation of composite grains in one direction results in several things. An ordered structure may provide a greater number of direct percolation paths. The orientation or microstructure of the PS grains changes the electrical properties of composites at the same concentration, as shown in Figures 3.15 and 3.16. Fluctuations in resistivity over PS-composites with the same concentration of filler material can be explained by the random orientation of the PS-grains. The small number of grains in 2 mm and 3 mm thick composites contributes to the prominence of this effect.

The frequency dependence of the ac conductivity contains information about the microstructure of the composites, particularly the concentration at which the composite is percolated. The frequency range of the dc conductivity region correlates to the degree of interconnectedness of the filler material in the composite. PS-composites with larger concentrations of filler have a larger value of f_c and therefore the filler is more interconnected for these composites. The larger the frequency dependent region is, the less interconnected the filler material is.[24] The ac conductivity region, where capacitance

dominates, represents a microstructure with filler material that is not well connected. In a PS-composite with a larger frequency dependent conductivity region, it can be said that there are more PS voids between neighboring particles that impeded the tunneling of charges to the next particle than for PS-composites with a larger frequency independent conductivity region.

4.2.4 Optical Properties Analysis and Discussion

When comparing the microstructure of a PS-composite with its optical properties, the filler concentration and dispersion, as well as the PS matrix particles microstructure, are important factors to consider. Given the size of the PS beads, the transmission of light through the composite may depend on the number of PS-grains present through the thickness of the composite. Light transmission is a non-uniform property for the PS-composites. Transmittance is dependent on the processing of the composite, particularly the arrangement of PS-grains as well as other factors. The arrangement of PS-grains in a 2 mm composite affects the transmission of light when there is a continuous phase of PS through the composite, since pure PS has a higher transmittance than any PS-composite. Additions of filler material change the microstructure and how it affects the optical properties of the PS-composite. For example, light incident upon MWNT and/or ITO particles is absorbed or scattered by the atomic structure of the particle.[5, 43, 72, 95] The interaction of light with ITO and/or MWNT filler particles impedes the propagation of light and the resulting PS-composite has a lower transmittance than that of pure PS, as shown in Figures 3.11, 3.19, and 3.25. The spectrophotometry measurement is made with a 2 mm^2 spot size, which is randomly positioned on the sample. This means that the beam

may be positioned on a grain boundary, in the middle of a PS grain, or on a PS grain with a PS-grain boundary underneath it. The transmission measurement has different values depending on the microstructure.

The microstructure of the filler material within the PS-composite defines a honey comb lattice, where the orientation, size, and geometry of the PS-grain has a distribution which is influenced by the random arrangement of PS pellets before pressing, as well as the deformation that results from pressing. This random honeycomb lattice geometry of the composite, results in changes to the composites transmittance between different locations on the composites surface. The filler material is concentrated at the grain boundaries and collects or aggregates in dense regions that correspond to the direction of deformation during pressing, which resemble striations. The preferential agglomeration of filler material at such grain boundaries is confirmed by Keyence 3D micrograph, as seen in Figures 3.31 – 3.33.

The PS-grain microstructure itself affects the transmission of light through the composite, and the microstructure of the fillers on the PS-grain boundary edges and faces. The filler material covering the PS-grain boundaries are scattering centers for impinged light, which impedes its transmission. The number of PS-grains that are oriented perpendicular to the pressing direction increases the bulk transmittance of the composite. In some cases PS-grains are continuous through the composites thickness, with no adjacent grains that form a filler boundary. Regions of the composite with an all PS phase through the composite have optical transmittance properties equivalent to the optical properties of a pure PS-phase or nearly so. The presence of an all PS phase through the composite as well as large PS-grains, the large distance between filler

interfaces, and the random ordering of the filler interface, require that the measurement of the PS-composites optical properties is a heterogeneous measurement. Since the in line transmission spot size is smaller than the PS-grain size, and therefore can possibly misrepresent the bulk transmittance through the PS-composite.

4.2.5 Mechanical Properties Analysis and Discussion

The fracture behavior of composites and the resulting fracture surface indicates that the filler material must have penetrated into the PS-grains during fabrication. The deformation of the PS-composites at sufficient force causes failure. The fracture surfaces shown in Figures 3.34 and 3.35 imply that there is penetration/migration of filler material into the PS-grain at the grain boundary, because of the enhanced mechanical integrity of the composite represented by the fracture surface. If no penetration or migration of filler into the PS-grain had occurred, the fracture of the composite would most likely occur at the PS-grain boundaries and would show the polyhedron shape of the grains. The same is true for PS/ITO and mixed ITO/MWNT/PS composites.

4.3 The Correlation between Time and the Electrical Properties of Composites Containing MWNT

An interesting result was found when PS/MWNT and PS/ITO composites were re-characterized with impedance spectroscopy six months after the initial characterization. The impedance response of the composites was affected by the age or life of the composite. In some cases, a second impedance semicircle appeared, as seen in Figures 3.26 and 3.27. The second semicircle was found to have an impedance response which was dependent on both the amplitude of the ac voltage and the dc bias voltage. The

impedance response after a time elapse confirms that these PS-composites are forming new less resistive conducting pathways. While changes in the PS-composites electrical properties are apparent, it is less clear what is causing this behavior. The following subsections explain this unexpected behavior by making informed assumptions and providing analysis based on these assumptions.

4.3.1 Time Dependence Analysis and Discussion

The time dependence of the impedance response for PS/MWNT and PS/ITO/MWNT composites is exclusive to PS-composites containing MWNT filler, as ITO PS-composites do not show this behavior. The mixed electrical properties of MWNT require that the PS-composites have interconnected pathways with some combination of metallic and semiconducting particle-particle "connections." During impedance measurements, a potential is applied to two sides of the PS-composite, after which charge carriers must conduct or collect at different interfaces along some pathway. From one side of the composite to the other the charge carriers must first be carried across the Aluminum sample holders to the Ag-electrodes (Ag paint). Next, the charges traverse the insulating and conducting interconnected-MWNT wire filler network in the PS-composite. After which the charge is then carried to the Ag-composite interface followed by the Al-Ag interface. After a time has elapsed, it is possible that these materials have interacted to increase the mobility of charge in the impedance test circuit.

As previously mentioned, when charge carriers conduct through interconnected pathways of filler, it can be assumed that there is some amount of charge tunneling through the PS between MWNT and/or ITO particles. The increase in charge mobility in PS-composites that occurs with time is not expected to occur during tunneling, because

the electrical properties of the PS are expected to remain unchanged.[95] Other possible changes in the charge mobility of this system are charge doping of MWNT with Ag particles from the test electrode. Ma et. al. described a process for doping CNT with Ag nanoparticles, which was used in an epoxy nanocomposite, where the composite with the Ag doped CNT showed a four orders of magnitude increase in electrical conductivity. [144] It is reasonable to assume that the Ag-paint electrodes are responsible for changes in charge mobility in the PS/MWNT composites.

4.3.2 Voltage Dependence Analysis and Discussion

Six months after the impedance of PS-composites was initially measured, in certain composites the impedance response had a second semicircle in the low frequency region of the Nyquist plot, as shown in Figure 3.27. It can be assumed that the doping of MWNT by Ag could cause new interfacial effects which cause a capacitive build up of charge when a low frequency ac voltage is applied. This new interface would cause charge to build up acting to effectively slow charge motion. The application of a higher ac voltage or dc bias voltage causes the second semicircle to diminish in size, as shown in Figure 3.27. The decrease in the size of the second semicircle may be due to the injection of charge into the sample. The two semicircle impedance response represents a material with two conducting phases with significantly different resistances.[137] A four order of magnitude increase in conductivity for Epoxy/Ag doped-CNT composites compared to non-Ag doped-CNT presented by Ma et. al. shows that Ag doped-CNT do indeed have a significantly higher conductivity than CNT alone when combined with Epoxy to form composites.[144]

CHAPTER 5

CONCLUSIONS AND FUTURE RECOMENDATIONS

5.1 Conclusions

PS-composites (PS/ITO, PS/MWNT, and PS/ITO) were successfully produced and analytically characterized. PS-composites exhibited notable electrical conductivity and optical transparency. The combination of ITO and MWNT in mixed ITO/MWNT PS-composites creates a unique microstructure that can improve their electrical properties as compared to PS/ITO composites, while maintaining sufficient transparency. The electrical and optical properties of PS-composites were substantially affected by the concentration of ITO, MWNT, or ITO/MWNT. Analysis of the ac conductivity impedance response of PS-composites showed an interesting correlation between concentration and multiple mechanisms of filler percolation in PS-composites. As the filler concentration is increased, the ac-conductivity analysis indicates a percolation mechanism occurs at low concentrations followed by another percolation mechanism which causes a more substantial increase in the composites electrical conductivity. The first percolation mechanism is assumed to create interconnected wires of filler material at the PS-grain edges; the second percolation mechanism creates interconnected wires on the grain boundaries.

The microstructure of PS-composites was found to affect the electrical properties of PS-composites, the orientation of PS-grains showed this effect. Ordering of the PS grains in PS/MWNT composites created a cellular structure which was found to have a higher

electrical conductivity than a PS/MWNT composite with a randomly ordered microstructure. The electrical conductivity of PS-composites containing MWNT was found to have a dependence on the lifetime of the composite. Initial impedance measurements had a different response than subsequent measurements. Specifically, the resistivity of the PS/MWNT composites decreased as a function of time when a sufficient amount of time had elapsed (~3 months). Subsequently, in some cases, the PS/MWNT composites had a voltage dependent impedance response. Inspection of the fracture surface of PS-composites is believed to indicate that the mechanical properties of the PS-composites are enhanced by the addition of both ITO and MWNT. The fracture surface of the PS-composites may prove that filler material infiltrates into the PS grains because it does not fracture at grain boundaries.

5.2 Future Recommendations

Further work in this field should focus on several factors, studying jamming transitions, optimizing electrical and optical properties, and working with different materials systems to further the development of thin transparent conducting composites.

The understanding of PS/ITO, PS/MWNT, and PS/ITO/MWNT composites provided by this research can be used to tailor polymer/ITO/MWNT composites for application in optoelectronics, particularly transparent electrodes. Changing the polymer matrix to another polymer system, such as PET, could be used to make flexible transparent electrodes. ITO thin films are typically used as transparent electrodes, as mentioned in Section 1.2.2 but these films are subject to brittle failure. Researchers can correlate the effects of additions of MWNT and/or ITO material to PS-composites presented in this

research to a proposed composite system. Further research could also focus on increasing both the conductivity and optical transparency of polymer/ITO/MWNT composites. Polymer-composites have a good chance to enhance the bending force before fracture is experienced in flexible opto-electronic devices. Devices to consider when using a transparent polymer-composite electrode are solar cells, LED displays, and optical sensors. The amount of ITO and/or MWNT used in the PS-composites in this research, is very small, which suggests that compared to traditional optoelectronic devices which use transparent conducting oxides, the PS-composites may prove to be less expensive. In addition, the electrical properties of PS-composites may be affected by small deformations and/or applied forces, which is another possible area to study for applications in mechanical sensors.

REFERENCES

[1] C. J. Capozzi and R. A. Gerhardt, "Novel percolation mechanism in PMMA matrix composites containing segregated ITO nanowire networks," *Advanced Functional Materials*, vol. 17, pp. 2515-2521, 2007.

[2] R. Andrews, D. Jacques, M. Minot, and T. Rantell, "Fabrication of carbon multiwall nanotube/polymer composites by shear mixing," *Macromolecular Materials and Engineering*, vol. 287, pp. 395-403, 2002.

[3] V. Antonucci, G. Faiella, M. Giordano, L. Nicolais, and G. Pepe, "Electrical Properties of Single Walled Carbon Nanotube Reinforced Polystyrene Composites," *Macromol. Symp.*, vol. 172-181, 2007.

[4] F. M. Du, J. E. Fischer, and K. I. Winey, "Coagulation method for preparing single-walled carbon nanotube/poly(methyl methacrylate) composites and their modulus, electrical conductivity, and thermal stability," *Journal of Polymer Science Part B-Polymer Physics*, vol. 41, pp. 3333-3338, 2003.

[5] R. B. H. Tahar, T. Ban, Y. Ohya, and Y. Takahashi, "Optical, structural, and electrical properties of indium oxide thin films prepared by the sol-gel method," *Journal of Applied Physics*, vol. 82, pp. 865-870, 1997.

[6] D. L. Ciprari, *Mechanical Characterization of Polymer Nanocomposites and the Role of Interphase*. 2004, Atlanta, Ga, M.S. Thesis: Georgia Institute of Technology.

[7] A. L. Gershon, A. K. Kota, and H. A. Bruck, "Characterization of Quasi-static Mechanical Properties of Polymer Nanocomposites Using a New Combinatorial Approach," *Journal of Composite Materials*, vol. 43, pp. 2587-2598, 2009.

[8] R. B. Mathur, S. Pande, B. P. Singh, and T. L. Dhami, "Electrical and mechanical properties of multi-walled carbon nanotubes reinforced PMMA and PS composites," *Polymer Composites*, vol. 29, pp. 717-727, 2008.

[9] T. X. Liu, I. Y. Phang, L. Shen, S. Y. Chow, and W. D. Zhang, "Morphology and mechanical properties of multiwalled carbon nanotubes reinforced nylon-6 composites," *Macromolecules*, vol. 37, pp. 7214-7222, 2004.

[10] A. H. Barber, S. R. Cohen, and H. D. Wagner, "Measurement of carbon nanotube-polymer interfacial strength," *Applied Physics Letters*, vol. 82, pp. 4140-4142, 2003.

[11] J. Waddell, R. Ou, C. J. Capozzi, S. Gupta, C. A. Parker, R. A. Gerhardt, K. Seal, S. V. Kalinin, and A. P. Baddorf, "Detection of percolating paths in polyhedral segregated network composites using electrostatic force microscopy and conductive atomic force microscopy," *Applied Physics Letters*, vol. 95, pp. 233122-1 - 233122-3, 2009.

[12] J. C. Grunlan, Y. S. Kim, S. Ziaee, X. Wei, B. Abdel-Magid, and K. Tao, "Thermal and mechanical behavior of carbon-nanotube-filled latex," *Macromolecular Materials and Engineering*, vol. 291, pp. 1035-1043, 2006.

[13] K. I. Winey, T. Kashiwagi, and M. F. Mu, "Improving electrical conductivity and thermal properties of polymers by the addition of carbon nanotubes as fillers," *Materials Research Society Bulletin*, vol. 32, pp. 348-353, 2007.

[14] H. E. Miltner, N. Grossiord, K. B. Lu, J. Loos, C. E. Koning, and B. Van Mele, "Isotactic polypropylene/carbon nanotube composites prepared by latex technology. Thermal analysis of carbon nanotube-induced nucleation," *Macromolecules*, vol. 41, pp. 5753-5762, 2008.

[15] Z. Wang, M. Lu, H. L. Li, and X. Y. Guo, "SWNTs-polystyrene composites preparations and electrical properties research," *Materials Chemistry and Physics*, vol. 100, pp. 77-81, 2006.

[16] M. N. Tchoul, W. T. Ford, M. L. P. Ha, I. Chavez-Sumarriva, B. P. Grady, G. L. Lolli, D. E. Resasco, and S. Arepalli, "Composites of single-walled carbon nanotubes and polystyrene: Preparation and electrical conductivity," *Chemistry of Materials*, vol. 20, pp. 3120-3126, 2008.

[17] J. R. Yu, K. B. Lu, E. Sourty, N. Grossiord, C. E. Konine, and J. C. Loos, "Characterization of conductive multiwall carbon nanotube/polystyrene composites prepared by latex technology," *Carbon*, vol. 45, pp. 2897-2903, 2007.

[18] K. B. Lu, N. Grossiord, C. E. Koning, H. E. Miltner, B. van Mele, and J. Loos, "Carbon Nanotube/Isotactic Polypropylene Composites Prepared by Latex Technology: Morphology Analysis of CNT-Induced Nucleation," *Macromolecules*, vol. 41, pp. 8081-8085, 2008.

[19] T.-M. Wu and E.-C. Chen, "Preparation and characterization of conductive carbon nanotube-polystyrene nanocomposites using latex technology," *Composites Science and Technology*, vol. 68, pp. 2254-2259 2008.

[20] J. Loos, N. Grossiord, C. E. Koning, and O. Regev, "On the fate of carbon nanotubes: Morphological characterisations," *Composites Science and Technology*, vol. 67, pp. 783-788, 2007.

[21] O. Regev, P. N. B. ElKati, J. Loos, and C. E. Koning, "Preparation of conductive nanotube-polymer composites using latex technology," *Advanced Materials*, vol. 16, pp. 248-251, 2004.

[22] D. Blond, W. Walshe, K. Young, F. M. Blighe, U. Khan, D. Almecija, L. Carpenter, J. McCauley, W. J. Blau, and J. N. Coleman, "Strong, tough, electrospun polymer-nanotube composite membranes with extremely low density," *Advanced Functional Materials*, vol. 18, pp. 2618-2624, 2008.

[23] C. Capozzi, S. Shackelford, R. Ou, and R. Gerhardt, *Study of Percolation in PMMA/Indium Tin Oxide Composites*, in *Materials Research Society*. 2004 meeting, symp. N3.13, pp. 303-308.

[24] C. J. Capozzi and R. A. Gerhardt, "Correlation of the ac Electrical Conductivity and the Microstructure of PMMA/ITO Nanocomposites That Possess Phase-Segregated Microstructures," *Journal of Physical Chemistry C*, vol. 112, pp. 19372-19382, 2008.

[25] S. Gupta, R. Q. Ou, and R. A. Gerhardt, "Effect of the fabrication method on the electrical properties of poly(acrylonitrile-co-butadiene-co-styrene)/carbon black composites," *Journal of Electronic Materials*, vol. 35, pp. 224-229, 2006.

[26] L. E. Levine, G. G. Long, J. Ilavsky, R. A. Gerhardt, R. Ou, and C. A. Parker, "Self-assembly of carbon black into nanowires that form a conductive three dimensional micronetwork," *Applied Physics Letters*, vol. 90, pp. 014101-3, 2007.

[27] R. Q. Ou, S. Gupta, C. A. Parker, and R. A. Gerhardt, "Fabrication and electrical conductivity of poly(methyl methacrylate) (PMMA)/Carbon black (CB) composites: Comparison between an ordered carbon black nanowire-like segregated structure and a randomly dispersed carbon black nanostructure," *Journal of Physical Chemistry B*, vol. 110, pp. 22365-22373, 2006.

[28] C. J. Capozzi, *Controlled Self-Assembly of ITO Nanoparticles Into Aggregate Wire Structures in PMMA-ITO Nanocomposites*, 2009, Atlanta, Ga, Ph.D. Thesis: Georgia Institute of Technology.

[29] C. J. Capozzi, Z. Li, R. J. Samuels, and R. A. Gerhardt, "Impedance spectroscopy and optical characterization of polymethyl methacrylate/indium tin oxide nanocomposites with three-dimensional Voronoi microstructures," *Journal of Applied Physics*, vol. 104, pp. 114902-114902-10, 2008.

[30] R. H. Baughman, A. A. Zakhidov, and W. A. de Heer, "Carbon nanotubes--the route toward applications," *Science*, vol. 297, pp. 787-792 2002.

[31] N. Grossiord, J. Loos, O. Regev, and C. E. Koning, "Toolbox for dispersing carbon nanotubes into polymers to get conductive nanocomposites," *Chemistry of Materials*, vol. 18, pp. 1089-1099, 2006.

[32] J. C. Grunlan, W. W. Gerberich, and L. F. Francis, "Lowering the percolation threshold of conductive composites using particulate polymer microstructure," *Journal of Applied Polymer Science*, vol. 80, pp. 692-705, 2001.

[33] M. Kozlowski and S. Frackowiak, "Chemical sensors based on polymer composites," *Sensors and Actuators B-Chemical*, vol. 109, pp. 141-145, 2005.

[34] B. L. He, Y. K. Zhou, W. J. Zhou, B. Dong, and H. L. Li, "Preparation and characterization of ruthenium-doped polypyrrole composites for supercapacitor," *Materials Science and Engineering a-Structural Materials Properties Microstructure and Processing*, vol. 374, pp. 322-326, 2004.

[35] K. Awasthi, A. Srivastava, and O. N. Srivastava, "Synthesis of carbon nanotubes," *Journal of Nanoscience and Nanotechnology*, vol. 5, pp. 1616-1636, 2005.

[36] R. Ramasubramaniam, J. Chen, and H. Y. Liu, "Homogeneous carbon nanotube/polymer composites for electrical applications," *Applied Physics Letters*, vol. 83, pp. 2928-2930, 2003.

[37] A. K. Kota, B. H. Cipriano, M. K. Duesterberg, A. L. Gershon, D. Powell, S. R. Raghavan, and H. A. Bruck, "Electrical and Rheological Percolation in Polystyrene/MWCNT Nanocomposites," *Macromolecules*, vol. 40, pp. 7400-7406, 2007.

[38] N. Grossiord, P. J. J. Kivit, J. Loos, J. Meuldijk, A. V. Kyrylyuk, P. van der Schoot, and C. E. Koning, "On the influence of the processing conditions on the performance of electrically conductive carbon nanotube/polymer nanocomposites," *Polymer*, vol. 49, pp. 2866-2872, 2008.

[39] O. Biham, A. A. Middleton, and D. Levine, "Self-organization and a dynamical transition in traffic-flow models," *Physical Review A*, vol. 46, pp. R6124-R6127 1992.

[40] G. F. Wang, X. M. Tao, and R. X. Wang, "Flexible organic light-emitting diodes with a polymeric nanocomposite anode," *Nanotechnology*, vol. 19, pp. 145201-1-145201-5, 2008.

[41] Wikipedia. *Static Electricity*. 2010 [cited 2010 February 22]; Available from: http://en.wikipedia.org/wiki/Static_electricity.

[42] J.B. Donnet, M.J. Wang, *Carbon Black: Science & Technology*. 1993., New York: Marcel Dekker.

[43] J. Y. Kim, M. Kim, H. M. Kim, J. Joo, and J. H. Choi, "Electrical and optical studies of organic light emitting devices using SWCNTs-polymer nanocomposites," *Optical Materials*, vol. 21, pp. 147-151, 2003.

[44] R. B. H. Tahar, T. Ban, Y. Ohya, and Y. Takahashi, "Tin doped indium oxide thin films: Electrical properties," *Journal of Applied Physics*, vol. 83, pp. 2631-2645, 1998.

[45] J. F. Gao, Z. M. Li, Q. J. Meng, and Q. Yang, "CNTs/UHMWPE composites with a two-dimensional conductive network," *Materials Letters*, vol. 62, pp. 3530-3532, 2008.

[46] J. M. Thomassin, X. Lou, C. Pagnoulle, A. Saib, L. Bednarz, I. Huynen, R. Jerome, and C. Detrembleur, "Multiwalled carbon Nanotube/Poly(epsilon-caprolactone) nanocomposites with exceptional electromagnetic interference shielding properties," *Journal of Physical Chemistry C*, vol. 111, pp. 11186-11192, 2007.

[47] S. C. Tjong, G. D. Liang, and S. P. Bao, "Effects of crystallization on dispersion of carbon nanofibers and electrical properties of polymer nanocomposites," *Polymer Engineering and Science*, vol. 48, pp. 177-183, 2008.

[48] C. A. Mitchell, J. L. Bahr, S. Arepalli, J. M. Tour, and R. Krishnamoorti, "Dispersion of functionalized carbon nanotubes in polystyrene," *Macromolecules*, vol. 35, pp. 8825-8830, 2002.

[49] M. Moniruzzam and K. I. Winey, "Polymer Nanocomposites Containing Carbon Nanotubes," *Macromolecules*, vol. 39, pp. 5194 - 5205, 2006.

[50] J. P. Jog, "Solid-State Processing of Polymers - a Review," *Advances in Polymer Technology*, vol. 12, pp. 281-289, 1993.

[51] A. Malliaris and D. T. Turner, "Influence of Particle Size on the Electrical Resistivity of Compacted Mixtures of Polymeric and Metallic Powders," *Journal of Applied Physics*, vol. 42, pp. 614-618, 1971.

[52] R. P. Kusy and D. T. Turner, "Electrical Conductivity of a Polyurethane Elastomer Containing Segregated Particles of Nickel," *Journal of Applied Polymer Science*, vol. 17, pp. 1631-1633, 1973.

[53] R. P. Kusy and D. T. Turner, "Electrical Resistivity of a Polymeric Insulator Containing Segregated Metallic Particles," *Nature-Physical Science*, vol. 229, pp. 58-62, 1971.

[54] R. P. Kusy, "Influence of Particle-size Ratio on Continuity of Aggregates " *Journal of Applied Physics*, vol. 48, pp. 5301-5305, 1977.

[55] R. Mukhopadhyay, S. K. De, and S. Basu, "Effect of Metal Concentration on Electrical-Conductivity and Some Mechanical-Properties of Poly(methyl methacrylate)-Copper Composites," *Journal of Applied Polymer Science*, vol. 20, pp. 2575-2580, 1976.

[56] S. Bhattacharya, S. Basu, and S. De, "Effect of Size, Shape and Oxide Content of Metal Particles on Formation of Segregated Networks in PVC Composites," *Composites*, vol. 9, pp. 177-183, 1978.

[57] G. Pinto and A. K. Maaroufi, "Conducting polymer composites of zinc-filled urea-formaldehyde," *Journal of Applied Polymer Science*, vol. 96, pp. 2011-2015, 2005.

[58] C. M. Chan, C. L. Cheng, and M. M. F. Yuen, "Electrical properties of polymer composites prepared by sintering a mixture of carbon black and ultra-high molecular weight polyethylene powder," *Polymer Engineering and Science*, vol. 37, pp. 1127-1136, 1997.

[59] J. Bouchet, C. Carrot, J. Guillet, G. Boiteux, G. Seytre, and M. Pineri, "Conductive composites of UHMWPE and ceramics based on the segregated network concept," *Polymer Engineering and Science*, vol. 40, pp. 36-45, 2000.

[60] C. E. Hoppe, F. Rivadulla, J. Vidal-Vidal, M. A. Lopez-Quintela, and J. Rivas, "Magnetic relaxation of gamma-Fe2O3 nanoparticles arrangements and electronic phase-segregated systems," *Journal of Nanoscience and Nanotechnology*, vol. 8, pp. 2883-2890, 2008.

[61] S. K. Bhattacharya and A. C. D. Chaklader, "Review on Metal-Filler Plastics.1.Electrical-Conductivity," *Polymer-Plastics Technology and Engineering*, vol. 19, pp. 21-51, 1982.

[62] A. Greco and A. Maffezzoli, "Polymer melting and polymer powder sintering by thermal analysis," *Journal of Thermal Analysis and Calorimetry*, vol. 72, pp. 1167-1174, 2003.

[63] T. J. Vink, W. Walrave, J. L. C. Daams, P. C. Baarslag, and J. Vandenmeerakker, "On the Homogeneity of Sputter-Deposited ITO Films.1.Stress and Microstructure," *Thin Solid Films*, vol. 266, pp. 145-151, 1995.

[64] S. J. Hong, J. W. Choi, and J. I. Han, "Effect of Heat Treatment on the Characteristics of ITO Nanoparticles for Inkjet Printing," *Journal of the Korean Physical Society*, vol. 53, pp. 2508-2511, 2008.

[65] L. J. Meng and M. P. dos Santos, "Properties of indium tin oxide films prepared by rf reactive magnetron sputtering at different substrate temperature," *Thin Solid Films*, vol. 322, pp. 56-62, 1998.

[66] I. Hamberg and C. G. Granqvist, "Evaporated Sn-Doped In_2O_3 Films - Basic Optical-Properties and Applications to Energy-Efficient Windows," *Journal of Applied Physics*, vol. 60, pp. R123-R159, 1986.

[67] K. L. Chopra, S. Major, and D. K. Pandya, "Transparent Conductors - a Status Review," *Thin Solid Films*, vol. 102, pp. 1-46, 1983.

[68] Y. Shigesato and D. C. Paine, "A Microstructural Study of Low-Resistivity Tin-Doped Indium Oxide Prepared by DC Magnetron Sputtering," *Thin Solid Films*, vol. 238, pp. 44-50, 1994.

[69] B. G. Lewis and D. C. Paine, "Applications and processing of transparent conducting oxides," *Materials Research Society Bulletin*, vol. 25, pp. 22-27, 2000.

[70] R. A. Gilstrap and C. J. Summers, "Synthesis and analysis of an indium tin oxide nanoparticle dispersion," *Thin Solid Films*, vol. 518, pp. 1136-1139, 2009.

[71] G. B. Gonzalez, T. O. Mason, J. P. Quintana, O. Warschkow, D. E. Ellis, J. H. Hwang, J. P. Hodges, and J. D. Jorgensen, "Defect structure studies of bulk and nano-indium-tin oxide," *Journal of Applied Physics*, vol. 96, pp. 3912-3920, 2004.

[72] C. J. Capozzi, I. N. Ivanov, S. Joshi, and R. A. Gerhardt, "The effect of the atmosphere on the optical properties of as-synthesized colloidal indium tin oxide," *Nanotechnology*, vol. 20, pp. 145701, 2009.

[73] R. A. Gilstrap, C. J. Capozzi, C. G. Carson, R. A. Gerhardt, A. Y. Borisevich, and C. J. Summers, "Synthesis of Nonagglomerated Indium Tin Oxide Nanoparticle Dispersions," *Advanced Materials*, vol. 20, pp. 4625-4625, 2008.

[74] G. Frank and H. Kostlin, "Electrical-Properties and Defect Model of Tin-Doped Indium Oxide Layers," *Applied Physics a-Materials Science & Processing*, vol. 27, pp. 197-206, 1982.

[75] D. M. Mattox, "Sol-Gel Derived, Air-Baked Indium Tin Oxide-Films," *Thin Solid Films*, vol. 204, pp. 25-32, 1991.

[76] S. Y. Han, D. H. Lee, G. S. Herman, and C. H. Chang, "Inkjet-Printed High Mobility Transparent-Oxide Semiconductors," *Journal of Display Technology*, vol. 5, pp. 520-524, 2009.

[77] K. Y. Kim and S. B. Park, "Preparation and property control of nano-sized indium tin oxide particle," *Materials Chemistry and Physics*, vol. 86, pp. 210-221, 2004.

[78] S. Iijima, "Helical Microtubes of Graphitic Carbon," *Nature*, vol. 354, pp. 56-58, 1991.

[79] S. Bredeau, S. Peeterbroeck, D. Bonduel, M. Alexandre, and P. Dubois, "From carbon nanotube coatings to high-performance polymer nanocomposites," *Polymer International*, vol. 57, pp. 547-553, 2008.

[80] E. T. Thostenson, Z. F. Ren, and T. W. Chou, "Advances in the science and technology of carbon nanotubes and their composites: a review," *Composites Science and Technology*, vol. 61, pp. 1899-1912, 2001.

[81] P. C. Ma, M. Y. Liu, H. Zhang, S. Q. Wang, R. Wang, K. Wang, Y. K. Wong, B. Z. Tang, S. H. Hong, K. W. Paik, and J. K. Kim, "Enhanced Electrical Conductivity of Nanocomposites Containing Hybrid Fillers of Carbon Nanotubes and Carbon Black," *American Chemical Society Applied Materials & Interfaces*, vol. 1, pp. 1090-1096, 2009.

[82] M. A. Valente, L. C. Costa, S. K. Mendiratta, F. Henry, and L. Ramanitra, "Structural and electrical properties of polystyrene-carbon composites," *Solid State Communications*, vol. 112, pp. 67-72, 1999.

[83] K. Wu, *Phase-segregated PS/CB, PS/SWNT, and PS/MWNT Composites*. 2008, Undergraduate Research, Georgia Institute of Technology Atlanta.

[84] R. Haggenmueller, W. Zhou, J. E. Fischer, and K. I. Winey, "Production and characterization of polymer nanocomposites with highly aligned single-walled carbon nanotubes," *Journal of Nanoscience and Nanotechnology*, vol. 3, pp. 105-110, 2003.

[85] B. Safadi, R. Andrews, and E. A. Grulke, "Multiwalled carbon nanotube polymer composites: Synthesis and characterization of thin films," *Journal of Applied Polymer Science*, vol. 84, pp. 2660-2669, 2002.

[86] F. Henry and L. C. Costa, "Percolation study by infrared thermography," *Microwave and Optical Technology Letters*, vol. 45, pp. 335-337, 2005.

[87] D. Rivin and Y. Suzin, "Calorimetric investigation of the interaction of carbon nanotubes with polystyrene," *Journal of Polymer Science Part B-Polymer Physics*, vol. 44, pp. 1821-1834, 2006.

[88] Y. J. Choi, S. H. Hwang, Y. S. Hong, J. Y. Kim, C. Y. Ok, W. Huh, and S. W. Lee, "Preparation and Characterization of PS/Multi-Walled Carbon Nanotube Nanocomposites," *Polymer Bulletin*, vol. 53, pp. 393-400, 2005.

[89] M. F. Mu, A. M. Walker, J. M. Torkelson, and K. I. Winey, "Cellular structures of carbon nanotubes in a polymer matrix improve properties relative to composites with dispersed nanotubes," *Polymer*, vol. 49, pp. 1332-1337, 2008.

[90] S. S. Kim and C. D. Han, "Effect of Thermal History on the Rheological Behavior of a Thermotropic Liquid-Crystalline Polymer," *Macromolecules*, vol. 26, pp. 3176-3186, 1993.

[91] S. H. Hwang, K. S. Yoo, C. N. Moorefield, S. W. Lee, and G. R. Newkome, "Thermal behavior of metallodendrimers possessing bis(terpyridinyl)Ru-(II) connectivity and different surface functionality," *Journal of Polymer Science Part B-Polymer Physics*, vol. 42, pp. 1487-1495, 2004.

[92] C. D. Han and J. K. Kim, "Molecular Theory for the Viscoelasticity of compatible Polymer Mixtures .2. Tube Model with Reptation and Constraint Release Contributions," *Macromolecules*, vol. 22, pp. 4292-4302, 1989.

[93] C. D. Han and M. S. Jhon, "Correlations of the 1st Normal Stress Difference with Shear-Stress and of the Storage Modulus with Loss Modulus for Homopolymers," *Journal of Applied Polymer Science*, vol. 32, pp. 3809-3840, 1986.

[94] C. D. Han, D. M. Baek, and J. K. Kim, "Effect of Microdomain Structure on the Order-Disorder Transition Temperature of Polystyrene-Block-Polyisoprene-Block-Polystyrene Copolymers," *Macromolecules*, vol. 23, pp. 561-570, 1990.

[95] J. Schaffer, A. Saxena, S. Antolovich, T. Sanders, and S. Warner, *The Science and Design of Engineering Materials*. 2 ed. 1999, New York: WCB McGraw Hill.

[96] *Overview of materials for polystyrene* 2010 [cited 2010 2/11]; Available from: http://www.matweb.com/search/DataSheet.aspx?MatGUID=df6b1ef50ce84e7995bdd1f6fd1b04c9&ckck=1.

[97] W. Bauhofer and J. Z. Kovacs, "A review and analysis of electrical percolation in carbon nanotube polymer composites," *Composites Science and Technology*, vol. 69, pp. 1486-1498, 2009.

[98] M. T. Connor, T. A. Ezquerra, and F. J. Balta Calleja, "Broadband ac conductivity of conductor-polymer composites," *Physical Review B*, vol. 57, pp. 2286-2294, 1998.

[99] X. Sun and M. Song, "Numerical Simulations of the Effect of Microstructure on AC Conductivity of MWCNT/Polymer Nanocomposites." *Macromolecular Theory and Simulations*, vol. 19, pp. 57-63, 2010.

[100] F. Henry and L. C. Costa, "Percolation and order-disorder transition," *Physica B-Condensed Matter*, vol. 387, pp. 250-258, 2007.

[101] L. A. Prystaj, *Effect of Carbon Filler Characteristics on the Electrical Properties of Conductive Polymer Composites Possessing Segregated Network Microstructures*, 2008, Atlanta, Ga, M.S. Thesis: Georgia Institute of Technology.

[102] S. Talapatra and R. Gerhardt, *Undergraduate research report on ABS/CB polymer composites*. 2008, Georgia Tech: Atlanta. p. 18.

[103] V. Bliznyuk, S. Singamaneni, R. Kattumenu, and M. Atashbar, "Surface electrical conductivity in ultrathin single-wall carbon nanotube/polymer nanocomposite films," *Applied Physics Letters*, vol. 88, pp., 2006.

[104] S. Ugur, O. Yargi, and O. Pekcan, "Conductivity percolation of carbon nanotubes (CNT) in polystyrene (PS) latex film," *Canadian Journal of Chemistry-Revue Canadienne De Chimie*, vol. 88, pp. 267-276.

[105] T. S. Lin, L. Y. Cheng, C. C. Hsiao, and A. C. M. Yang, "Percolated network of entangled multi-walled carbon nanotubes dispersed in polystyrene thin films through surface grafting polymerization," *Materials Chemistry and Physics*, vol. 94, pp. 438-443, 2005.

[106] M. B. Bryning, M. F. Islam, J. M. Kikkawa, and A. G. Yodh, "Very low conductivity threshold in bulk isotropic single-walled carbon nanotube-epoxy composites," *Advanced Materials*, vol. 17, pp. 1186 - 1191, 2005.

[107] C. C. Hsiao, T. S. Lin, L. Y. Cheng, C. C. M. Ma, and A. C. M. Yang, "Nanomechanical properties of polystyrene thin films embedded with surface-grafted multiwalled carbon nanotubes," *Macromolecules*, vol. 38, pp. 4811-4818, 2005.

[108] J. B. Bai and A. Allaoui, "Effect of the length and the aggregate size of MWNTs on the improvement efficiency of the mechanical and electrical properties of nanocomposites - experimental investigation," *Composites Part a-Applied Science and Manufacturing*, vol. 34, pp. 689-694, 2003.

[109] T. Kimura, H. Ago, M. Tobita, S. Ohshima, M. Kyotani, and M. Yumura, "Polymer composites of carbon nanotubes aligned by a magnetic field," *Advanced Materials*, vol. 14, pp. 1380-1383, 2002.

[110] A. B. Dalton, S. Collins, E. Munoz, J. M. Razal, V. H. Ebron, J. P. Ferraris, J. N. Coleman, B. G. Kim, and R. H. Baughman, "Super-tough carbon-nanotube fibers - These extraordinary composite fibers can be woven into electronic textiles," *Nature*, vol. 423, pp. 703-703, 2003.

[111] B. Vigolo, A. Penicaud, C. Coulon, C. Sauder, R. Pailler, C. Journet, P. Bernier, and P. Poulin, "Macroscopic fibers and ribbons of oriented carbon nanotubes," *Science*, vol. 290, pp. 1331-1334, 2000.

[112] F. M. Du, R. C. Scogna, W. Zhou, S. Brand, J. E. Fischer, and K. I. Winey, "Nanotube networks in polymer nanocomposites: Rheology and electrical conductivity," *Macromolecules*, vol. 37, pp. 9048-9055, 2004.

[113] J. L. Stevens, A. Y. Huang, H. Q. Peng, L. W. Chiang, V. N. Khabashesku, and J. L. Margrave, "Sidewall amino-functionalization of single-walled carbon nanotubes through fluorination and subsequent reactions with terminal diamines," *Nano Letters*, vol. 3, pp. 331-336, 2003.

[114] E. K. Hobbie, B. J. Bauer, J. Stephens, M. L. Becker, P. McGuiggan, S. D. Hudson, and H. Wang, "Colloidal particles coated and stabilized by DNA-wrapped carbon nanotubes," *Langmuir*, vol. 21, pp. 10284-10287, 2005.

[115] R. Andrews and M. C. Weisenberger, "Carbon nanotube polymer composites," *Current Opinion in Solid State & Materials Science*, vol. 8, pp. 31-37, 2004.

[116] S. Barrau, P. Demont, E. Perez, A. Peigney, C. Laurent, and C. Lacabanne, "Effect of palmitic acid on the electrical conductivity of carbon nanotubes-epoxy resin composites," *Macromolecules*, vol. 36, pp. 9678-9680, 2003.

[117] F. M. Du, J. E. Fischer, and K. I. Winey, "Effect of nanotube alignment on percolation conductivity in carbon nanotube/polymer composites," *Physical Review B*, vol. 72, pp. 4, 2005.

[118] R. Haggenmueller, H. H. Gommans, A. G. Rinzler, J. E. Fischer, and K. I. Winey, "Aligned single-wall carbon nanotubes in composites by melt processing methods," *Chemical Physics Letters*, vol. 330, pp. 219-225, 2000.

[119] C. A. Mitchell and R. Krishnamoorti, "Dispersion of single-walled carbon nanotubes in poly(epsilon-caprolactone)," *Macromolecules*, vol. 40, pp. 1538-1545, 2007.

[120] X. S. Yi, C. Z. Wu, and D. L. Ma, "Property balancing for polyethylene-based carbon black-filled conductive composites," *Journal of Applied Polymer Science*, vol. 67, pp. 131-138, 1998.

[121] C. H. Poa, S. R. P. Silva, P. C. P. Watts, W. K. Hsu, H. W. Kroto, and D. R. M. Walton, "Field emission from nonaligned carbon nanotubes embedded in a polystyrene matrix," *Applied Physics Letters*, vol. 80, pp. 3189, 2002.

[122] S. T. Kim, H. J. Choi, and S. M. Hong, "Bulk polymerized polystyrene in the presence of multiwalled carbon nanotubes," *Colloid and Polymer Science*, vol. 285, pp. 593-598, 2007.

[123] N. Sluzarenko, B. Heurtefeu, M. Maugey, C. Zakri, P. Poulin, and S. Lecommandoux, "Diblock copolymer stabilization of multi-wall carbon nanotubes in organic solvents and their use in composites," *Carbon*, vol. 44, pp. 3207-3212, 2006.

[124] T.-E. Chang, A. Kisliuk, S. M. Rhodes, W. J. Brittain, and A. P. Sokolov, "Conductivity and mechanical properties of well-dispersed single-wall carbon nanotube/polystyrene composite," *Polymer*, vol. 47, pp. 7740-7746, 2006.

[125] D. Qian, E. C. Dickey, R. Andrews, and T. Rantell, "Load transfer and deformation mechanisms in carbon nanotube-polystyrene composites," *Applied Physics Letters*, vol. 76, pp. 2868-2870, 2000.

[126] L. Jin, C. Bower, and O. Zhou, "Alignment of carbon nanotubes in a polymer matrix by mechanical stretching," *Applied Physics Letters*, vol. 73, pp. 1197-1199, 1998.

[127] J. J. Ge, H. Hou, Q. Li, M. J. Graham, A. Greiner, H. Reneker Darrell, W. Harris Frank, and Z. D. Cheng Stephen, "Assembly of well-aligned multiwalled carbon nanotubes in confined polyacrylonitrile environments: Electrospun composite nanofiber sheets " *Journal of American Chemical Society*, vol. 126, pp. 15754-15761, 2004.

[128] J. B. Gao, A. P. Yu, M. E. Itkis, E. Bekyarova, B. Zhao, S. Niyogi, and R. C. Haddon, "Large-scale fabrication of aligned single-walled carbon nanotube array and hierarchical single-walled carbon nanotube assembly," *Journal of the American Chemical Society*, vol. 126, pp. 16698-16699, 2004.

[129] H. Q. Hou, J. J. Ge, J. Zeng, Q. Li, D. H. Reneker, A. Greiner, and S. Z. D. Cheng, "Electrospun polyacrylonitrile nanofibers containing a high concentration of well-aligned multiwall carbon nanotubes," *Chemistry of Materials*, vol. 17, pp. 967-973, 2005.

[130] F. Ko, Y. Gogotsi, A. Ali, N. Naguib, H. H. Ye, G. L. Yang, C. Li, and P. Willis, "Electrospinning of continuons carbon nanotube-filled nanofiber yarns," *Advanced Materials*, vol. 15, pp. 1161-1165, 2003.

[131] C. A. Dyke and J. M. Tour, "Covalent functionalization of single-walled carbon nanotubes for materials applications," *Journal of Physical Chemistry A*, vol. 108, pp. 11151-11159, 2004.

[132] J. B. Gao, M. E. Itkis, A. P. Yu, E. Bekyarova, B. Zhao, and R. C. Haddon, "Continuous spinning of a single-walled carbon nanotube-nylon composite fiber," *Journal of the American Chemical Society*, vol. 127, pp. 3847-3854, 2005.

[133] S. Chatterjee, "Polymer–ITO nanocomposite template for the optoelectronic application," *Journal of Materials Science*, vol. 43, pp. 1696-1700, 2008.

[134] H. Miyazaki, T. Ota, and I. Yasui, "Solar Energy Materials and Solar Cells : Design of ITO/transparent resin optically selective transparent composite," *Solar Energy Materials and Solar Cells*, vol. 79, pp. 51-55, 2003.

[135] Y. Leterrier, L. Medico, F. Demarco, J. A. E. Manson, U. Betz, M. F. Escola, M. K. Olsson, and F. Atamny, "Mechanical integrity of transparent conductive oxide films for flexible polymer-based displays," *Thin Solid Films*, vol. 460, pp. 156-166, 2004.

[136] Y. Leterrier, "Durability of nanosized oxygen-barrier coatings on polymers - Internal stresses," *Progress in Materials Science*, vol. 48, pp. 1-55, 2003.

[137] R. A. Gerhardt, *Impedance Spectroscopy and Mobility Spectra*, in *Encyclopedia of Condensed Matter Physics*, G. Bassani, G. Liedl, and P. Wyder, Editors. 2005, Elsevier. p. 350-363.

[138] Z. Li, *Three-dimensional optical characterization of heterogeneous polymer systems*. 2004, Altlanta, Ga, M.S. Thesis: Georgia Institute of Technology.

[139] A. Ierczynska, J. Friedrich, H. E. Maneck, G. Boiteux, and J. K. Jeszka, "Segregated network polymer/carbon nanotubes composites," *Central European Journal of Chemistry*, vol. 2, pp. 363-370, 2004.

[140] *Cheaptubes.com the source for short nanotubes-Short CNTs*. 2010 [cited 2010 1/21]; Available from: http://www.cheaptubesinc.com/ShortCNTs.htm#Short_MWNTs_8-15nm_OD.

[141] C. Capozzi and R. Gerhardt, "Effect of Processing on the Microstructure and Electrical Conductivity of Hot Pressed PMMA/ITO Bulk Nanocomposites," in *Fall 2006 Materials Research Society Meeting Procedings*, vol. 907, pp. FF12.19, 2006.

[142] O. J. OaeLoan, M. R. Evans, and M. E. Cates, "Jamming transition in a homogeneous one-dimensional system: The bus route model," *Physical Review E*, vol. 58, pp. 1404-1418, 1998.

[143] V. Pryamitsyn and V. Ganesan, "Origins of Linear Viscoelastic Behavior of Polymer−Nanoparticle Composites," *Macromolecules*, vol. 39, pp. 844-856, 2006.

[144] P. C. Ma, B. Z. Tang, and J.-K. Kim, "Effect of CNT decoration with silver nanoparticles on electrical conductivity of CNT-polymer composites," *Carbon*, vol. 46, pp. 1497-1505, 2008.

VITA

JOHN M. BOYEA

BOYEA was born in Atlanta, Georgia. He completed a dual degree engineering program through Berry College, in Rome, Georgia, and the Georgia Institute of Technology, in Atlanta, Georgia. He has a B.S. in physics as well as a B.S. in Materials Science and Engineering, from Berry and Georgia Tech respectively, which were obtained in 2008. Mr. Boyea is a strong supporter of sustainable practices and technology. Away from school and research, he enjoys digital music production and cycling around Atlanta and on bike trails.